Adaptation in Bipedal Locomotion: Insights from Dynamic Modelling, Numerical Optimization, and Neuro-fuzzy-genetic Programming

by

Mehran Armand

A thesis
presented to the University of Waterloo
in fulfilment of the
thesis requirement for the degree of
Doctor of Philosophy
in
Mechanical Engineering and Kinesiology

Waterloo, Ontario, Canada, 1998

©Mehran Armand 1998

National Library of Canada
Acquisitions and Bibliographic Services
395 Wellington Street
Ottawa ON K1A 0N4
Canada

Bibliothèque nationale du Canada
Acquisitions et services bibliographiques
395, rue Wellington
Ottawa ON K1A 0N4
Canada

Your file Votre référence

Our file Notre référence

The author has granted a non-exclusive licence allowing the National Library of Canada to reproduce, loan, distribute or sell copies of this thesis in microform, paper or electronic formats.

L'auteur a accordé une licence non exclusive permettant à la Bibliothèque nationale du Canada de reproduire, prêter, distribuer ou vendre des copies de cette thèse sous la forme de microfiche/film, de reproduction sur papier ou sur format électronique.

The author retains ownership of the copyright in this thesis. Neither the thesis nor substantial extracts from it may be printed or otherwise reproduced without the author's permission.

L'auteur conserve la propriété du droit d'auteur qui protège cette thèse. Ni la thèse ni des extraits substantiels de celle-ci ne doivent être imprimés ou autrement reproduits sans son autorisation.

0-612-30584-8

Canada

The University of Waterloo requires the signatures of all persons using or photocopying this thesis. Please sign below, and give address and date.

Acknowledgments

I have been accompanied, and guided by many people through this journey. My gratitude to my supervisors, Professor Jan Huissoon and Professor Aftab Patla for their support and encouragement. To Jan who was always open to my problems and skillfully walked with me through every single detail. To Aftab who taught me how to have vision; see through the problems, and look at the big picture.

Many thanks to my committee members. To Dr. Zernicke who patiently read through my thesis and gave me many constructive critiques and ideas. To Dr. Dubey whom I will always respect his knowledge and wisdom. To Dr. Jim Frank for his input on the neural part of this work. I can hardly remember enjoying any class as much as his. To Dr. Calamai who taught, examined, provided valuable input, and finally optimized (maximized) my understanding of the optimization part of this work.

Many other professors and friends have provided valuable input to this work. I was privileged to discuss research issues with Dr. David Winter. Dr. McPhee, generously, spent time to discuss my problems in multi-body dynamics. I could not have asked for more from Dr. Amir Khajepour. He gave ideas, discussed my research, read my paper, and most of all was a valuable friend. My friend, Dr. Farid Golnaraghi, has always been extremely supportive (and a bit of a pain!). His presence usually raised a happy spirit in our automation group.

I would like to acknowledge all the secretaries and staff that have been so caring and have assisted me throughout these four years. I especially like to give my sincere thanks to Kathy Roenspiess, Sue Guckenberger, Diane Hause, Ruth Gooding, Julie Cassaubon, and Elaine Garner. My thanks also go to Victor Kiss, Paul Guy, Cathy Silcher, Dr. Kristina Gielo-Perczak, John Pezak, and Marius van Reenen.

My most memorable accomplishment in this journey was the friends I found in both the engineering and kinesiology departments. Milad Ishac's footsteps are all over my thesis. He shared my accomplishments and whines all through the last four years. Many thanks for many memorable and enjoyable, long working days and nights to Djamil

Bulahbal, Fariborz Fariborzi, Dr. Lin, Shahyar Ziae, and Robert Madjka. Thanks to my buddies Lillian Gobi, Antonio Quedo, Elaine Little, Shierly Reitdyk, Allen Adkin, Steve Hill, Nicole Wynberg and all others in the neural control lab. Special thanks to Dr. Hamid Ahmadian, Toni Perhasto, Sultan Sediqui, David Purcell, Corey Richards, Richard Li and all others in the automation group.

To my friends, Jalals, Homayoon, Manouchehr, and Mehrnoosh. I felt your supports all through my happy and sad times. I feel the events of our lives have done nothing but strengthen our friendships. I sincerely value your friendships.

To all my family, especially to my mother Zahra, and to my sisters Monir and Mahasty. We, together, have gone through so much and shared lots of joy and sorrow. Thank you for having faith in me. Thanks for your support, care, and love. Although thanks are not sufficient to express the way I feel.

To my wife Grace, who has actively shared and supported me at every step in this road. Your presence in my life has made this journey so much more beautiful and meaningful. For all you have brought to my life, I am in debted to you, forever.

Finally, I dedicate this thesis to the one who traveled with me to the end, and every evening added that little happiness I needed to carry on. He finally passed on in his own journey just after I reached the end of this one. In his beloved memory, I finish this work.

It is no small a thing

to have enjoyed the sun,

to have lived light in the spring,

to have loved, to have thought,

to have dreamed, to have done.

In Memory of My Father

Ali Naghi Armand

Abstract

A human ambulator continuously adapts to changing terrain conditions by modifying the dynamics of movement of its own components and their relationship to the external world. The study of human locomotion as a biological model of adaptation, inspires research in a variety of disciplines. Examples include applications where a robot is required to maneuver on uneven terrain, the assessment of gait abnormalities in humans, and the improvement of rehabilitation strategies.

In this work, the study of adaptation of human gait is carried out by the development of neuro-musculo-skeletal models. The models developed proceed from the skeletal system inwards; i.e., the skeletal system is modelled first, the muscles are added next, and finally the central control system is developed.

Skeletal models (rigid bodies) are developed with various levels of complexity (2-D and 3-D). The results show translational energy applied at the hip joint provides a given toe elevation for minimal energy cost. This strategy is most effective when initiated during the double support phase, and results in increased hip elevation velocity at toe-off. Also found is that the leading limb ankle push-off is the most effective strategy for increasing hip elevation velocity at the start of the swing phase. In addition, contributions of intersegmental dynamics are greater when active (flexor) control is implemented at the knee joint compared to control at the hip joint.

Next, bi-articular muscles are added, and the muscle force inputs are optimized to best satisfy the postulated objectives for landing stability, obstacle clearance, and efficiency of movement. The simulation results demonstrate that the use of bi-articular muscles is sufficient to clear a range of obstacles with the trailing limb (obstacle encountered during early swing). Stride length or landing stability objectives need not be specified, suggesting a simpler control of trailing limb trajectory by the central nervous system (CNS). In contrast, while the use of bi-articular muscles can be sufficient to clear obstacles with the leading limb (obstacle encountered during mid to late swing), a stable landing and smooth toe and knee trajectories are compromised without suitable initial conditions at toe-off.

A proactive (feed-forward) control system for a novice ambulator is developed by combining a neural network model, fuzzy logic control, genetic optimization, and reinforcement learning. The ambulator, after performing several trials, learns to relate visual inputs of the obstacle size and location to limb movement dynamics. The ambulator learns to produce the muscle forces and joint velocities required to step over an obstacle. This is done within a feed-forward network of neurons.

The neuro-fuzzy-genetic model is also used for performing muscle force optimization. Some of the findings are: a) for the leading limb stepping over an obstacle, less active control during the swing phase and more planning during the double support phase are required; b) for the trailing limb, modifying the initial velocities at toe-off is not sufficient to achieve obstacle clearance and landing stability, and the addition of muscles is required to produce a satisfactory trajectory; and c) the model is able to achieve an adaptive behavior. The model demonstrates satisfactory performance over a range of obstacles without re-learning the neural weights and activation functions.

Finally, the modelling approach is applied to gain insight to *reactive* balance control strategies during locomotion. Specifically, the available response time for recovery from an unsuccessful step over an obstacle (tripping) is considered. The simulation results show that the available response time increases with obstacle compliance, size, and its location within the stride. It also depends on the velocity of the swing foot and the location of the center of mass at the time of impact. The simulation suggests that at normal speeds and smaller obstacles, polysynaptic responses to tripping are the only possible option for the human ambulator. Only if the obstacle is hit in early swing, is a voluntary response to the trip possible.

Contents

List of Tables

List of Figures

Chapter 1

Introduction

Locomotion is an integral part of an animal's activity for survival. Like other biological mechanisms, evolution has sculptured locomotion to increase an animal's adaptability to its environment. Interestingly, for transportation on ground, legged locomotion has been the most common choice of nature. Its outstanding feature, compared to wheel and track type of locomotion, is the ability of the animal to use isolated foot holds, thereby increasing maneuverability when negotiating uneven terrain.

In humans, bipedal locomotion has freed the forelimbs for other activities. This is obtained at the expense of the development of more sophisticated motor acts: the main priority for the quadruped or hexapod locomotor is to generate a sequence of limb movements to produce gait. In bipedal locomotion, however, the balance constraint and narrower base of support are an added complexity on top the motor control problem.

The study of bipedal locomotion, and in particular obstacle avoidance as one of its main features, is advantageous to a variety of disciplines. It is important in assessing gait abnormalities in humans and improving rehabilitation strategies. Its advantages have also been recognized in the field of mobile robots, especially in applications where a robot is required to maneuver on uneven terrain.

To develop a comprehensive understanding of the bipedal locomotor behavior, it is

necessary to draw on and interpret the existing knowledge in a variety of disciplines. Engineering techniques can be used to develop models for bipedal locomotion and to search for answers to many observed behaviors in the study of the human locomotor. On the other hand, the experimental analysis and observations on human locomotor behavior can assist us to develop human-like bipeds, which is one of the goals of bipedal locomotion studies.

Modelling is the major thrust of this thesis. Models of different complexities are used to gain insights into the adaptability of human locomotion.

1.1 Some Issues in Stepping over Obstacle Strategies

This thesis follows two themes: modelling the adaptation of human locomotion to new environmental conditions (specifically when stepping over obstacles) and a search for strategies used for this adaptation (with specific attention to the hip elevation strategy for obstacle avoidance).

Redundancy is the key to adaptation of the human locomotor in the ever-changing environment. An excess number of degrees of freedom in the lower limbs' skeletal system offers a great deal of flexibility in modifying a limb trajectory when obstacles are encountered in the pathway. In addition, usually more than one muscle acts upon a joint, thus providing several options for producing a specific joint torque and/or changing the stiffness in the joints. Evolution has not sufficed to all these: some muscles span two joints; some of these bi-articular muscles are the principal actuators for producing the required joint torques during locomotion. Added to this complexity is the redundancy in the locomotor's sensory system. The integration of the several sensory inputs play an important role in the ambulator's response to the environment. The failure of some of the sensory systems, muscle actuators, and/or segment joints are compensated by other sensors, muscle actuators, and/or joint torques respectively.

Can mathematical models provide insights to how the central nervous system (CNS) deals with the redundancy problem in various levels? What are the CNS objectives when grouping and integrating information and harnessing the degrees of freedom in a certain way? Many researchers have used optimization methods to solve the redundancy problem for muscles spanning one joint. These studies led to the examination of several potential optimization objectives. However, limited success was obtained in reproducing the EMG results for muscle activation. More recent optimization research looked at the effect of the dynamics of movement between segments. One limitation is that muscle activities show variability between subjects. There exists a range of solutions for performing a movement task; the optimization routines, however, usually end up with one optimal solution for muscle forces.

The adaptation of bipedal locomotion must be viewed beyond optimization for certain obstacle size in a pathway. Adaptation can be viewed as the ability to perform an appropriate (not necessarily optimal) response to a new condition. Thus, an adaptive model must keep several venues open for further expansion and inclusion of other necessary behaviors, having the ability to add new layers of control to its existing ones. The design and simulation of adaptive models have attracted more research energy over the last decade. However, very little work has been dedicated to developing such models for understanding human locomotion.

The other theme in this thesis is to understand the strategies used for the human adaptation when stepping over the obstacles. Intuitively, we tend to think of people flexing their swinging limb's knee and hip to achieve more toe elevation when stepping over higher obstacles. However, recent experiments show that the strategy of elevating the swing hip is more correlated to the obstacle height, than the former two strategies. Does this observed phenomena have any mechanical relevance? How is it produced in humans? How does it compare to other strategies? The presented work has exhausted various modelling techniques to gain some insights to these questions.

1.2 Thesis Organization

The models presented vary in levels of complexity (e.g., from 2-D to 3-D). The models proceed from the skeletal system inwards. The skeletal system is modelled first (chapters 2 and 3), muscles are added in chapter 5, and control systems are added in chapters 6 and 7. Thus, each chapter is a step taken towards the development of a neuro-musculo-skeletal model of human locomotion.

Each chapter deals with a specific phase of this work. Therefore, each chapter includes its own literature survey, method, results, and discussion.

Chapter 2 describes the formulation of a planar biomechanical link-segment model and how it is used to study the role of active torques and forces, and intersegmental dynamics during the swing phase of locomotion over level ground and obstacles. The material in this chapter was presented at the 8th biennial conference of the Canadian Society of Biomechanics, Calgary (1994).

Chapter 3 synthesizes the problem of walking over obstacles through the development of 3-D models of the swing and double support phases of locomotion. The models are based on experiments conducted while human subjects stepped over obstacles. The major focus of the synthesis approach is to understand the effects of hip elevation on the limb trajectory. The material in this chapter was presented at the 9th biennial conference of the Canadian Society of Biomechanics, Burnaby, B.C.(1996).

Chapter 4 describes a methodology that simplifies the use of Lagrangian multipliers for a multibody dynamical system with nonholonomic constraints. The method is applied to formulate the link-segment models used for simulation of gait. The material in this chapter was presented at the 18th annual conference of the IEEE Engineering in Medicine and Biology Society, Amsterdam (1996).

Chapter 5 presents numerical optimization approaches for investigating the objectives the CNS may use to produce a desired limb trajectory over an obstacle. As well, the method determines the active controls required when an obstacle is encountered at various locations during the swing phase of locomotion. The material in this chapter

is accepted for publication in the IEEE Transactions on Rehabilitation Engineering, and was also presented in the 17th annual conference of the IEEE Engineering in Medicine and Biology Society, Montreal (1995).

Chapter 6 describes a model developed to address the problem of learning and adaptation in a novice locomotor. It combines neural network models, fuzzy linguistic control, genetic optimization, and reinforcement learning in order to develop a robust model of learning and adaptation. This model is also used to ascertain the level of active control necessary for stepping over obstacles.

While previous chapters considered proactive control (planning the movement before encountering the obstacle) of gait, the model developed in Chapter 7 looks at the reactive control strategies for recovering from a trip over an obstacle. The material in this chapter was presented in the Neural Control of Movement meeting, Mexico (1997).

Finally, chapter 8 summarizes the contributions of this thesis. It also points out limitations of this work and future directions that this research should take to move towards a better understanding and modelling of the adaptation in bipedal locomotion.

Chapter 2

The Role of Active Torques and Forces and Intersegmental Dynamics in the Control of the Swing Phase of Locomotion

A biomechanical model is developed to study the role of active torques and forces and intersegmental dynamics while walking over level ground and uneven terrain. The simulation results clearly show that the locomotor control system exploits the mechanical interactions between segments to simplify control of the swing phase of locomotion. Two major findings are: (a) while walking over level ground, there are no initial conditions at toe-off that can produce a swing phase that provides adequate ground clearance and stable landing, although minimal active control exerted at the ankle joint is sufficient to achieve a *normal* swing phase. This suggests that the control system utilizes the passive mechanical interactions between segments to reduce the energy cost of this movement. (b) Obstacle avoidance strategies used by subjects to elevate the limb are most economical in terms of energy cost, while ensuring stable landing. Specifically, translational energy applied at the hip joint provides a given toe elevation for minimal energy cost, but severely compromises subsequent landing.

This strategy is most effective when it is initiated during the double support phase. In addition, contributions of intersegmental dynamics are greater when active (flexor) control is implemented at the knee joint compared to control at the hip joint. This work shows the usefulness of modelling to provide insights into the locomotor control system.

2.1 Introduction

Knowledge of the plant is essential for the development of a control system. From an engineering perspective, the control system has to account for the limitations of the plant and exploit the desirable features of the plant to simplify the control. Researchers studying the control of movement have begun to examine the contributions of the effector system dynamics to the observed control strategies. Bernstein [10] in his seminal work clearly stressed the need for studying the contributions of the passive forces and moments to the final expression of movement, arguing that skilled movements exploited these passive forces to control movements simply and efficiently.

The dominant contribution of passive forces to the pendular motion of the swing limb is well demonstrated by the dynamic walking machine of McGeer [51] which walked and balanced with sole gravitational effect provided by the slope of the terrain without any active control. Research has shown the similarity of the swing phase limb trajectory to that of compound pendular motion purely under gravitational force (Mochon and McMahon [53, 54]). Normal swing motion, as reflected in swing times, is possible under gravitational force only without any need for active muscle involvement. However, in their model the foot was rigidly attached to the distal link. Mena, Mansour, and Simon [52] presented a three degree of freedom model with a normal hip trajectory. Their model included the foot of the swinging limb. They concluded that active muscle control at the ankle joint is required to generate a normal swing. We extend the work of these previous studies by performing a dimensional search analysis to identify if there is any set of initial conditions, resulting from active

muscle control during the double support phase, that can produce a normal swing phase motion over level ground. To adequately assess the swing phase motion, we develop a number of criteria.

Next, we address the role of active muscle control and intersegmental dynamics when walking over obstacles in the travel path. Zernicke et al. [90] separated the torques due to gravity, generalized muscle forces (active muscle contraction and passive deformation of muscle and other tissues) and motion dependent torques. They compared the changes in these torque components from walking to running, and concluded that the role of generalized muscle forces become more predominant during running than normal walking. Empirical studies on obstacle avoidance in humans have shown contribution of specific groups of muscle activity during the double support phase and the swing phase [50, 60, 63]. How does such an increase in the role of active torques and forces affect the intersegmental dynamics? McFadyen and Winter [50] showed that while going over obstacles "additional knee and hip flexion is achieved not by a higher hip pull-off power but rather by reduced knee extensor activity during late stance thus allowing the knee to flex more; and further augmented by an active knee flexor moment immediately after toe-off". Patla et al. [62] provided experimental evidence that translational power at the hip joint, in addition to the knee joint rotational power, is a major contributor to limb elevation for obstacle avoidance. This suggests that muscle action in the stance limb can cause flexion of the swing limb. In this work, we use the model to understand the reasons behind the observed strategies for achieving limb elevation. We also explore the influence of timing of the hip joint reaction force (which is responsible for the hip translational power) on limb elevation.

2.2 The Biomechanical Model and Assumptions

A four degree of freedom model with added hip elevation capability was developed for this study. The model consists of four links representing the thigh, the leg, the

foot of the swing leg, and the stance leg (Figure 2.1). To simplify the equations of motion, the following assumptions were made: (a) motion was primarily restricted in the sagittal plane; (b) joints were modelled as hinge joints; and (c) for each segment the mass distribution was assumed uniform. Anthropometric data were taken from Dempster provided in Winter [83]. The Lagrangian method was used to derive the equations of motion. The general form of the equations are described in Appendices A and B. The simultaneous numerical integration of these equations was performed using a variable step size 4th and 5th order Runge-Kutta-Fehlberg method.

The uni-directional non-linear dampers (Figure 2.1) model the anatomical constraints (knee hyperextension, ankle plantarflexion, and ankle dorsiflexion). The equations defining the damper dynamics (e.g. knee hyperextension) are :

$$M_k = \frac{A}{1 + exp((\theta_3 - \theta_2)S)} \times (\dot{\theta}_3 - \dot{\theta}_2) \tag{2.1}$$

where:

$$A = \begin{cases} 0 & if\ \dot{\theta}_3 \leq \dot{\theta}_2 \\ 100 & if\ \dot{\theta}_3 > \dot{\theta}_2 \end{cases} \tag{2.2}$$

The value of S was chosen to ensure the damper becomes active close to full knee extension (typically $S = -100$).

The uni-directional feature ensures that the movement is limited only when moving toward anatomical limits, without locking the segment at that limit. Damping becomes significant only at joint angles close to the anatomical limits, and the slope S can be adjusted to avoid impact at the joint limits. Such a damper has the unique feature of modelling the inelastic collision at the joint limits, which is more representative of the physical condition than an elastic collision, which will generate oscillatory motion due to the spring. The limited time length of the simulation and the significant joint limit sensitive amplitude of the damping force generated, guarantee that the joint angle will never exceed the joint limit.

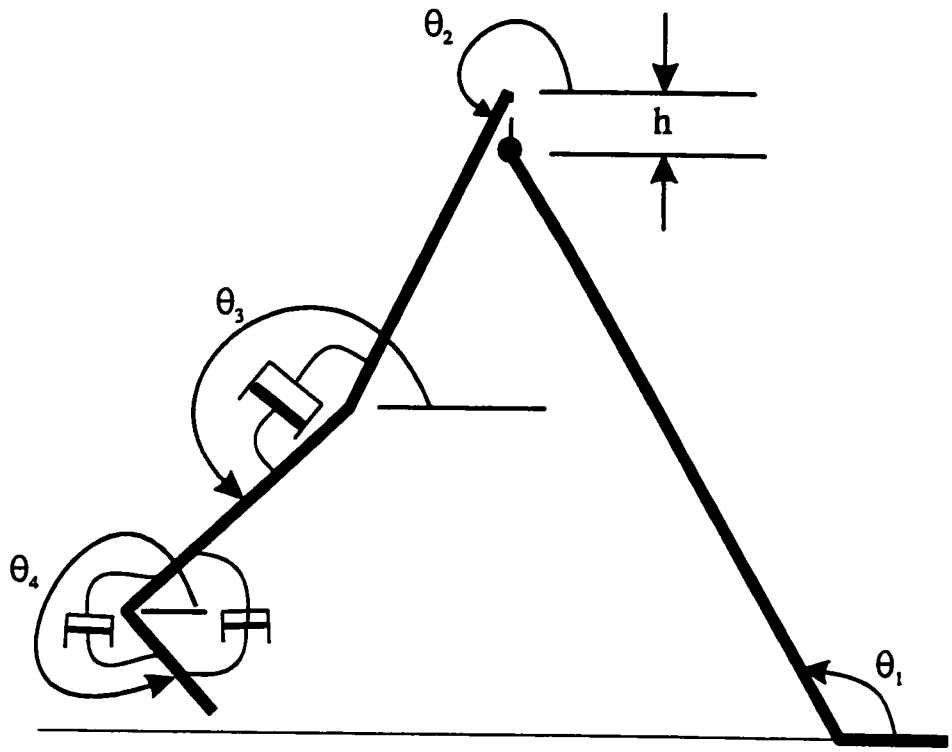

Figure 2.1: **A schematic diagram showing a 4 degree of freedom model which includes the segments for the swing limb (thigh, leg and foot) and one segment for the stance limb. Uni-directional non-linear dampers are used to model anatomical constraints. Hip hiking capability is included.**

Each possible swing was determined by a set of seven initial conditions (three initial angles and four initial angular velocities). The eighth parameter (the stance leg angular displacement) was determined from the kinematic condition at toe-off. To establish a basis for comparison of results, we started with a set of experimental initial conditions during toe-off [83] and varied the parameters around this point. The initial conditions were adjusted from the experimental values to compensate for the assumption that the stance limb was considered as a rigid link.

2.3 Control of Swing Limb Trajectory Over Level Ground

Before proceeding with the simulations, it is necessary to define the characteristics of a *successful* swing. When performing a normal swing over level ground, five desired objectives should be accomplished (Figure 2.2). For each desired objective, control parameters can be defined. Maintaining all of these control parameters within an acceptable range will then ensure the performance of a successful swing. Figure 2.2 summarizes the desired objectives and the corresponding control parameters. Note that the acceptable range is usually defined by the higher and lower limits. We have proposed these limits only as a basis for comparison. Foot/floor clearance must be greater than zero to avoid tripping. The upper bound for toe elevation is chosen to be 1.5 times the average observed in subjects [82]. Stable landing is achieved based on two criteria: first, the center of mass at landing is posterior to the swing toe; second, the velocity of the center of mass is less than the average observed during the swing phase (1.4 m/s from reference [82]). To minimize slipping, we have chosen to limit the velocity of the foot at landing to 1.5 times its average experimental value (.4 m/s from reference [82]). A step length within 20observed for normal walking speeds (from reference [82]) is chosen to be an acceptable range. Maintaining all of these control parameters within an acceptable range will then ensure the performance of a successful swing. Now we can address one of the questions posed in the introduction.

Desired Objective	Control Parameter	Acceptable Range
Avoid Tripping	Foot/floor clearance	$Y_{toe} > 0$
Minimize Potential Energy	Minimize max. Y_{toe}	$Y_{toe\_max} < 1.5 \times 0.13^{*}$
Achieve Stable Landing	Foot anterior to C.M. Upper bound for $V_{C.M.}$	$X_{toe} - X_{C.M.} > 0$ $V_{C.M.} < 1.5 \times 1.4^{*}$
Minimize Slipping	Upper bound for V_{foot} at landing	$V_{foot} < 1.5 \times 0.4^{*}$
Cover Reasonable Distance/Step	Normal step length	Within 20% of the step length of 0.5 meters

*Experimental values

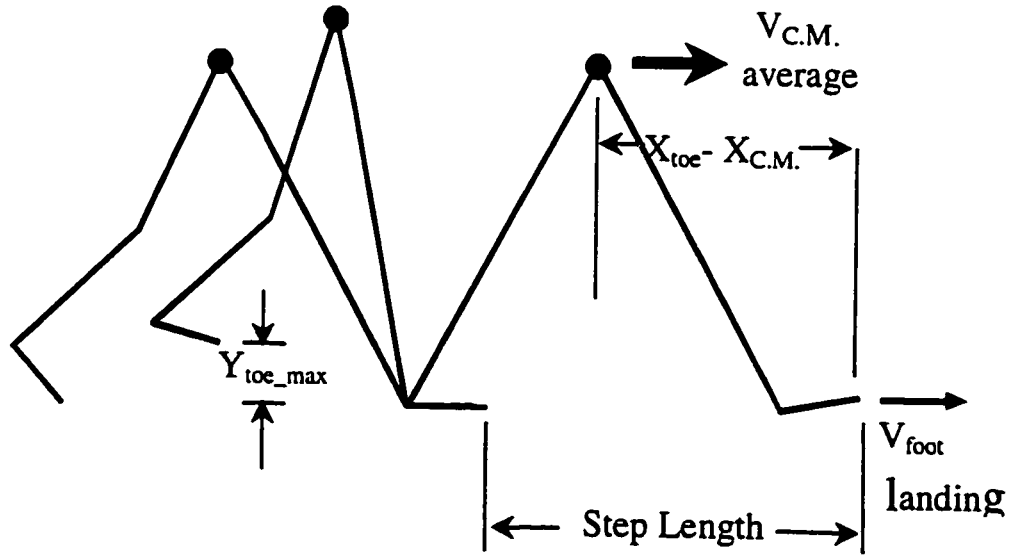

Figure 2.2: **A schematic diagram identifying objectives that have to be met for a successful swing phase along with the relevant control parameters.**

2.3.1 Is Any Set of Initial Conditions at Toe-off Sufficient for Performing a "Normal" Swing Under Gravitational Force Alone?

Simulation Procedure

Once we established key control parameters for evaluating a *normal* swing, a full dimensional search strategy was developed to find a *set* of initial conditions which maintain all the control parameters within the acceptable range, and hence, does not violate the desired objectives. Note that a full dimensional search not only varies each initial condition independently, but also varies all combinations of initial conditions, and checks the results with the acceptable range of values for the control parameters.

However, to reduce the required simulation effort, sets of pre-factorial simulations were performed to identify parameter ranges from within which acceptable solutions would be possible, and to identify trends between parameter variations and the resultant swing trajectory. Amongst others, these pre-factorial studies provided range limits on the ankle angular velocities in both limbs. For example, $V_{C.M.}$ was found to be significantly dependent on the stance ankle angular velocity. Likewise, landing with the heel within acceptable control parameter bounds required an initial dorsiflexor activity on the swing limb's ankle. These pre-factorial results enabled the search space to be reduced to a three level investigation for ankle angular velocities, and five levels for the three angular displacements (thigh, knee and ankle). However, 20 levels were considered for the most significant variables (the thigh and knee angular velocities). These ranges are summarized in Table 2.1.

Results & Discussion

It is clear that there are no initial conditions at toe-off, which can produce a normal swing phase in the absence of any active muscle forces. A select group of results from the simulation is summarized in Table 2.2 (the corresponding stick figures shown in

Variables	Range of Variation	Levels
θ_2 (deg)	250 to 280	3
θ_3 (deg)	225 to 255	3
θ_4 (deg)	285 to 315	3
θ'_1 (rad/s)	-1 to -3	5
θ'_2 (rad/s)	0 to 5	20
θ'_3 (rad/s)	-4 to 1	20
θ'_4 (rad/s)	0 to 5	3

Table 2.1: **The parameter ranges and the levels of investigation for each parameter during simulation for swing phase over level ground under gravitational force alone. The various terms are defined in captions for Figures 2.1 and 2.2.**

Figure 2.3) to guide our discussion. When initial conditions are set close to experimental values [83], the swing limb tends to land with the toe. To avoid this situation, a dorsi flexor initial velocity (as opposed to a plantar flexor initial velocity) was applied. Even with a relatively high dorsi flexor initial angular velocity, landing with the heel only occurs when a knee *extensor* velocity instead of the experimentally observed knee flexor velocity is applied (row 7). In such a situation, the minimal foot/floor clearance would be the limiting factor. To achieve a normal swing, these should be combined with higher stance leg velocities (row 7). However, higher stance leg velocities would result in higher hip velocities, which are not desirable. As well, independent increase of the stance leg angular velocity will increase both toe clearance and hip velocity, both undesirable (row 2). Increasing the angular velocity of the swing thigh leads to larger landing velocities with the toe (row 5); however, decreasing this velocity leads the body to an unstable landing (row 4). The latter effect was observed when the backward leg velocity was increased (row 6).

Also notable from Table 2.2 is the very different values of the foot velocity at landing (column 7) from that of normal values (except for row 3 which refers to a successful swing). One major difference is that in row 3 the knee reached full extension (see also Figure 2.3). Therefore an energy transfer form the swing leg to thigh occurred (through the damper) which resulted in arresting the leg velocity and significantly reducing it. Another reason for the variability observed in the landing foot velocity was that the swing foot segment was the last link in the link segment chain. Therefore, any variation in the links' initial velocities would alter the swing foot velocity.

In summary, the results of the simulation suggest that reliance on purely passive dynamics may allow the subject to clear the ground, but the step length, landing velocity, and posture are compromised. This would certainly affect the execution of the next step. Therefore, there is a need for some active control during the swing phase. As previously noted, the main problem in achieving a satisfactory swing arises from the inability of the foot to clear the ground during its free pendular motion. As a

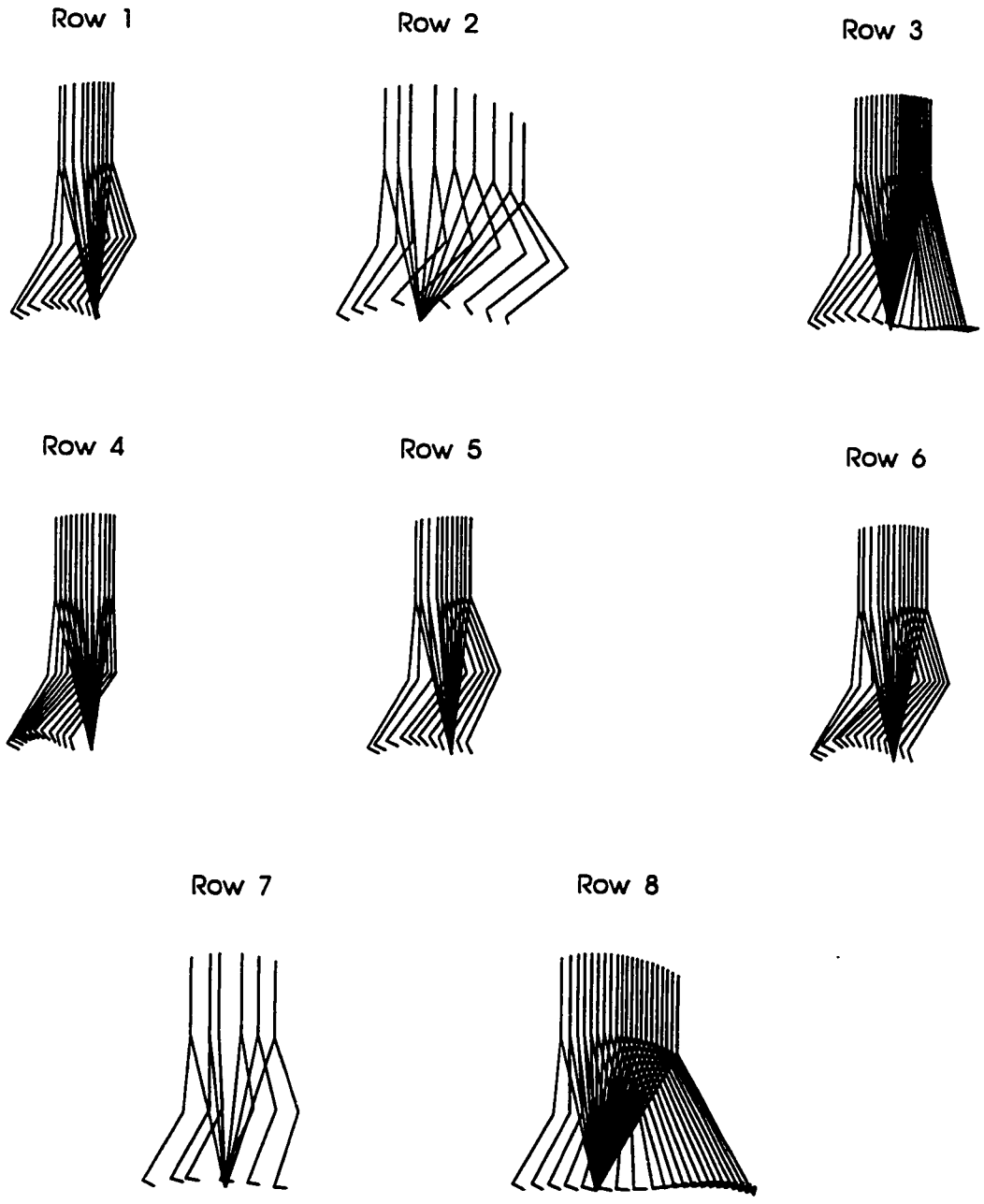

Figure 2.3: **Stick diagrams for the various scenarios shown in Table 2.2. The time interval between the two consecutive stick diagrams is 0.02 seconds.**

$\theta_1 = 103.7$ $\theta_2 = 265.4$ $\theta_3 = 240.2$ $\theta_4 = 300.0$ (deg.) (*): constrained ankle motion				Stride Length (m)	Max. Y_{toe} (m)	V_{foot} landing (m/s)	X_{toe} -$X_{C.M}$ (m)	$V_{C.M}$ Average (m/s)	Landed on
θ'_1 (rad/s)	θ'_2 (rad/s)	θ'_3 (rad/s)	θ'_4 (rad/s)	Normal Values (Winter, 1992)					
				1.00	.13	.4	.3	1.4	heel
				Simulation Results					
-1.5	2.5	-2.5	5.0	0.58	0.07	2.81	-0.03	1.41	toe
-3	2.5	-2.5	5.0	1.01	0.11	3.07	-0.11	2.86	toe
-1	2.5	-2.5	-2.5*	1.06	0.08	0.19	0.34	0.89	heel
-1.5	1	-2.5	5.0	0.39	0.08	2.09	-0.25	1.41	toe
-1.5	3	-2.5	5.0	0.68	0.06	3.15	0.06	1.42	toe
-1.5	2.5	-3.5	5.0	0.62	0.10	2.61	-0.09	1.42	toe
-3.0	2.5	0.5	5.0	0.84	0.04	4.23	0.13	2.44	heel
-1.5	2.5	0.5	0.5*	1.63	0.06	4.48	0.45	1.40	heel

Table 2.2: **Simulation results for swing phase over level ground under gravitational force alone for a range of initial conditions at toe-off. The various terms are defined in captions for Figures 2.1 and 2.2. The corresponding stick Diagrams are shown in Figure 2.3.**

solution to this problem, a dorsi flexor initial velocity was applied to the ankle. Such a solution is not only unrealistic, but also it still does not generate a normal swing. Empirical data suggest active dorsiflexor control at the ankle joint in addition to hip and knee flexor control at the end of the swing phase [83]. We applied a moment to the ankle to maintain it in a neutral position throughout the course of the swing phase, and examined the control parameters defined before. To maintain the ankle at a constant angle during the course of the swing, an extra constraint was introduced to the system. The augmented method [1] was used to include such a constraint to the set of equations. This method utilizes the equations of motion, together with the differentiated form of the constrained equations to form a set of (# DOF + # Constraints) second order differential equations to be integrated simultaneously.

The simulation results show that the model with this constraint can perform a normal swing for some range of initial conditions (see Figure 2.3 and row 3 of Table 2.2). This result is in agreement with the work of Mochon and McMahon [53] who showed a three degree of freedom model can perform a normal swing. Since the mass of the foot is relatively small, it does not have a significant intersegmental influence on other segments. Therefore, for performing a normal swing, an active moment applied at the ankle combined with free pendular motion of the other segments is sufficient. To understand the reason for more proximal muscle involvement at the end of the swing phase, we would have to include the upper body in our model.

In the above discussion, while the dimensional search demonstrates the need for active control of the ankle, it does not directly imply that no combination of segmental properties exists that can provide a solution that satisfies all the criteria. However, the addition of more detail (such as segmental initial accelerations and segmental properties) to the search parameters, will greatly increase the required simulation effort. Utilizing optimization was deemed to be a better approach.

Our point here is that on observing trends in the solution space that would seem to indicate that no parameter combination will produce the required result, it is reasonable to apply active control. The introduction of active control will widen the

range of variables (initial conditions at toe-off, and segment properties) that result in a successful swing, hence increasing the robustness of the strategy.

2.4 Control of the Swing Limb Trajectory Over Obstacles During Locomotion

Next we focus our modelling effort to the problem of how a change in terrain conditions, specifically existence of obstacles, would change the locomotor swing pattern. Specifically, we address the following questions: a) Why is the translational energy applied at the hip joint a dominant contributor to limb altitude control?; b) Should a vertical force at the hip joint be applied starting in the double support phase, or only during the swing phase to achieve higher limb elevation?; and c) Why is active (flexor) control at the knee joint and not at the hip joint preferred to elevate the limb? Before we proceed to answer these questions, we need to revise the criteria for a successful swing. Instead of minimum toe clearance, we must include maximum toe elevation and the spatial (with respect to toe-off) location of this maximum toe elevation.

2.4.1 Why is Translational Energy Applied at the Hip Joint a Dominant Contributor to Limb Altitude Control?

Patla et al. [62] have shown that during the swing phase, vertical hip translational power and rotational knee power are major contributors to the limb elevation during obstacle avoidance. They found that the integral of the vertical hip translational power and the knee rotational power (from toe-off to the time the limb was over the obstacle) were highly correlated with obstacle height (Figure 2.4). We have extended our model to gain insight into these observed strategies for limb elevation.

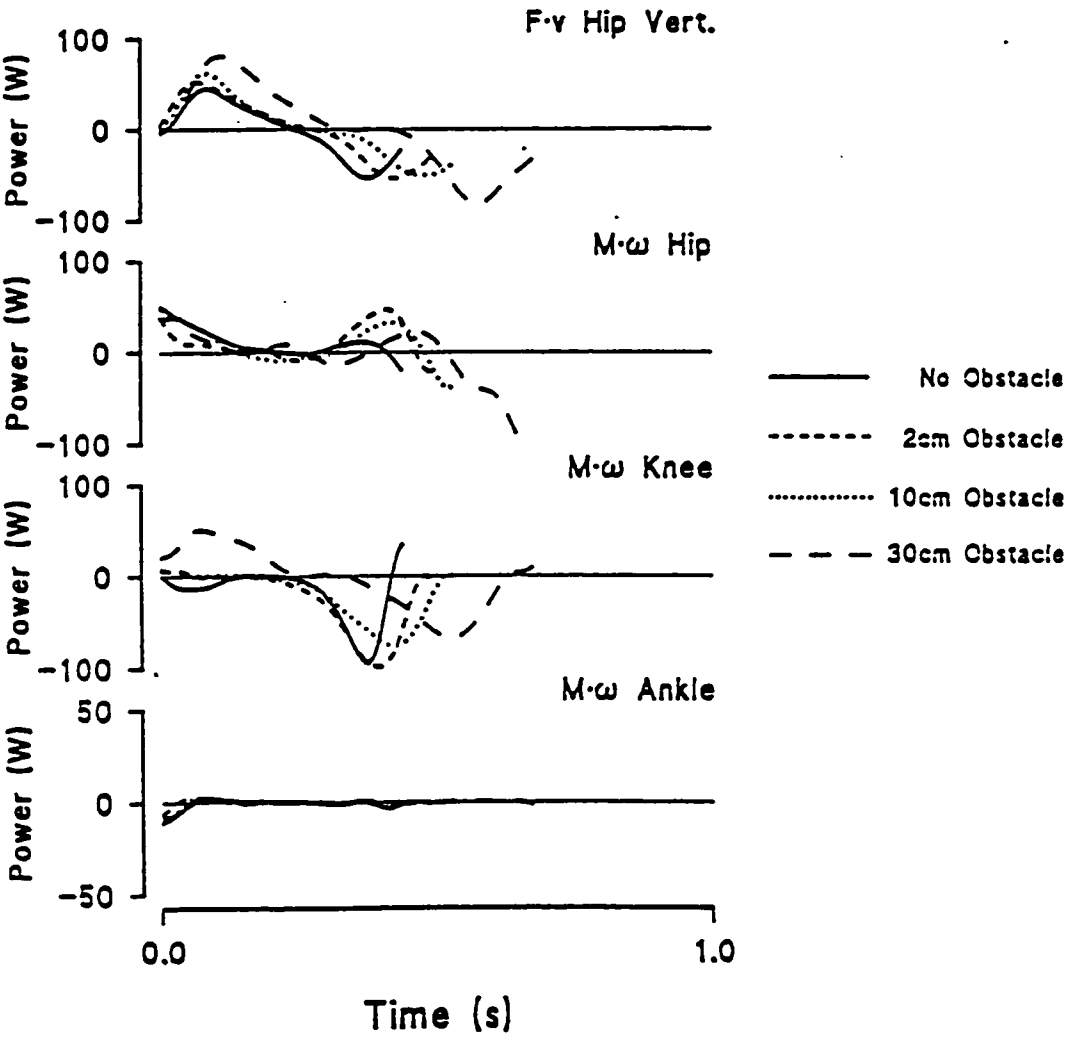

Figure 2.4: **Power profiles (translational power at the hip joint - F.v; Rotational power at the hip, knee and ankle joint) from toe-off to subsequent foot contact over different height obstacles (from [62]).**

Simulation Procedure

The effects of increasing the knee flexor torque, the hip flexor torque, and hip vertical displacement, applied independently, on limb elevation were examined. Hip vertical displacement was modelled as a sinusoidal vertical hip movement, $h(t) = h_0.sin(\omega_s.t)$, with respect to the stance leg position. The desired magnitude of the hip elevation was therefore h_0, while $\omega_s.t$ represents the complete swing phase cycle. It was also assumed that the weight of the point mass (representing the weights of the head, arms and trunk) was shifted over the stance leg. Rotational and translational energies were calculated for hip/knee flexor torques and the vertical force resulting from the vertical hip elevation respectively. The translational energy calculated in this way does not consider the energy required to shift the pelvis or any necessary work on the head, arms, and trunk (HAT). The justification for this assumption is that when the weight of the HAT is shifted over the stance leg, the amount of work required to tilt the pelvis is negligible when compared to that required to elevate the swing limb. A more detailed investigation would require a more realistic (3-D) model, which is outside the scope of the present work.

Results & Discussion

The contributions of translational and rotational joint energies to toe elevation are shown in Figure 2.5. For a given amount of energy, translational energy applied at the hip joint results in the highest toe elevation, followed by rotational joint energy applied at the knee, while rotational energy applied at the hip joint results in the smallest increase in toe elevation. As well, the rate of increase in toe elevation follows the same trend (Figure 2.5). This explains the dominating role of these two strategies for limb elevation. We conclude that in agreement with experimental observations [62], translational energy applied at the hip and rotational energy applied at the knee can provide most efficient limb elevation for obstacle avoidance. The evident difference between the required knee rotational energy versus the hip translational energy also indicates that even when the work required to tilt the pelvis is added, the

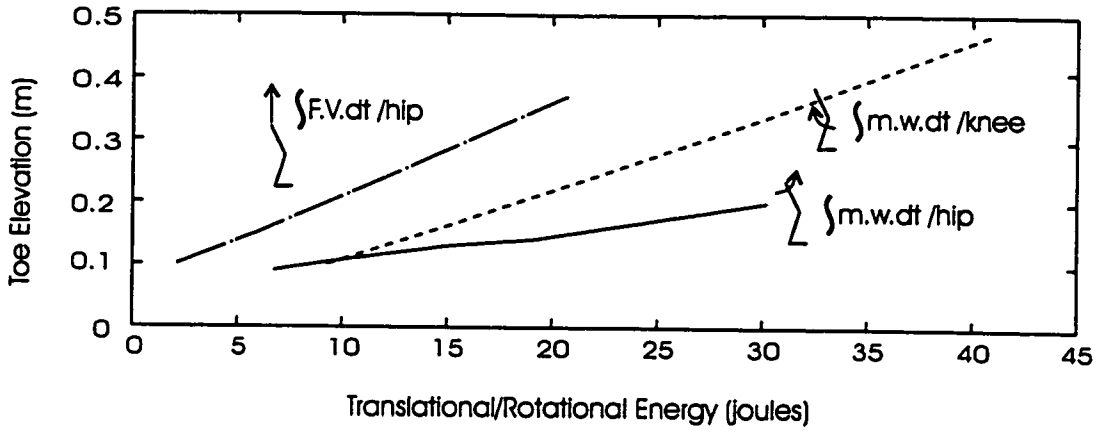

Figure 2.5: **Plots showing toe elevation as a function of translational energy applied at the hip joint, rotational energy applied at the knee, and the hip joint. Note that these results were obtained by applying each of three energies to the model independently.**

hip translational energy remains more efficient than the other methods.

A natural question resulting from these simulation results is as follows: If translational energy applied at the hip joint is most efficient, then why do subjects also use active control at the knee joint during obstacle avoidance [62, 50]? The answer to this question lies in the landing velocities and posture following obstacle avoidance when different strategies are used (Table 2.3). It is clear that translational energy applied at the hip joint may result in high toe elevation, but subsequent landing is severely compromised. In particular, the body centre of mass is very close, and in some cases anterior to the toe at landing (Column 6 in Table 2.3). Therefore, observed obstacle avoidance strategies represent a compromise between efficient limb elevation and stable landing.

$\theta_1 = 103.7$ $\theta_2 = 265.4$ $\theta_3 = 240.2$ $\theta_4 = 300.0$ (deg.)	Stride Length (m)	Max. Y_{toe} (m)	X-pos. of Max. Y_{toe} (m)	V_{toe} Landing (Horz.) (m/s)	V_{toe} Landing (Vert.) (m/s)	X_{toe} - X_{CM} (m)	V_{CM} Avrg. (Horz.) (m/s)	Swing Time (s)	Landed on
Increasing Hip Flexor Torque from 5.0 (N.m) to 25.0 (N.m)	0.83	0.08	0.38	3.29	-0.77	0.14	1.41	0.33	toe
	1.08	0.10	0.45	3.54	-0.64	0.30	1.42	0.39	toe
	1.40	0.13	0.55	2.35	-0.46	0.50	1.43	0.48	heel
	1.65	0.16	0.66	1.70	-1.10	0.62	1.45	0.55	heel
	1.85	0.20	0.78	1.50	-1.61	0.72	1.47	0.62	heel
Increasing Knee Flexor Torque From -2.5 (N.m) to -12.5 (N.m)	0.82	0.10	0.39	2.97	-1.06	0.09	1.42	0.36	toe
	0.96	0.16	0.47	2.86	-1.53	0.11	1.44	0.44	toe
	1.06	0.24	0.53	2.60	-2.10	0.10	1.46	0.51	toe
	1.11	0.34	0.60	2.16	-2.60	0.03	1.47	0.58	toe
	1.15	0.47	0.66	1.59	-3.22	-.08	1.49	0.68	toe
Increasing Hip Hiking from 2.0 (cm) to 8.0 (cm)	0.82	0.10	0.30	2.95	-1.06	0.08	1.43	0.36	toe
	0.91	0.15	0.47	2.73	-1.53	0.07	1.45	0.43	toe
	1.00	0.24	0.52	2.40	-2.12	0.03	1.47	0.51	toe
	1.08	0.37	0.59	1.89	-2.85	-0.07	1.50	0.62	toe

Table 2.3: **Simulation results for swing phase over obstacles under three different active controls applied independently during the swing phase. The various terms are defined in captions for Figures 2.1 and 2.2.**

2.4.2 What Phase is Most Efficient for Applying Hip Translational Force During Obstacle Avoidance?

Simulation Procedure

The non-zero first derivative of the vertical hip displacement, $h(t) = h_0.sin(\omega_s.t)$ at $t = 0$, implies the existence of an initial hip vertical velocity at toe-off. This initial condition indicates that a vertical force is applied during the double support phase by muscles in the stance limb. The alternative scenario is that hip displacement

starts with zero vertical velocity at toe-off, thus representing the condition when vertical hip force is applied during the swing phase only. To model this situation, the hip elevation term can be represented at $h(t) = h_0.(1 - cos(2\omega_s.t))/2$, where $0 <= \omega_s.t <= \pi$ again represents the swing phase cycle. Both formulae define half a cycle sinusoidal hip elevation. As well, in the first derivatives of those two formulae: $\dot{h}(t) = h_0.\omega_s.cos(\omega_s.t))$ and $\dot{h}(t) = h_0.\omega_s.sin(2.\omega_s.t))$, the velocity amplitudes $(h_0.\omega_s)$ are the same.

Results and Discussion

To gain some insight about the effect of the phase of application of the hip elevation, the magnitude of hip elevation (h_0) versus the maximum resulting toe elevation is shown in Figure 2.6. Note that the other experimental initial conditions were similar for both cases and that no torque pulse on knee or hip was applied. As shown in Figure 2.6, applying a vertical force to hip starting during the double support phase results in higher toe elevation than applying this force only during the swing phase of locomotion. These results are in agreement with observed changes in locomotor patterns (muscle activity, kinetics) for obstacle avoidance prior to the onset of the swing phase [50, 60, 63].

These results can be directly observed from the governing equations of motion: the translational (first and second) terms in the right hand side of the equations for M1 to M4 (Appendicies A and B) have the same sign. In the conventional sense, the effect of the gravitational term will be to lower the limbs during swing. Now if $\ddot{h}$ has a negative sign, these first two terms will oppose each other. In other words, by shaping and reducing the gravitational terms, the hip translational term will be fully capable of controlling the limb elevation. However, to produce such an effect, it is necessary to introduce an initial upward translational velocity to the hip, which will be caused by the relevant muscle forces prior to toe-off. The first equation for hip elevation $(h(t) = h_0.sin(\omega_s.t))$ produces such a situation, and the results shown in Figure 2.6 clearly demonstrate the effect.

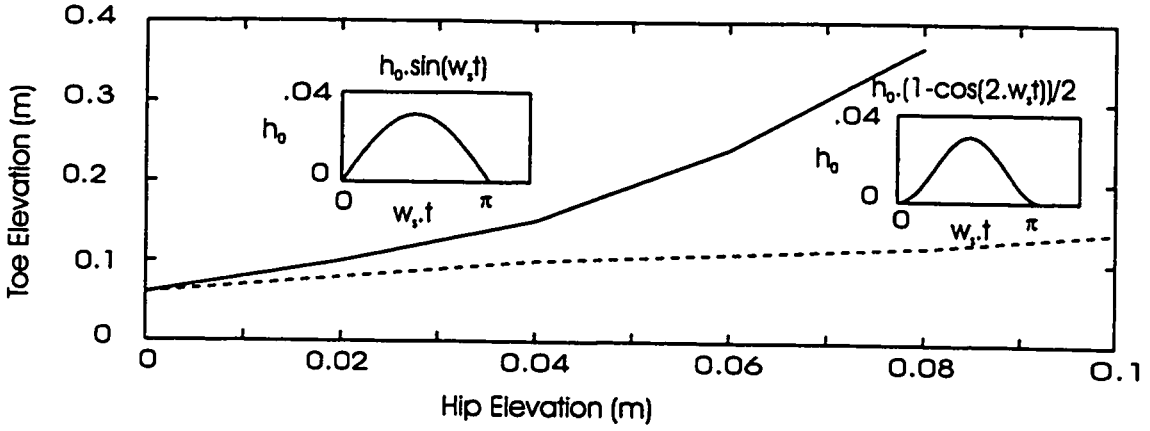

Figure 2.6: **Plots showing toe elevation as a function of hip elevation translational energy applied at the hip joint when the hip elevation was initiated during the double support phase and when the hip elevation was applied only during the swing phase. The corresponding functions for a typical 3 cm hip elevation are also shown.**

Even a simplified planar model used in this study is able to provide insights into the experimental observations (Figure 2.4) [62, 82]. Determination of sources of hip elevation will of course require more complex models.

2.4.3 Why is Active Flexor Control at the Knee Joint Preferred Over Control at the Hip Joint to Achieve Limb Elevation?

Simulation Procedure

Experimentally observed initial conditions were applied to the link segment model. Flexor torque pulses were applied at the hip and knee joints. To avoid the foot from plantar flexing during the swing phase, two dorsi flexor pulses were applied to the ankle joint. The first pulse started at the beginning of the swing to counteract the plantar flexor velocity during push-off. The second torque pulse was applied at

the point in the swing at which a flexor velocity exists, and the joint angle was 90 degrees (start of plantar flexion), provided it did not interfere with the first torque pulse. While maintaining the same ankle torque pulses, the effect of changing the magnitude of the knee and hip flexor torques, in different combinations were studied.

Results & Discussion

Figure 2.7 illustrates that an increase of the hip flexor torque and the knee flexor torque increase the foot/floor clearances as expected. As shown in Figure 2.7, for the same value of the maximum toe elevation, a lower range of knee flexor torques compared to hip flexor torques is required. This, together with Figure 2.5, confirms that active control at the knee joint is a more efficient strategy for obstacle avoidance and requires less effort than active control at the hip joint. This is in agreement with the experimental results of McFadyen and Winter [50] and Patla et al. [62] showing the predominant contribution of active control about the knee joint during obstacle avoidance. To understand why active control at the knee joint is better than active control at the hip joint, consider the relative intersegmental contributions.

Increasing the hip flexor torque (with no knee torque pulse and two ankle torque pulses) resulted in an increase in knee flexion, although it had a minimal effect on the location of maximum knee flexion (Figure 2.8). Increasing the knee flexor torque resulted in a greater increase in both magnitude and location at which maximum hip flexion occurred (Figure 2.9). These results clearly show that intersegmental contributions are greater when knee flexor torque is applied compared to hip flexor torque.

Furthermore, as knee flexor torque was increased, a backward shift was observed in the location of occurrence of maximum ankle dorsi flexion. In contrast, increasing the hip flexor torque results in a slight forward shift of the location of maximum ankle dorsi flexion. However, the onset of the second dorsi flexor torque varied minimally with change in the magnitude of hip and knee torques. Therefore such shifts are the results of longer swing lengths due to greater knee flexion but lesser hip flexion. The

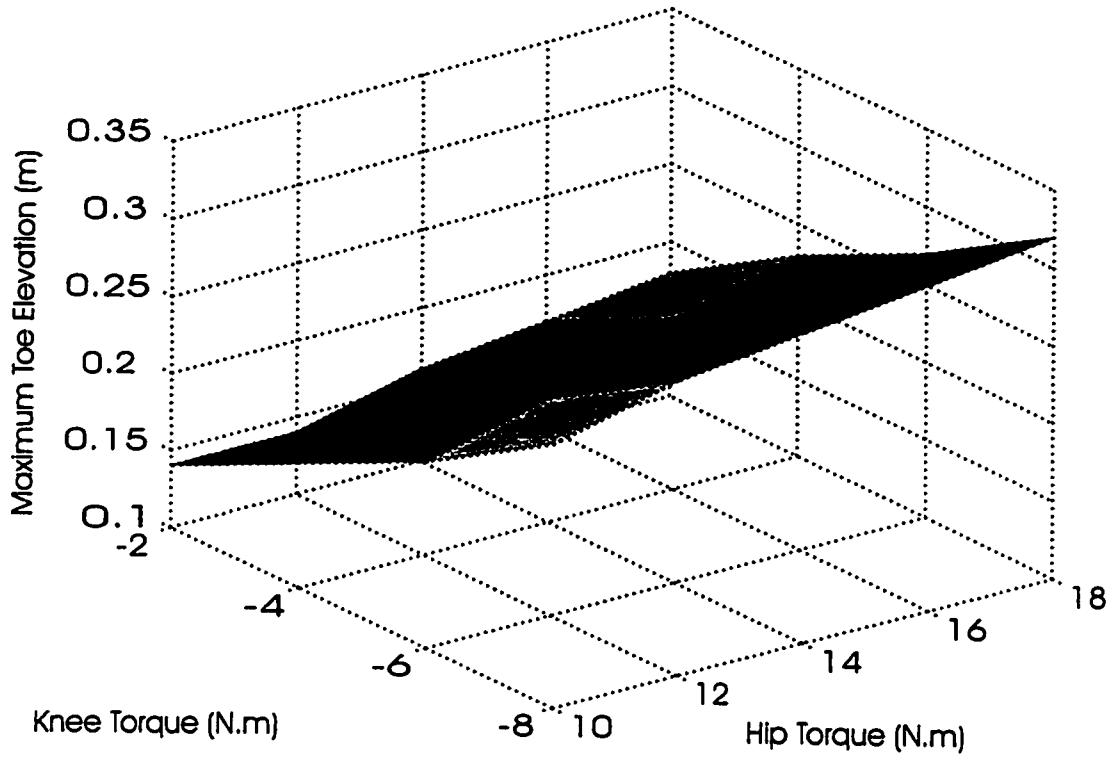

Figure 2.7: **A surface plot showing maximum toe elevation achieved for various combination of knee and hip flexor torques. Note the convention: counterclockwise torque is +ve.**

results (Figure 2.9) clearly show that the knee flexor torque has a definite effect on increasing the swing length.

In summary, the lower magnitudes of knee flexor torque required for obstacle avoidance and its greater intersegmental influences, explains why we use this strategy instead of hip flexor torque strategy.

2.5 Conclusions and Future Directions

We proposed that a biomechanical model of the swing phase of locomotion would be useful to understand the role of active torques and forces and intersegmental dynamics during the swing phase of locomotion over level ground and obstacles. Simulations

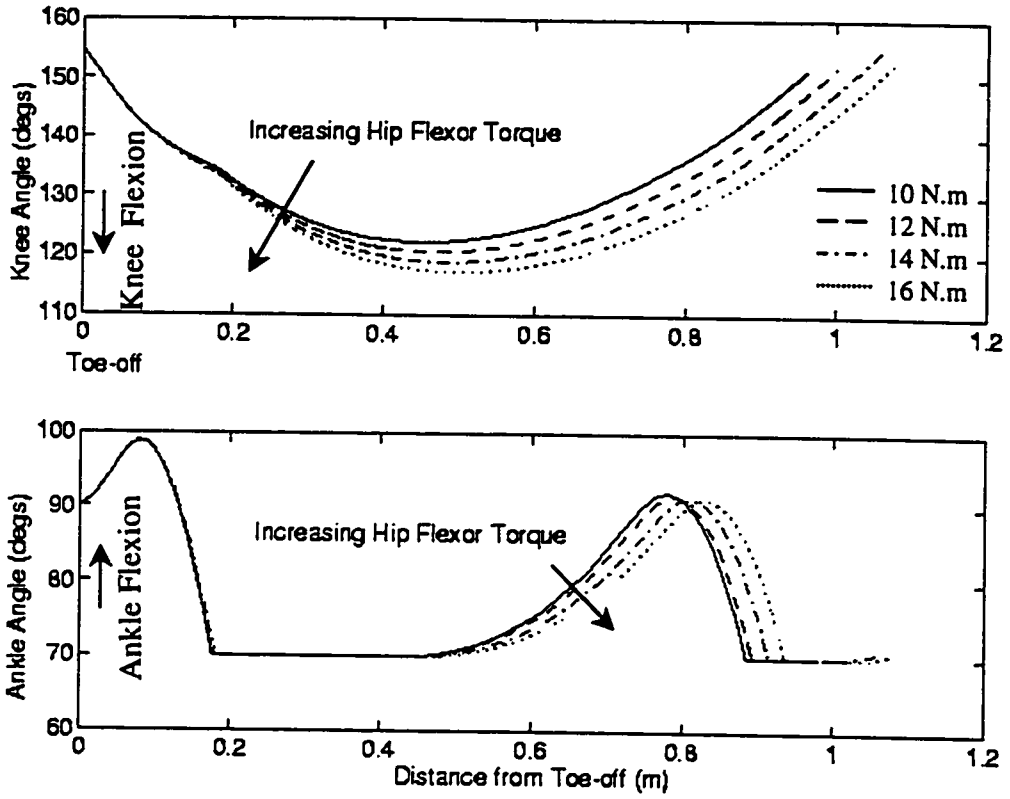

Figure 2.8: **Relative knee and ankle angle profiles as a function of distance from toe-off for different values of applied hip flexor torque.**

using this model have shown that mechanical interactions between segments provide energy efficiency for walking on level ground and stepping over obstacles. It is clear that the control system exploits these features of the effector system to regulate locomotor patterns for different terrains.

Although the proposed model provides some insight on the control of the swing phase of locomotion, many questions remain unanswered. A natural follow-up to this work is empirically identifying how hip elevation is achieved, and using the simulation model to understand the basis for the selection of the strategies. This will require expanding the model to three dimensions, and adding upper limbs.

The choice of control parameters, whether the parameters chosen are complete, and the type of control parameters required when studying the limb trajectory over

obstacles, are other issues that require some method of verification using optimization methods and will be discussed in the next chapter.

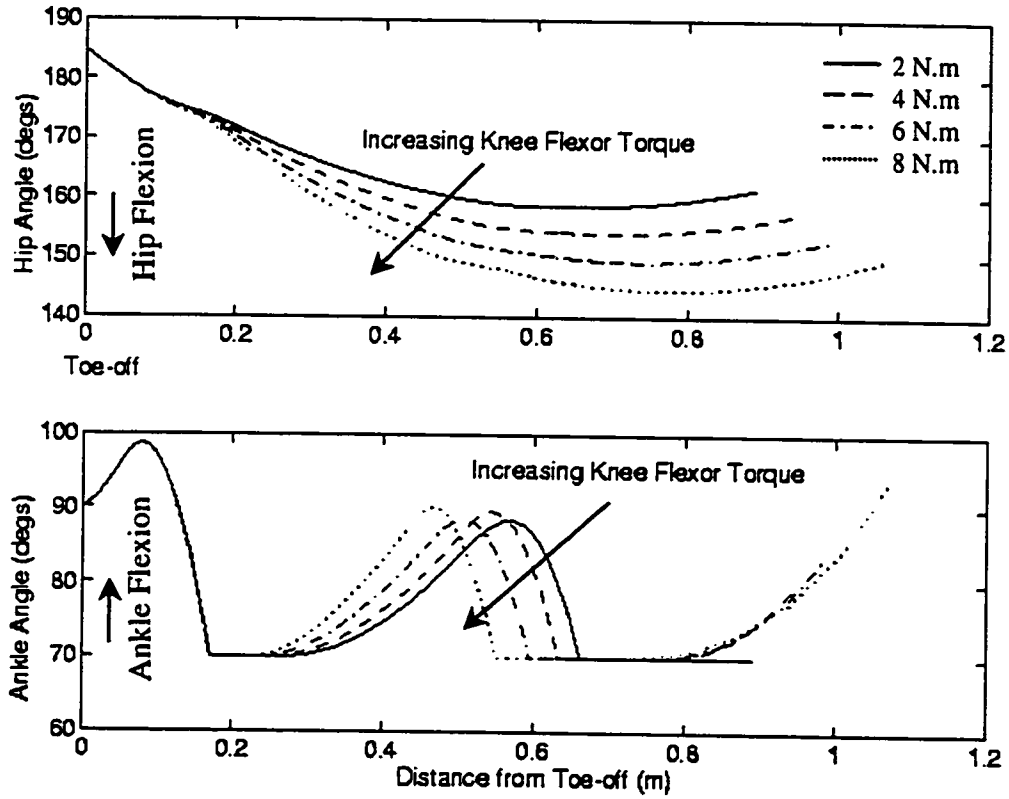

Figure 2.9: **Relative hip and ankle angle profiles as a function of distance from toe-off for different values of applied knee flexor torque.**

Chapter 3

3D Biomechanical Models: Identifying Optimal Hip Elevation Strategies to Control the Swing Limb Trajectory

Recent experimental studies have demonstrated the dominant contribution of translational hip energy to swing toe elevation when stepping over obstacles during bipedal locomotion. In this chapter we investigate potential strategies for elevating the hip using simulation models. The effects of these strategies during both the double support and swing phases on the resulting toe elevation are identified. Results show that hip vertical translation is most effective when resulting from torques and forces initiated during the double support phase. Also found was that the leading limb ankle push-off is the most effective strategy for increasing hip elevation velocity at the start of the swing phase.

3.1 Introduction

Design of prosthesis and rehabilitation of gait amputees are both concerned with the advantages of different strategies for stepping over obstacles. In fact, stepping over obstacles is an integral part of gait evaluation during rehabilitation procedures. The major challenges in the field of bipedal locomotion are the control of balance and stability. Thus while the most significant feature that legged locomotion provides is the ability to step over obstacles, this has attracted relatively little attention in bipedal modelling and gait simulation.

Experimental studies of obstructed gait by McFadyen and Winter [50] concluded that the additional swing limb flexion to step over an obstacle is achieved by a combination of increasing hip pull-off power, reducing knee extensor activity during late stance, followed by active knee flexor moment during the swing phase. Recently Patla and Prentice [61] provided evidence that translational power at the hip joint is the dominant contributor to limb altitude control.

The use of forward solution linkage models for synthesis of normal walking (e.g. Mena et al. [52]; Mochon McMahon [53]; Onyshko and Winter [57]; Pandy and Berme [58]) and paraplegic gait (e.g. Yamaguchi and Zajac [85]) is well established. To investigate the strategies observed when stepping over obstacles, in previous chapter we developed [5] a planar forward solution linkage model and studied the independent effects of knee flexor torque, hip flexor torque, and hip vertical force to swing toe elevation. It was shown that the contribution of hip translational energy to toe elevation is more than the contribution of knee and hip rotational energies. We also applied two sinusoidal trajectory constraints to the hip and showed that higher toe elevations result when the hip vertical force is initiated during the double support phase (prior to the swing limb's toe-off). These results were in agreement with the observed changes in locomotor pattern prior to the onset of the swing phase [63].

These findings suggested that while muscle action in the stance limb can cause flexion of the swing limb, the locomotor pattern during the double support phase has a major influence on observed toe elevation during the swing phase. The first goal

of this work was to identify the most effective available strategies for achieving hip elevation. The second goal was to investigate how changes in locomotor pattern prior to the onset of swing affect toe elevation.

3.2 Methods

3.2.1 Experimental Protocol

The main objective of the experiments was to generate a data-base of kinematics for the modelling technique (the models are described in the next section). Four healthy male subjects were required to step over one of six different height obstacles placed halfway along a 12 meter track. The obstacles ranged from .5 cm to 38 cm in height. An OPTOTRAK imaging system was used to capture the 3-D marker positions during gait. Twenty four markers were positioned on eight segments: the feet, legs, thighs, pelvis, and trunk of the subjects (3 markers per segment). The principal axis of each segment was found using extra digitized points on each segment (two on the foot and one on the shank, thigh, and trunk). The relative Euler angles for the eight segments were calculated from the absolute marker coordinates.

3.2.2 Modelling the Swing Phase

Possible sources of hip elevation are shown in Figure 3.1. We further divided the sources into two groups: The first group provided stance limb interaction (including stance limb ankle plantar flexion, knee extension, and hip extension) which basically elevated the stance hip and the swing hip. The second group included pelvic elevation, and the action of the trunk muscles. This group basically elevated the swing hip with respect to the stance hip.

In order to isolate the sources of hip elevation, three different models were developed. Model I was a six degree of freedom (DOF) model without pelvic elevation for investigating stance limb interaction effects on toe elevation. The effect of stance

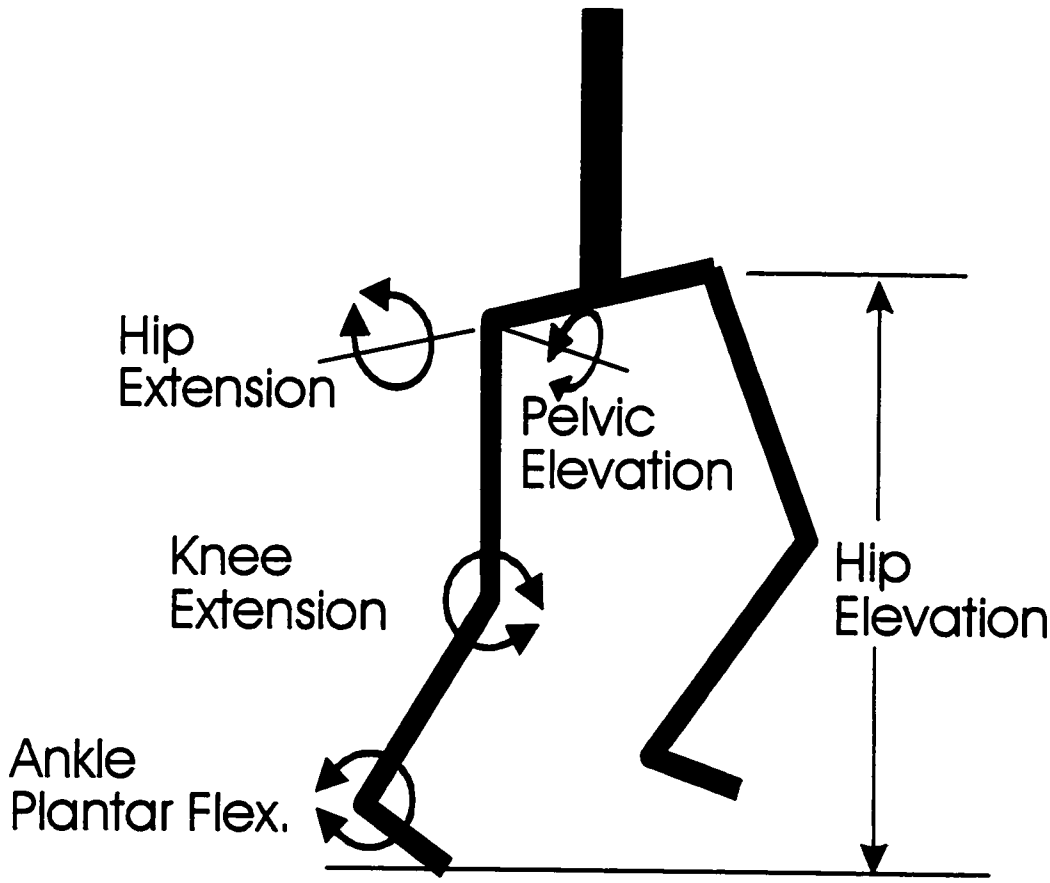

Figure 3.1: **Possible sources of hip elevation during the swing phase of stepping over obstacles.**

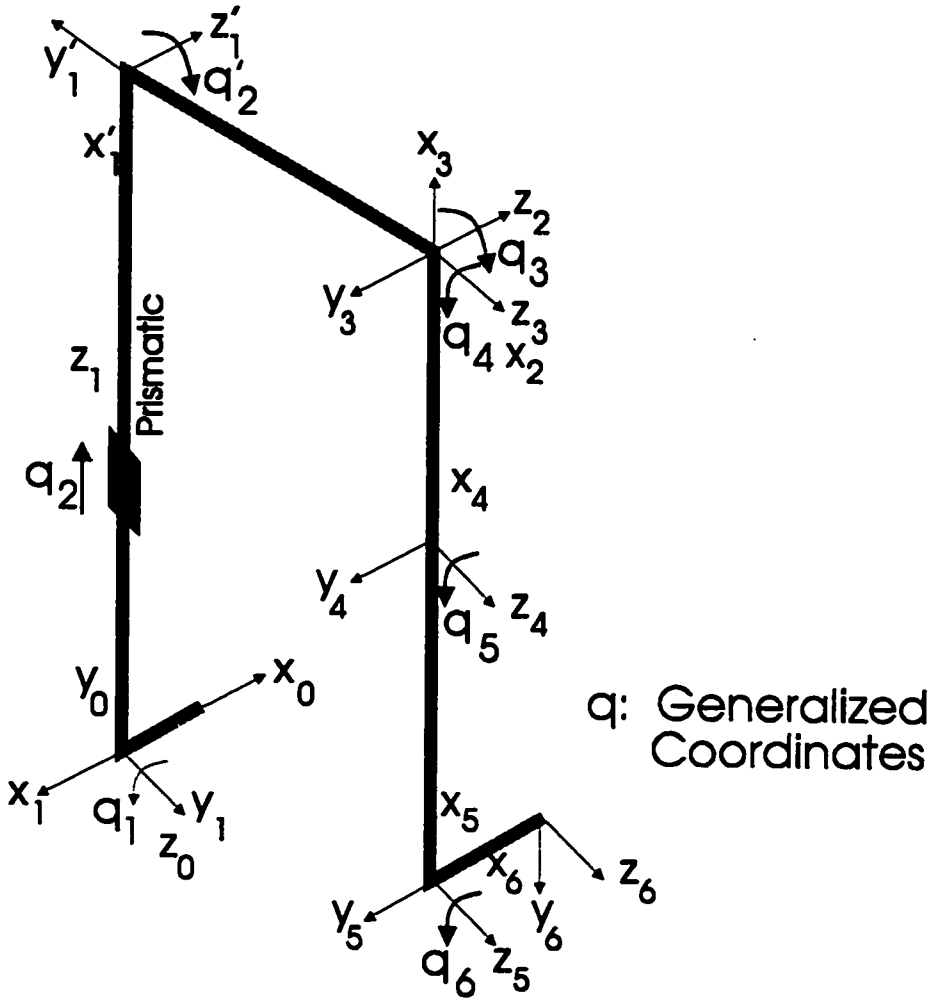

Figure 3.2: **3-D analytical models. The relative frames are attached to the segment joints.**

limb joint interactions was modelled using a single prismatic joint (q_2 in Figure 3.2). In Figure 3.2, $q_i (i = 1 \cdots n)$ are the generalized joint coordinates and the model has n degree of freedom. Model II was also a six DOF model, but with q_2 replaced by stance hip abduction/adduction (q_2'). Model III included both stance knee flexion/extension and stance hip abduction/adduction and flexion/extension. This eight DOF model was used to examine the combined effects of these two groups of hip elevators. Note that from the experimental data, pelvic tilt was found to be negligible and was not included in the models.

A symbolic program in MAPLE was developed to generate the equations of motion from the Lagrange formulation. The validity of the program was checked by comparing the derived equations of motion with those of SCARA and STANFORD manipulators, and a double pendulum. The relative coordinates of each segment were defined using the Denavit-Hartenberg (DH) convention (Appendix G). Once the transformation between the principal axes of the experimental model (developed from marker positions) and those of models I, II, and III were found, the displacements, velocities, and accelerations were obtained by inverse kinematics (see Appendix G).

3.2.3 Modelling the Double Support Phase

The double support phase was modelled from heel-off of the support limb to toe-off of the leading limb. During this period, the movement of the limb can be approximated with a ball-joint connecting the metatarsal-phalangeal (MP) joint to the ground and rotating around a fixed point.

However, the accumulating errors during simulation caused the position of the MP joint not to be fixed in space. These errors were primarily due to mapping the experimental data for eight segments (each with 6 DOF) to the simulation models with only six or eight DOF, and in which fixed segment lengths and simplified joints were assumed. To fix the position of the MP joint in space, the experimental data were corrected using a secant minimization with BFGS updates [26]. The minimization procedure found the minimal joint angle changes of the swing hip abduction/adduction, hip flexion/extension, and ankle plantar/dorsi flexion at each time step during the double support phase, to fix the position of the MP joint in space. These joint angle modifications were found to be moderate, without serious effect on the continuity of the resulting torques and forces, and usually required between 5 to 55 trials for successful convergence.

These constrained multibody systems can be modelled using the augmented method [2]:

$$\begin{bmatrix} D & B^T \\ B & 0 \end{bmatrix} \begin{Bmatrix} \ddot{q} \\ \lambda \end{Bmatrix} = \begin{Bmatrix} C \\ G \end{Bmatrix} + \begin{Bmatrix} Q \\ \dot{g} \end{Bmatrix} \tag{3.1}$$

where $[D(q)]$ is the inertia matrix, $[C(q,\dot{q})]$ are the Cristofell terms, $\{G\} = -[\dot{B}]\{\dot{q}\}$, $\{g\} = [B]\{\dot{q}\}$ and $\{Q\}$ is the vector of generalized forces and torques acting on this system. For the inverse dynamics problem, all the left hand side terms except $\{\lambda\}$ (the Lagrangian multipliers) are known. However, in next chapter we show that for this case, $\{\lambda\}$ is the vector of ground reaction forces measurable by a force plate. We also can detect the end of the double support phase and the beginning of the swing phase by monitoring λ_2 (the vertical ground reaction force measurable by the force plate).

3.3 Results and Discussion

Both experimental evidence (Patla and Prentice [61]) and our planar model [5] had shown that the hip translational energy during the swing phase is highly correlated with the obstacle height. This might be because of velocity components of energy $\int F.v.dt$ or the hip vertical force during swing. We first investigated these two possibilities by developing Models I, II, and III for the swing phase. Next, we extended the models to the double support phase to investigate which strategy can contribute most to hip vertical velocity at toe-off.

3.3.1 Effect of Scaling the Hip Vertical Force and Hip Velocity at Toe-Off

Figure 3.3 shows the stance hip vertical force from the experimental results from one of the subjects. With the initial velocities and displacements at toe-off set to the experimental values, the portion of the hip vertical force in excess of the body weight (the portion of the stance hip force prior to the time shown by the vertical dashed line in Figure 3.3), was scaled. As evident from these results, a variation of 40% in

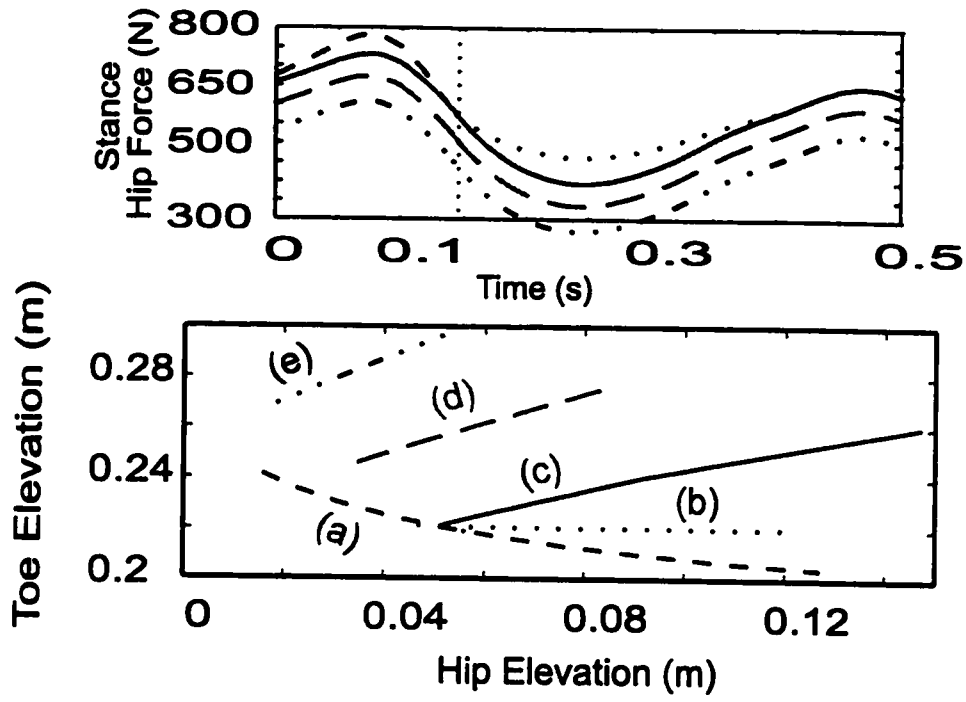

Figure 3.3: **Effects of varying hip translational velocity at toe-off and hip vertical force during swing phase on maximum toe elevation: increasing the portion of hip vertical force in excess to the body weight (a), increasing the portion of hip vertical force less than the body weight (b), increasing the hip vertical translational velocity at toe-off (c), and reducing the bias of the hip vertical translational force to 90% (d), and 80% (e) of its original value (while increasing the hip translational velocity).**

the vertical force about its nominal value (middle curve) resulted in a decrease of 5% in toe elevation of the swing limb. The major effect of these forces was to increase the distance between the stance ankle and hip (prismatic length in case of Model I).

The effect of scaling the negative portion of the hip vertical force (the portion below the body weight) is also shown in Figure 3.3. Increasing this also resulted in higher hip elevation with less than 5% effect on toe elevation. Reducing this force had a major effect on increasing hip elevation and swing length, while having minor effect on toe elevation. As a result, increasing the hip vertical force during the swing

phase was not the cause of observed toe elevation when stepping over obstacles.

All three models I, II, and III demonstrated the same results. Therefore, no matter what the origin of hip vertical force generation during the swing phase, increasing the hip vertical force does not produce significant toe elevation. However, the experimental results show that there is an increase in hip elevation force with obstacle height. Our model shows that the existence of a positive component of vertical force is not for increasing toe elevation, although it may be there to satisfy other requirements. For instance, hip flexors such as the psoas muscle also create hip elevation. Therefore flexing the hip always results in some hip hiking (elevation of the swing hip with respect to the stance hip). Hip hiking may also be used as a means of shifting the centre of mass of the body from one leg to the other leg in order to maintain equilibrium.

The initial hip velocity at toe-off was next increased from its nominal (experimental) value. As evident from Figure 3.3, such an increase in hip vertical velocity at toe-off had a more significant effect on toe elevation in comparison to the previous two methods. This was in agreement with the previous chapter's results obtained from the planar model.

However, the striking result was that by reducing the bias in hip vertical force, the ratio of toe-elevation to hip-elevation improved significantly. The results for 10% and 20% reductions of the nominal value are shown in Figure 3.3. A linear improvement is evident when the initial velocities are increased. This clearly shows that the mechanism which makes hip elevation the most effective is *a combined effect of increasing the initial hip translational velocity during the double support phase and reducing the anti-gravitational upward force on the hip during the swing phase.*

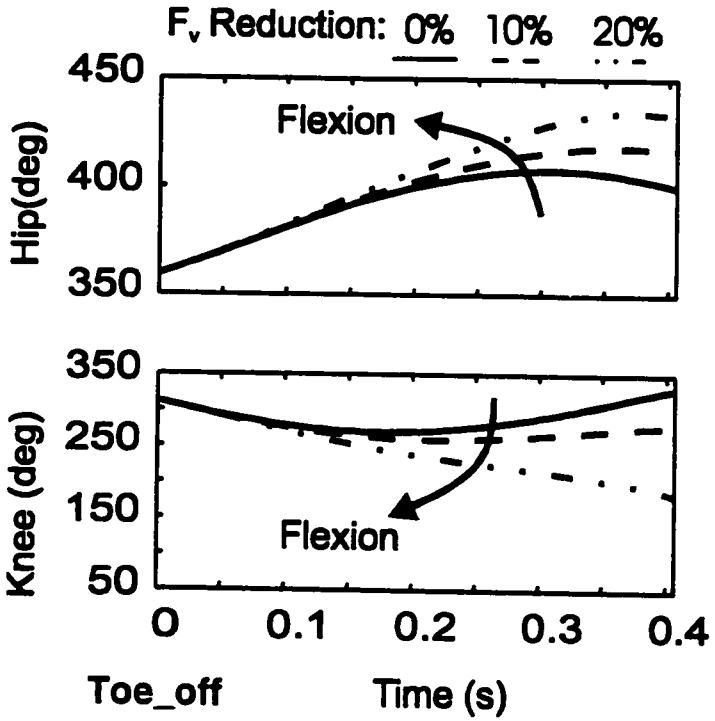

Figure 3.4: **Effect of 10 and 20% reduction in the hip vertical translational force on the knee and hip flexion when stepping over an obstacle. The hip at neutral position (no flexion, no extension) has an angle of 360 degrees(in Figure 3.2, X_3 and X_4 must be colinear). The knee at full extension has an angle of 360 degrees (in Figure 3.2, X_4 and X_5 must be colinear).**

3.3.2 Gravity Causes Toe Elevation Through Intersegmental Dynamics

To understand how reducing hip translational upward force results in increasing toe elevation, the intersegmental dynamics were studied. As shown in Figure 3.4, reducing the upward force bias during the swing phase results in additional flexion of both knee and hip joints, the direct result of which is an increase in toe clearance over the obstacle.

Winter [84], using kinematic link analysis has shown that hip abduction can produce relatively more toe elevation than other strategies. Our dynamic model shows

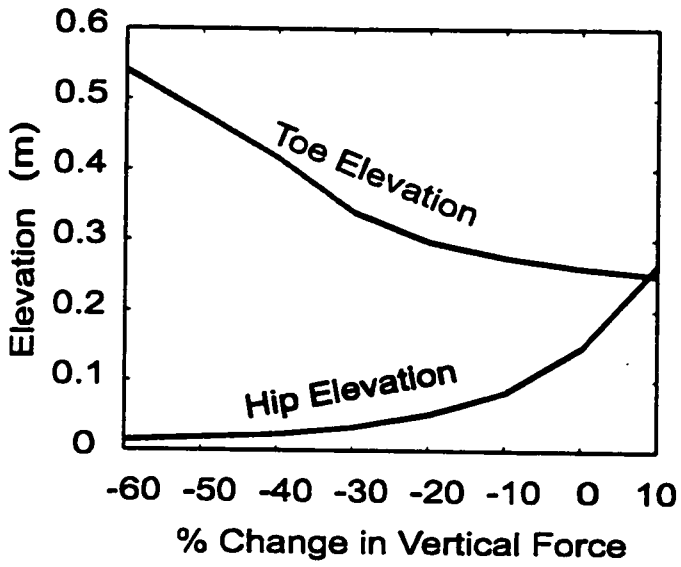

Figure 3.5: **Effect of reducing hip vertical translational force on maximum hip elevation and maximum toe elevation.**

that intersegmental effects of hip hiking during the swing phase is different from what kinematics show. Although elevating the hip can geometrically result in more toe elevation, the intersegmental dynamics of the linkage system acts in a way that increasing the hip hiking force reduces toe elevation.

Figure 3.5 shows that by reducing hip upward vertical force from 10% above its nominal value to 60% below the nominal value, maximum toe elevation increases while maximum hip elevation decreases. In other words, increasing the effect of gravitational forces will increase maximum toe elevation.

To avoid the collapse of segments when reducing the hip upward translational force to up to 60% over its nominal value, it was necessary to increase the translational velocity at toe-off. Therefore, for the purpose of this demonstration, the value of the hip translational velocity at toe-off was boosted 6 times above its nominal value. The observed excessive hip elevation at the nominal value for the hip vertical force is due to this extra initial velocity.

These results demonstrate that an increase of hip vertical velocity at toe-off is not

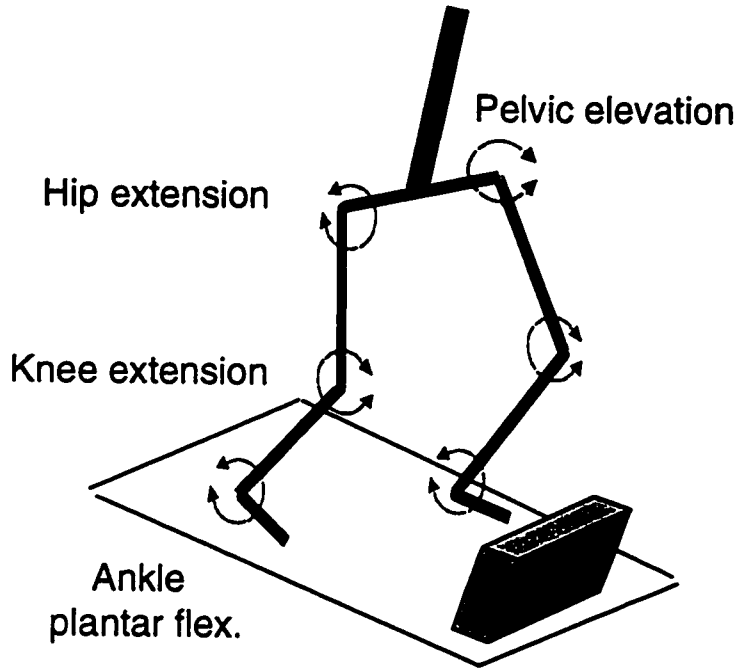

Figure 3.6: **Possible sources for increasing hip translational energy at toe-off.**

only for achieving additional toe-elevation; the extra energy supplied prevents the collapse of the linkage system when anti-gravitational forces which also elevate the limb are reduced. Next, we examine how the hip translational velocity at toe-off is increased.

3.3.3 Increasing the Hip Vertical Velocity at Toe-off

The hip translational velocity at toe-off is the result of interaction of many muscle forces and joint torques during the double support phase, the possible sources of which are shown in Figure 3.6. Here we chose to group our candidates as a) trailing limb ankle dorsiflexors, b) trailing limb interactions, c) leading limb hip abduction/adduction, d) leading limb hip flexion/extension, e) leading limb knee flexion/extension, f) ankle plantar/dorsi flexion.

Our goal was to study the independent effect of each of these on the leading hip

translational velocity. One obvious problem is that each of the above mentioned strategies affects not only the hip translational velocity, but also the other joint velocities via intersegmental dynamics. Hence, we were interested in finding a strategy that has a dominant effect on increasing the hip translational velocity, but with minimal effects on the other joints.

We varied the torques around each generalized coordinate (Figure 3.7) and observed their effects on maximum toe elevation. Note that the torques during the swing phase were kept the same as the experimental values, while only the torques during the double support phase were scaled.

Three levels of increase (10, 20, and 40%) for each torque or force around generalized coordinates are shown in Figure 3.8 (the generalized coordinates and their corresponding torques and forces are shown in Figure 3.7). Increasing leading limb plantar flexor torque during the double support phase (acting on q_6) increases maximum toe elevation; however, it also has some effect on the swing length. Although increased toe elevation can also be achieved by decreasing the leading limb hip extensor torque, and/or increasing knee flexor torque, their effect on the stride length is very significant. The trailing limb hip elevator force (prismatic force) has relatively less effect on the stride length; however, its effect on maximum toe elevation is minimal.

In summary, it seems there is a trade-off between toe elevation and stride length resulting from each of these strategies. For knee flexor and hip extensor torque, the dominating factors are significant changes of toe trajectory and stride length. However, increasing hip elevator force and leading limb plantar flexor torque does not change the stride length as significantly as the previous two strategies.

Figure 3.9 shows the effect of increasing each of the torques around generalized coordinates on the generalized velocities of the other joints.

We are looking for a strategy that produces maximum $\dot{q}_2$ (Figure 3.9a) while having minimal effect on the other velocities (Figure 3.9b). It is evident that increasing the leading limb knee extensor torque, $T(q_5)$, reduces $\dot{q}_2$ and has severe effects on

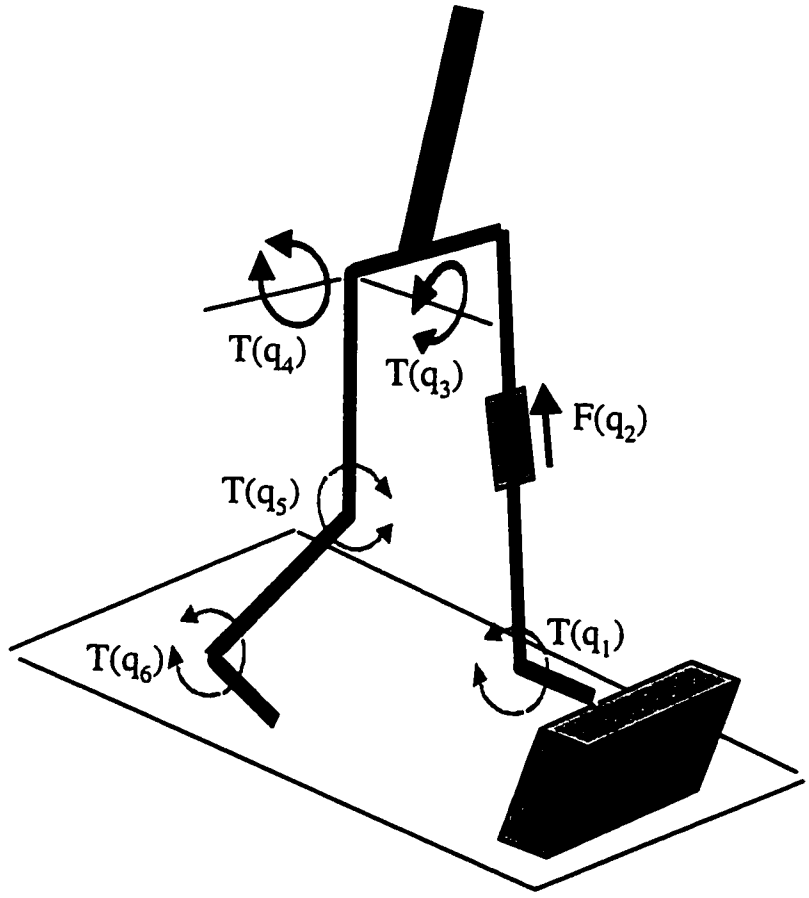

Figure 3.7: **Torques and forces around generalized coordinates: $T(q_1)$ the trail limb plantar flexor torque; trail hip elevation force, $F(q_2)$; lead limb abductor torque, $T(q_3)$; lead hip extensor torque $T(q_4)$; lead knee extensor torque $T(q_5)$; and lead ankle plantar flexor torque $T(q_6)$.**

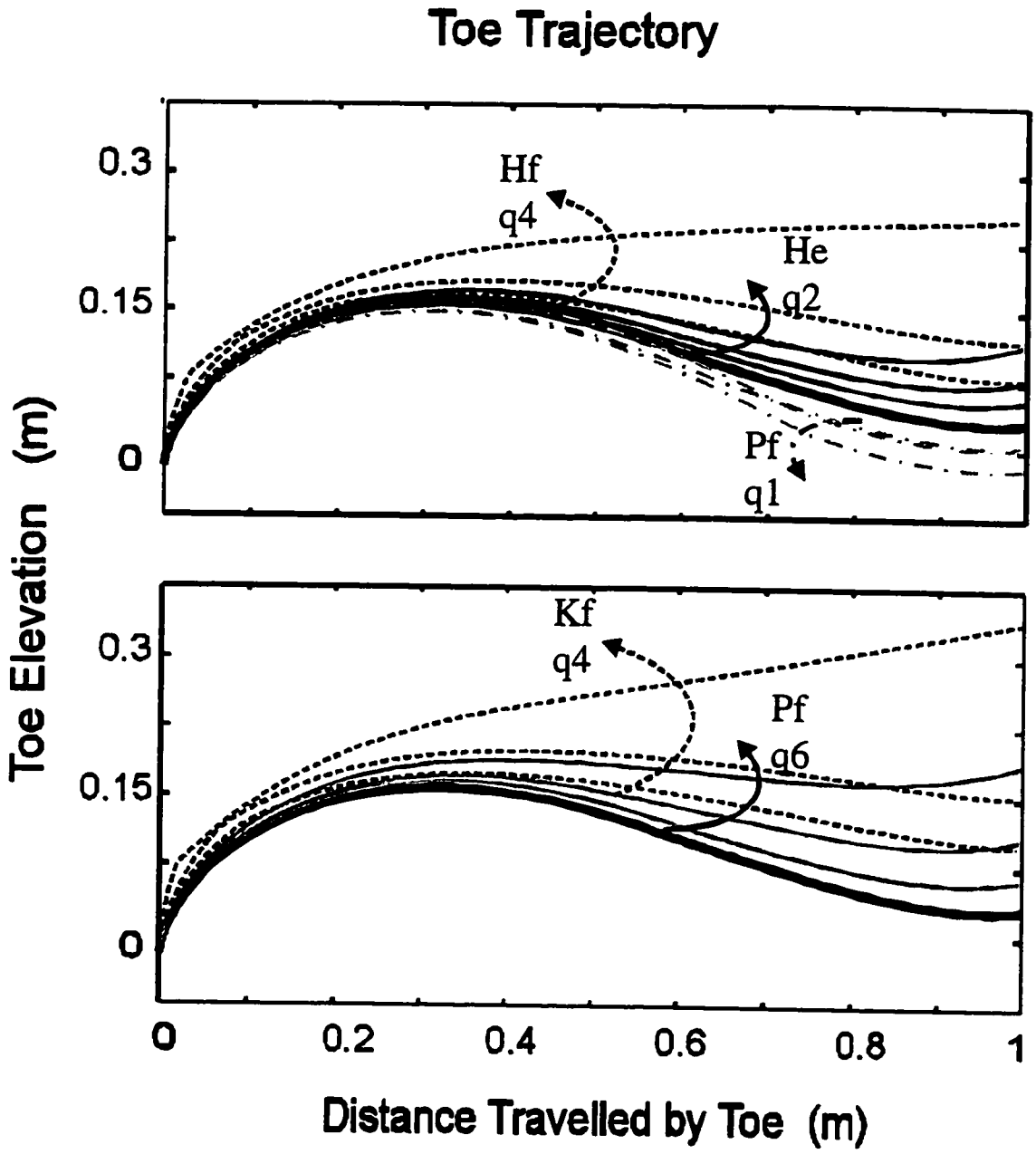

Figure 3.8: **Changes in the swing toe trajectories when increasing the leading limb plantar flexor torque (pf), knee flexor torque (kf), hip extensor torque (he), and the trailing limb hip translational force (ht). Each torque/force and its corresponding generalized coordinate is shown in Figure 3.7.**

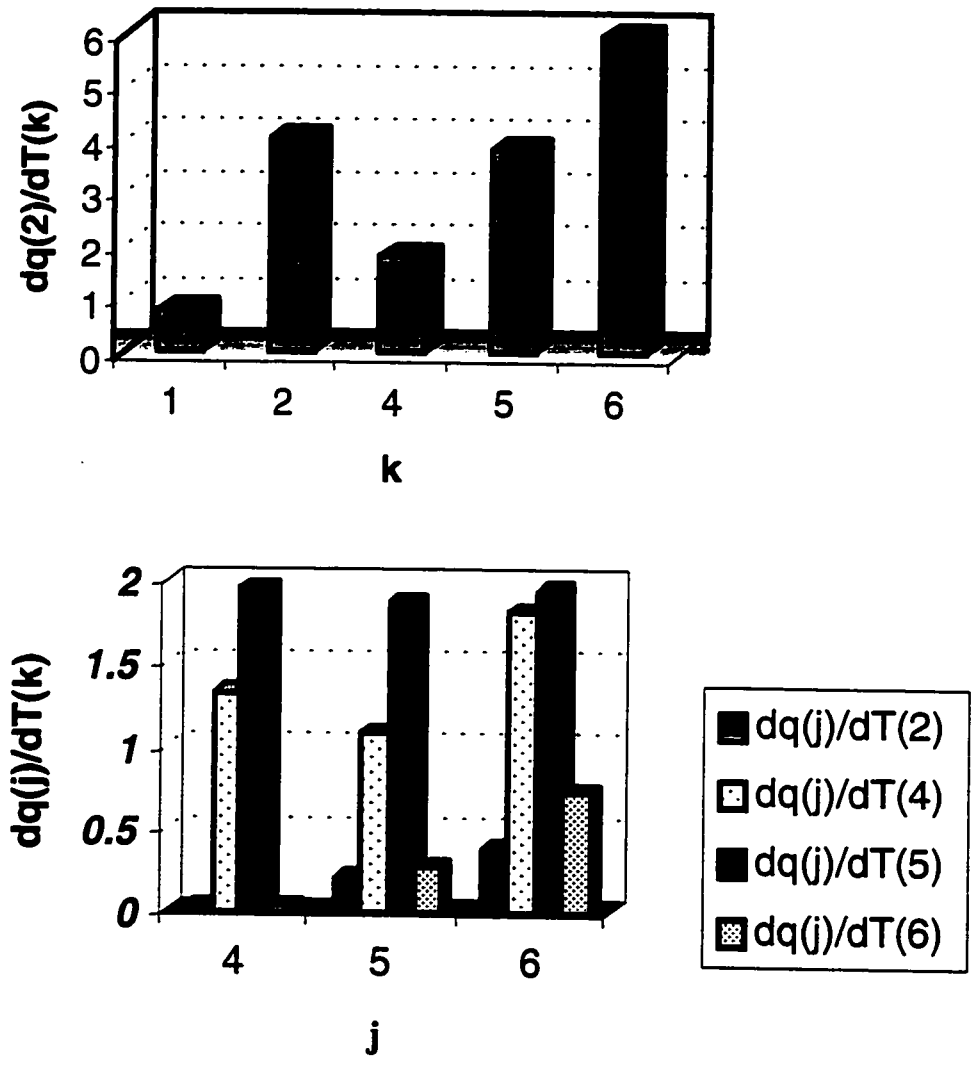

Figure 3.9: **Effect of increasing each of the generalized torques/forces during the double support phase (a) on hip elevation velocity at toe-off, (b) on other generalized velocities at toe-off. Each torque/force and its corresponding generalized coordinate are shown in Figure 3.7.**

other generalized velocities. Increasing leading limb's hip extensor torque, $T(q_4)$, has a moderate effect on $\dot{q}_2$ and a major effect on the other joints. The trailing limb translational force, $T(q_2)$, increases $\dot{q}_2$ and has minimal effect on other velocities. A more pronounced increase in hip elevation velocity is observed when the leading limb plantar flexor torque, $T(q_6)$, is increased. These forces, torques and their generalized coordinates are shown in Figure 3.7. Again, this strategy has minor effect on other joint velocities. In summary, increasing leading limb plantar flexor torque seems to be the most effective strategy for increasing hip translational velocity at toe-off.

3.4 Conclusion

Recent research has shown that hip elevation is the dominant strategy for stepping over an obstacle. The 3-D models that we developed in this study show that reducing hip vertical translational force during the swing phase results in increasing maximum toe elevation. In other words gravity, via intersegmental dynamics, helps elevate the limb during the swing phase. This, together with increasing hip vertical translational velocity at toe-off, is the most effective strategy for obtaining maximum toe elevation when stepping over obstacles.

The approaches used for modelling and simulation of the double support phase showed that the most effective strategy for increasing hip translational velocity at toe-off is lead limb ankle push-off. It was found that this strategy has minimal effect on other joint velocities at toe-off, while maximizing the hip translational velocity. These results clearly show that exploring the proper and effective methods for increasing the efficiency of walking is often counter intuitive; models are necessary to investigate these methods.

Chapter 4

Simplifying Biomechanical Modelling Problems using the Physical Meaning of Lagrangian Multipliers

In many multibody models for biomechanical applications, some of the constraint forces are directly measurable. In this note we make use of the physical meaning of Lagrangian multipliers to simplify the solution for such problems. This method is also useful when some of the constraint forces have to be measured and/or when a constraint violation has to be checked. Two biomechanical examples are given to demonstrate how this method simplifies both inverse and forward solutions of a multibody system.

4.1 Introduction

Multibody dynamics have found a wide range of applications in biomechanical modelling. Quite often, in the modelling of biomechanical systems, constraints are active

only for a range of motion. In these cases, it is normally desirable to derive the equations of motion first, and then build the closed loop and prescribed motion constraints into the model. In this way, premature introduction of constraints to the dynamical system can be avoided. In addition, specifically for linkage systems widely used in biomechanical analysis, the constraint Jacobian is in general a transcendental function of independent variables. This creates difficulty in deriving one independent variable in terms of others. Thus, for large dynamical systems, it is not always desirable to reduce the number of equations of motion by introducing kinematic constraints at early stages.

An alternate method is to increase the number of equations by introducing constraint forces via Lagrange multipliers. In this case, for a system with n independent generalized coordinates and m constraints, $n + m$ equations are used to describe the dynamics of the system, although the system has only $n - m$ degrees of freedom.

The increased computational effort required to calculate indeterminate multipliers has resulted in coordinate reduction methods attracting special attention. The goal of these methods, in general, was to eliminate Lagrangian multipliers from the equations of motion. The works of Hemami and Weimer [35], Singh and Likins [71], Kamman and Huston's [42] embedding method based on the zero eigenvalue theorem of Walton and Steeves [3], and the Pseudo Upper Triangular Decomposition Method (Amirouche and Tongyi [3]) are examples of coordinate reduction methods.

In many dynamical models, specifically biomechanical models, Lagrangian multipliers are directly measurable. Thus, introducing them to the systems of equations can actually simplify the problem. In some cases Lagrangian multipliers present the constraint forces in global coordinates, usually measurable by existing instrumentation used in biomechanics labs. We present two simple biomechanical examples to show how (1) predetermination of the Lagrangian multipliers simplifies the calculation of inverse dynamics, and (2) how addition of these to the systems of equations allows specific forces of constraints to be monitored.

4.2 Lagrangian Multipliers - A Special Case

Consider a system described by n generalized coordinates $q_1, q_2, ..., q_n$. Also consider a non-holonomic constraint ϕ applied to the system with equations of motion as follows:

$$\frac{d}{dt}\left(\frac{\partial L}{\partial \dot{q}_i}\right) - \frac{\partial L}{\partial q_i} + \lambda B_i = Q_i \qquad (i = 1, \ldots, n) \tag{4.1}$$

where L is the Lagrangian, $B_i = \frac{\partial \phi}{\partial q_i}$ is the Jacobian constraint, and Q_i is the external force. It is known that λB_i is the constraint force corresponding to q_i (e.g. Goldstein [30]). Also, it can be shown that λ is usually a force of constraint (e.g. Groesberg [32]).

As a special case of interest, if the following condition exists:

$$\frac{\partial \phi}{\partial q_i} = \frac{\partial x_k}{\partial q_i} \tag{4.2}$$

(where x_k is a coordinate in an arbitrary frame of reference), then the Lagrangian multiplier, λ, will be the constraint force corresponding to the x_k coordinate. Condition (4.2) implies that we have found a coordinate x_k along which the constraint acts.

As we have not found an explicit declaration of condition (4.2) in the literature, we demonstrate the analytical reasons for this condition. The reader who is most interested in the application of this method can directly move to the next section.

The non-holonomic or holonomic constraint ϕ in the set of n independent generalized coordinates can be defined as:

$$\sum_{i=1}^{n} \frac{\partial \phi}{\partial q_i} dq_i + \frac{\partial \phi}{\partial t} dt = 0 \tag{4.3}$$

where ϕ is the function of q's and time (t). Now consider a transformation from a set of $m > n$ coordinates to the set of n generalized coordinates such that:

$$
\begin{aligned}
x_1 &= f_1(q_1, q_2, \ldots, q_n, t) \\
x_2 &= f_2(q_1, q_2, \ldots, q_n, t) \\
&\vdots \\
x_m &= f_m(q_1, q_2, \ldots, q_n, t)
\end{aligned}
\tag{4.4}
$$

The constraint equation in the set of new m coordinates which are not independent is:

$$
\sum_{k=1}^{m} \frac{\partial \phi}{\partial x_k} dx_k + \frac{\partial \phi}{\partial t} dt = 0 \tag{4.5}
$$

Now if there is a $k \in [1, m]$ such that condition (4.2) is satisfied, then writing the constraint force as:

$$
c_i = \lambda B_i = \lambda \frac{\partial \phi}{\partial q_i} \tag{4.6}
$$

and substituting (4.2) in (4.6) yields:

$$
c_i = \lambda \frac{\partial \phi}{\partial q_i} = \lambda \frac{\partial x_k}{\partial q_i} \tag{4.7}
$$

The virtual work of the constraint force in generalized coordinates for virtual displacements δq_i is:

$$
\delta W = \sum_{i=1}^{n} c_i \delta q_i = 0 \tag{4.8}
$$

Substituting (4.7) into (4.8) yields:

$$
\delta W = \sum_{i=1}^{n} \lambda \frac{\partial x_k}{\partial q_i} \delta q_i = 0 \tag{4.9}
$$

The coordinates $(x_1, x_2, \ldots, x_m)$ are related to coordinates $(q_1, q_2, \ldots, q_n)$ via (4.4). Differentiating (4.4) and setting $\delta t = 0$ results in expressing small virtual displacements of δx_k in terms of virtual displacements of δq_i. We obtain

$$\delta x_k = \sum_{i=1}^{n} \frac{\partial x_k}{\partial q_i} \delta q_i \tag{4.10}$$

where $\frac{\partial x_k}{\partial q_i}$ is a function of q's and time t. By substituting (4.10) into (4.9)

$$\delta W = \sum_{i=1}^{n} \lambda \frac{\partial x_k}{\partial q_i} \delta q_i = \lambda \delta x_k = 0 \tag{4.11}$$

This clearly shows that the Lagrangian multiplier, λ, is the constraint force in the direction of the coordinate δx_k.

For simplicity, the case has been shown for one λ, since we were interested in a specific direction of a specific λ. If the general form of several constraints on each equation were used ($\sum \lambda_i B_{ij}$), then we could reformat the problem to maintain our specific λ and its Jacobian in the left hand side of equation (4.1) while treating the rest of the constraits as external forces by transfering them to the right hand side of (4.1).

4.3 Implications

Assume that for a system with n generalized coordinates, the coordinate x_k is in the direction of the global Cartesian axis X. From what was shown it can be immediately concluded that if condition (4.2) is satisfied, λ will be the constraint force corresponding to the global axis X.

In many biomechanical applications such as gait studies, some constraint forces in the global frame are directly measurable. Hence, by monitoring λ, the phases of the gait cycle in a linkage model can be easily monitored. As well, use of λ as a determinate variable can simplify the modelling process and assist in dealing with

the modelling errors. The following two examples of link-segment models for gait, emphasize the above points. An example for handling the geometrical constraints using the above method will be discussed first. The second example uses the method to find the reaction force due to a prescribed motion constraint.

4.3.1 Geometrical Constraints

One of the problems with linkage modelling of biomechanical systems is error accumulation, especially for forward solution models. The sources of errors are usually the simplifications on the skeletal model, assumptions such as fixed segment lengths and pin joints, as well as numerical integration of the equations of motion. In an example of a 3-D model in the previous chapter, the kinematic data collected from an OPTOTRAK imaging system showed that the metatarsal-phalangeal (MP) joint was rotating around a fixed point from heel-off to toe-off of the same limb during the double support phase of locomotion, as shown in Figure 4.1a. However, direct transformation of the ground reaction force to the generalized coordinates and then solving the equations without using constraints, resulted in a movement of the MP joint (Figure 4.1b). This conflicts with the experimental results. To avoid this, it was necessary to add constrained equations to fix the MP joint.

Now consider a simple planar model of the double support phase. The model and its generalized coordinates are shown in Figure 4.2. Assume force plate data are collected only under the MP joint in contact with the ground.

Consider the global coordinates, XY. The constraints can be defined as:

$$\begin{aligned} \phi_1 &= X - R_1 = x_1 - R_1 = l_1\cos(q_1) + l_2\cos(q_2) + l_3\cos(q_3) - R_1 = 0 \\ \phi_2 &= Y - R_2 = x_2 - R_2 = l_1\sin(q_1) + l_2\sin(q_2) + l_3\sin(q_3) - R_2 = 0 \end{aligned} \qquad (4.12)$$

Clearly for:

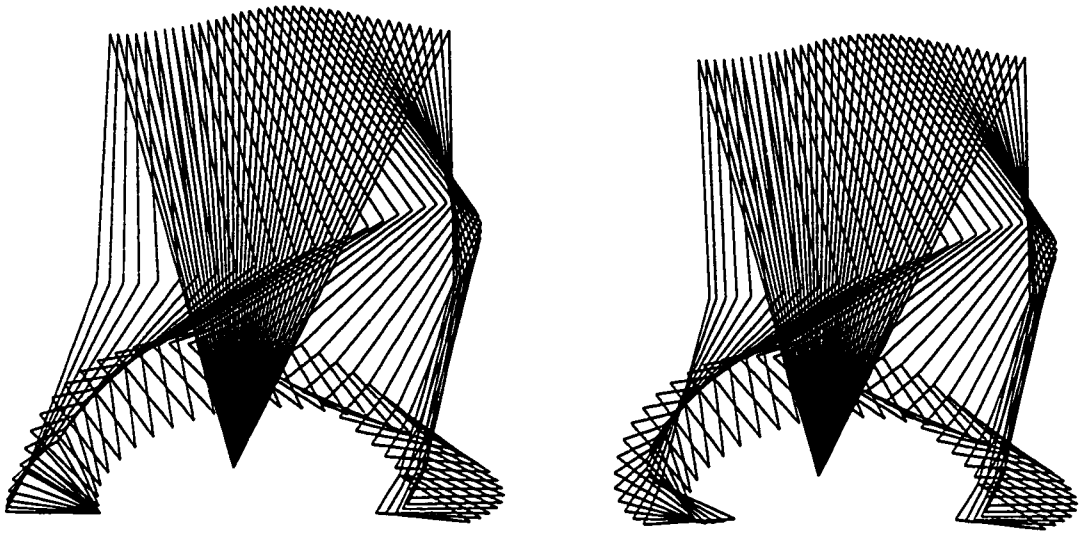

(a) (b)

Figure 4.1: **Model simulation a) using the proposed method. b) without using the proposed method.**

$$\{\phi\} = \begin{Bmatrix} \phi_1 \\ \phi_2 \end{Bmatrix} \qquad \{x\} = \begin{Bmatrix} x_1 \\ x_2 \end{Bmatrix} \tag{4.13}$$

we have:

$$\left[\frac{\partial \phi}{\partial x}\right] = \begin{bmatrix} 1 & 0 \\ 0 & 1 \end{bmatrix} \tag{4.14}$$

and the constraint Jacobian matrix of this system is:

$$[B] = \left[\frac{\partial \phi}{\partial q}\right] = \begin{bmatrix} -l_1 \sin(q_1) & -l_2 \sin(q_2) & -l_3 \sin(q_3) \\ l_1 \cos(q_1) & l_2 \cos(q_2) & l_3 \cos(q_3) \end{bmatrix} \tag{4.15}$$

Using (4.14), condition (4.2) is satisfied:

$$\frac{\partial \phi_k}{\partial q_i} = \sum_l \frac{\partial \phi_k}{\partial x_l} \frac{\partial x_l}{\partial q_i} = \frac{\partial x_k}{\partial q_i} \tag{4.16}$$

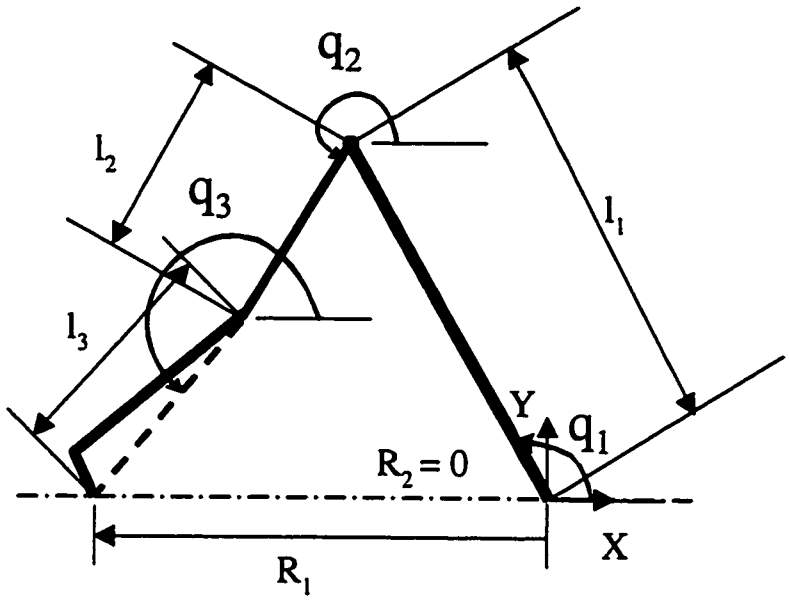

Figure 4.2: **Planar model for double support phase.**

where $k = 1, 2$. From (4.16) we conclude that λ_1 and λ_2 are the constraint forces in the direction of the respective global coordinates X and Y.

Using the differentiated form of the constraint equations, we may choose to formulate the equations of motion for this system as:

$$\begin{bmatrix} D & B^T \\ B & 0 \end{bmatrix} \begin{Bmatrix} \ddot{q} \\ \lambda \end{Bmatrix} = \begin{Bmatrix} C \\ G \end{Bmatrix} + \begin{Bmatrix} f \\ \dot{g} \end{Bmatrix} \tag{4.17}$$

where $[D(q)]$ is the inertia matrix, $[C(q, \dot{q})]$ are the Christoffel symbols, $\{G\} = -[\dot{B}]\{\dot{q}\}$, $\{g\} = [B]\{\dot{q}\}$ and f is the vector of generalized forces acting on this system.

When solving the inverse problem, since λ_1 and λ_2 are the forces measured with the force plate, all the terms in the left hand side of the equation (4.17) are known. Therefore, the forces and torques on the right hand side can be determined by simple matrix multiplication of the left hand side of this equation. The equation satisfies the constraint of rotation around the MP joint.

Also, if the forward solution model with given external forces and the constraint

over the MP joint had to be solved, the calculated value of λ_2 would have been the ground vertical reaction force and its zero value would determine when the toe-off occurred. Note that, the solution to the second row implies that MP joint only allows rotation around a fixed point (for more detail on equation (4.17), refer to [2]).

4.3.2 Prescribed Motion Constraints

Consider the linkage system shown in Figure 4.3. Here, $h(t)$, the model's hip elevation during the swing phase, is given by a constraint trajectory:

$$h(t) = h_0 \sin(wt) \tag{4.18}$$

where $wt = \pi$ at the end of one swing cycle. To find the vertical reaction force due to this constraint trajectory, all we have to do is to consider a new coordinate x in the direction of h, such that $h = x$. The constraint equation is:

$$\phi = x - h_0 \sin(wt) = q_2 \sin(q_1) - h_0 \sin(wt) = 0 \tag{4.19}$$

$$\frac{\partial \phi}{\partial x} = 1 \qquad [B] = \left[\frac{\partial \phi}{\partial q}\right] = \begin{bmatrix} q_2 \cos(q_1) & \sin(q_1) & 0 & 0 \end{bmatrix} \tag{4.20}$$

As before, by the chain rule, and using the above equation we can satisfy (4.2):

$$\frac{\partial \phi}{\partial q_i} = \frac{\partial \phi}{\partial x}\frac{\partial x}{\partial q_i} = \frac{\partial x}{\partial q_i} \tag{4.21}$$

Now the forward solution of the equation (4.17) will also calculate λ, the constraint force corresponding to the x coordinate. Therefore by applying extra coordinate in the direction of constraint force, the desired reaction force due to hip hiking can directly be calculated. Obviously, calculation of other unnecessary constraint forces (other joint reaction forces) can be avoided using the Lagrange formulation.

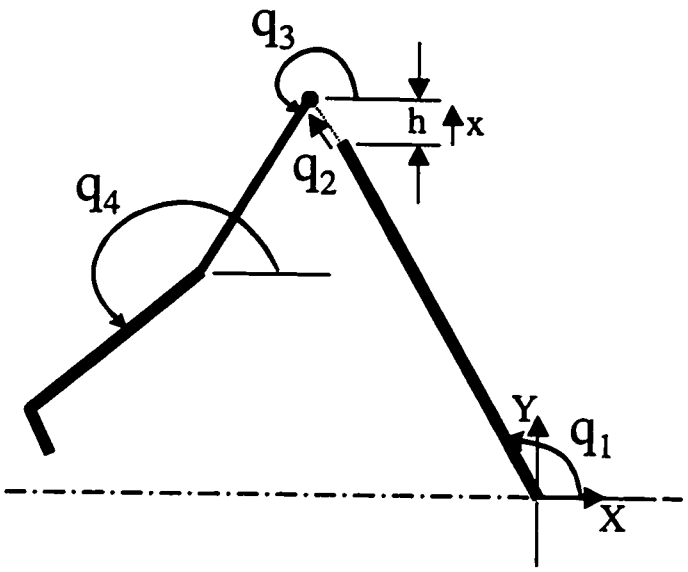

Figure 4.3: **Planar model with hip hiking constraint.**

4.4 Conclusions

The method presented simplifies the derivation of the solution to the equations of motion whenever some of the constraint forces are available, and/or in the case where a constraint force in a specific direction is to be calculated. Therefore, the method will be useful when monitoring some constraint forces is necessary. Two examples for geometrical and prescribed motion constraints in biomechanics have been given, and the ease of application of the method to these problems demonstrated.

Chapter 5

Stepping over Obstacles during Locomotion: Insights from Multi-Objective Optimization on a Set of Input Parameters

In this study we investigate possible objectives that the central nervous system (CNS) may consider in planning a strategy for stepping over an obstacle. A link segment simulation model has been developed based on Lagrangian dynamics, with which muscle force inputs can be optimized to best satisfy the postulated objectives for landing stability, obstacle clearance, and efficiency of the movement. A direct optimization approach with multi-objective criteria based on the kinematics and kinetic characteristics of the swing phase of locomotion is used in the simulation. The role of initial conditions at toe-off and bi- articular muscle forces during the swing phase was also investigated. The optimization was performed for both leading limb and trailing limb during the swing phase (We step over the obstacle first with the leading limb followed by the trailing limb).

The simulation results demonstrate that the use of bi-articular muscles is sufficient to clear a range of obstacles with the trailing limb (obstacle encountered during early

swing). Stride length or landing stability objectives need not be specified suggesting a simpler control of trailing limb trajectory by the CNS. In contrast while the use of bi-articular muscles can be sufficient to clear obstacles with the leading limb (obstacle encountered during mid to late swing), a stable landing and smooth toe and knee trajectories are compromised without suitable initial conditions at toe-off. The results suggest that the set of postulated objectives for the lead limb is necessary, although not sufficient.

5.1 Introduction

When we step over an obstacle in the travel path, the swing limb trajectory is modified considerably from that used for normal level-ground locomotion. Several empirical studies have described changes in the limb kinematics, kinetics, and muscle activity during this adaptive locomotion [60, 14, 50, 63, 15]. What is less clear is the criterion (or criteria) used by the central nervous system (CNS) to come up with the observed movement pattern.

During normal level ground locomotion, researchers have used various single criterion optimization methods to explain the specific recruitment of muscles for validating the predicted muscle recruitment profiles based on experimentally measured muscle activity profiles [34, 17, 64, 37, 16]. Lack of agreement between predicted muscle recruitment with the muscle activity profiles have led researchers to speculate that perhaps more than one aspect is optimized during locomotion [16]. While most optimization methods have been geared towards decomposing joint torques into muscle forces, Pandy et al. [59] have used optimal control theory to optimize bi-articular muscle forces in maximum high jumping. Also, Chou et al. [15] have used minimum energy and dynamic programming to predict swing ankle trajectory. They found that predictions were good for level ground; however, they are not acceptable during locomotion over uneven terrain.

Stepping over obstacles is a prime example where several objectives have to be

simultaneously optimized; it is critical to not only elevate the limb over the obstacle to avoid tripping, but also to achieve controlled landing to avoid slipping. Experimental work has shown that several key characteristics of the swing limb trajectory (related to slipping and tripping) are regulated within limits when stepping over obstacles of varying heights [63].

Our goal is to use a multi-objective optimization approach to generate the swing limb trajectory over an obstacle. It is clear that the initial conditions at the end of the stance phase and the activity of various swing limb muscles are responsible for the generation of the swing limb trajectory. In this study the multi-objective algorithm optimizes selected critical initial conditions and pulse parameters of the bi-articular muscles during the swing phase. The choice of these control inputs is consistent with the experimental work that has shown bi-articular muscles play a dominant role in the control of the swing limb over obstacles [63].

5.2 Multi-objective Optimization Model

The flow diagram of the optimization model is shown in Figure 5.1. This is based on a link segment model of the lower limbs, the inputs to which are the muscle force pulses and the initial conditions for the step cycle. For a given set of initial conditions and temporal muscle activation profiles, the limb trajectory is calculated by integrating the forward model. Selected characteristics of the resultant trajectory are combined to produce a signature metric, which becomes the objective function value for a direct or a variable metric optimization procedure. Maximization of this metric results in a minimal overall error between the desired and calculated trajectory characteristics, thus yielding the required temporal muscle activation profiles and initial conditions to achieve this.

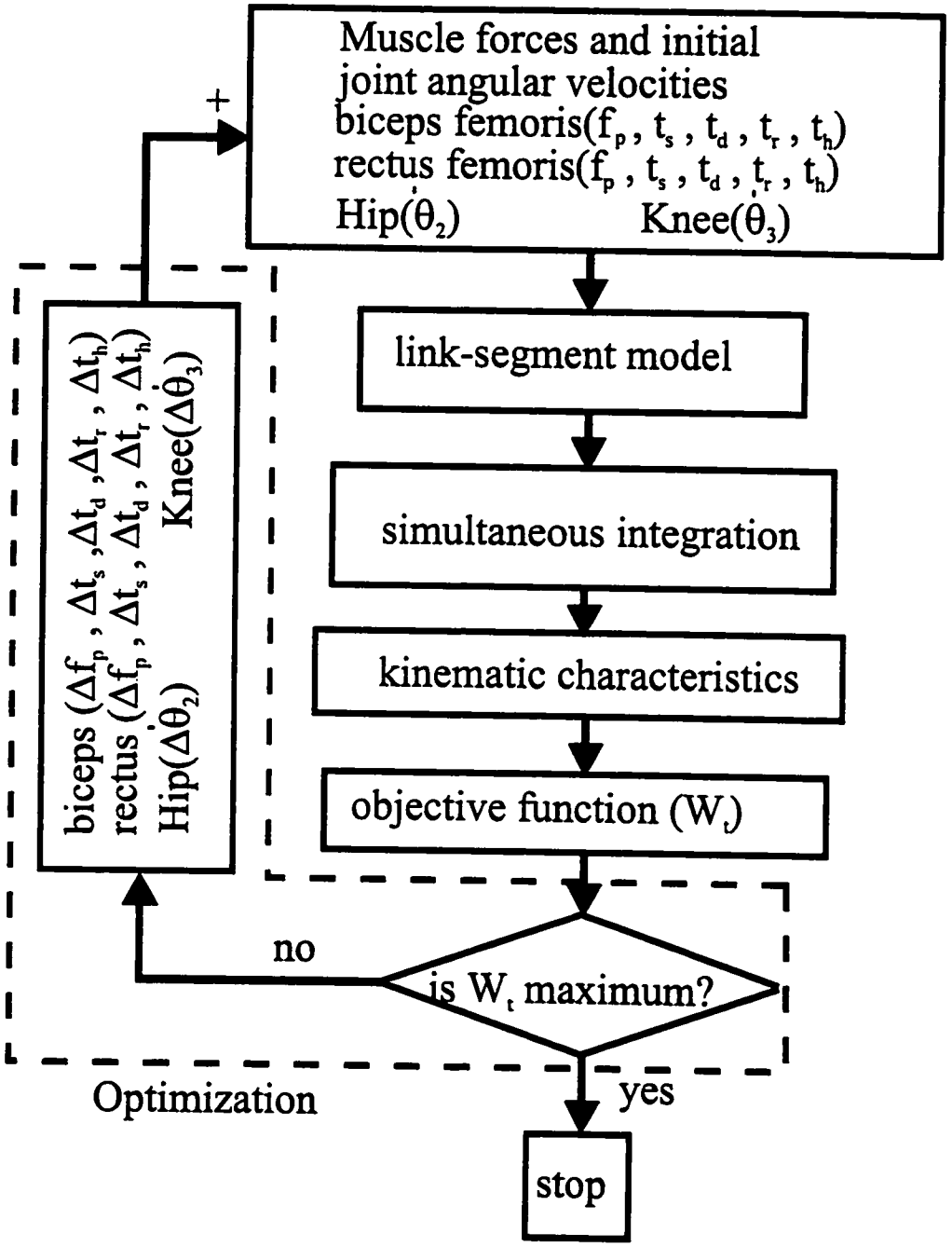

Figure 5.1: **The optimization algorithm. Details for each block are described in the method section. The parameters shown in the top block are described in Figures 5.2 and 5.3.**

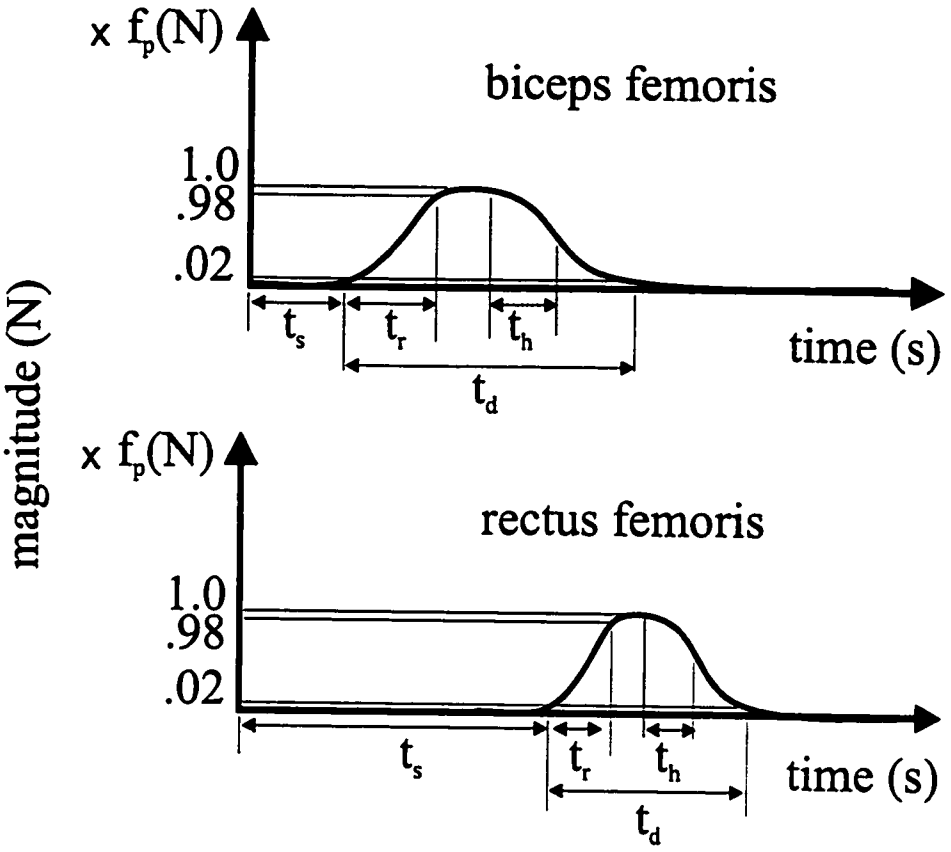

Figure 5.2: **Parameters describing single pulse muscle force: peak force (f_p), pulse start time (t_s), pulse duration (t_d), pulse rise time (t_r), and pulse half relaxation time (t_h).**

5.2.1 Input Parameters

One or more pulses characterize each muscle force activation profile (Figure 5.2). Each pulse is described by five parameters: start time (t_s) duration (t_d), peak amplitude (f_p), rise time (t_r), and half relaxation time (t_h).

Research has shown that the two bi-articular muscles, rectus femoris and biceps femoris, have significant activity during the swing phase of obstructed gait [50, 63]. Biceps femoris has two peaks of activity: the first peak starts prior to heel contact and continues during early swing. In our model, the focus is mostly on the early activity of biceps femoris, which plays a critical role in elevating the limb over the

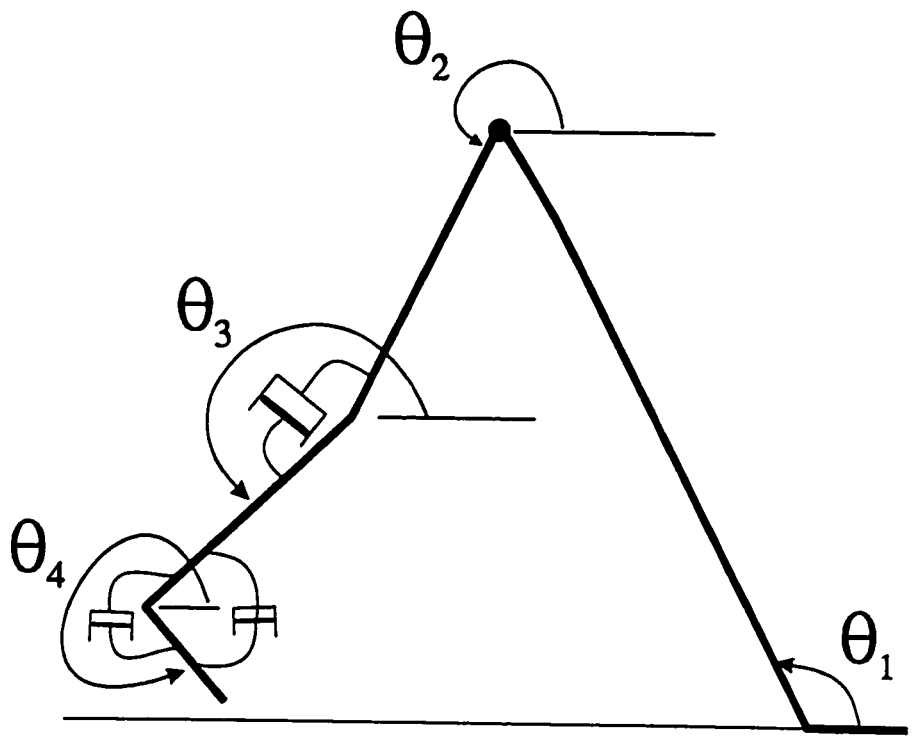

Figure 5.3: **A 4 degree of freedom planar model with pin joints. The model includes the segments for the swing limb (thigh, leg, foot) and one segment for the stance limb. Three uni-directional non-linear dampers are used to model anatomical constraints.**

obstacle. At the end of the swing phase, non-linear dampers (Figure 5.3) become active. The forces exerted by these dampers model both passive forces arising at the joint limits, and the second burst of activity in biceps femoris during late swing. The activity of rectus femoris generally occurs after clearing the obstacle, and is used to provide stable landing and adequate step length.

Two single-pulse activities for each muscle were used in the simulation. In addition to the ten control parameters defining these two pulses (five per pulse, as described above), initial velocities of the hip and knee joints at toe-off were also treated as control parameters for the model. These initial velocities result from muscle activity prior to toe-off.

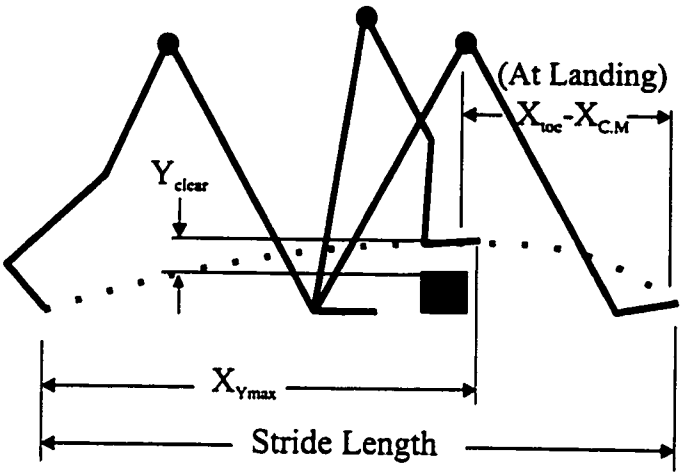

Figure 5.4: **Criteria used to characterise swing limb trajectory: toe clearance over obstacle (Y_{clear}), location of the maximum toe elevation ($X_{Y_{max}}$), stride length, and a measure of landing stability ($X_{toe} - X_{C.M.}$) measured at foot contact (we refer to it as stability margin).**

5.2.2 Model Definition

A symbolic program was written in MAPLE to generate the equations of motion and the constraint Jacobian as required. Lagrangian dynamics were used to derive the equations of motion (see Appendices A and B). For the planar models, both segment absolute angles (Figure 5.3) and relative joint angles can be used to describe the model. The description file for the program specifies the segments, position of the generalized coordinates (using the Denavit-Hartenberg convention [72], Appendix G), the type of joints, and the movement constraints.

For this study, a four degree of freedom planar model consisting of the thigh, the leg, and the foot of the swing limb, and a single link stance limb was used (Figure 5.3). The anatomical constraints were modeled as uni-directional non-linear dampers in which the damper coefficient increases exponentially close to the joint limit, and is described as a function of joint displacement. For example, the knee damper equation is as follows:

$$M = \frac{A}{1 + exp((\theta_3 - \theta_2) \times S)} \times (\dot{\theta}_3 - \dot{\theta}_2) \tag{5.1}$$

where: $A = 0 \; if \; \dot{\theta}_3 < \dot{\theta}_2$

The coefficients A and S were set to ensure that the damper becomes highly active in a region close to knee full extension (typically $A = 100$, $S = -100$). θ_2, θ_3 and their time derivatives (thigh and leg segment angular positions and velocities as defined in Figure 5.3) are the variables of this equation.

5.2.3 Experimental Data Set Source

Kinematic and muscle activity patterns for individuals (age range 18-21 years) stepping over obstacles of different heights (10.5 to 38 cm) in the travel path have been collected in our lab and are described in detail elsewhere [63, 61]. Obstacles were visible from the start and individuals walked at a natural self-selected pace and stepped over the obstacle. The toe trajectories for individual participants show similar patterns (see Figure 3 from [63]). Average values for selected kinematic parameters and average toe spatial trajectory from this data set were selected and used in this modelling work as described in the following section.

5.2.4 Kinematic Characteristics

The derived equations of motion have the format:

$$D(\theta)\,\ddot{\theta} + C(\theta, \dot{\theta}) + \Psi(\theta) = \tau - M(\theta, \dot{\theta}) \tag{5.2}$$

Here, D is the inertia matrix, C represents the velocity dependent terms, and Ψ includes potential terms (defined in Appendices A and B). The 4-5th order Runge-Kutta-Fehlberg numerical integration method with variable step size was used to compute the kinematics.

To describe the swing limb trajectory, certain trajectory characteristics must be defined. We have previously proposed a set of characteristics for a normal swing [5]; if the trajectory satisfies these characteristics, a successful swing is achieved. However, when stepping over an obstacle, all of these characteristics need not be satisfied. For instance, some landing stability can be sacrificed since corrective action could be taken in the next step. On the other hand, other characteristics such as the position of maximum toe clearance around the obstacle region become more significant.

Experimental studies on obstacle avoidance during locomotion show that the following trajectory characteristics are tightly controlled:

1. Toe clearance over an obstacle falls within a limited range, for a range of obstacle heights [63, 15]. This appears to be a compromise between increased efficiency (optimizing the lower limbs potential energy) and maintaining a safety margin for clearing the obstacle.

2. The distance to an obstacle from the toe-off position is usually about 60% of the total swing length; this ensures a safe landing while providing a reasonable stride length across the obstacle [63].

3. Maximum toe-clearance usually occurs just after crossing an obstacle [63]. The proximity of maximum toe clearance to obstacle location minimizes the lower limbs potential energy over the obstacle.

To describe any given trajectory over an obstacle, we use the four trajectory characteristics shown in Figure 5.4. Toe clearance (Y_{clear}) occurs over the obstacle while maximum toe elevation can occur anywhere between toe-off and landing, and the position at which this occurs with respect to toe-off is given by ($X_{Y_{max}}$). Landing stability is characterized by the distance between the toe on landing and the center of mass ($X_{toe}X_{C.M.}$), while stride length is simply as shown. It is realized that dynamic stability is influenced not only by the position of center of mass with respect to the base of support, but also its velocity. In this model we simply ensure that the center

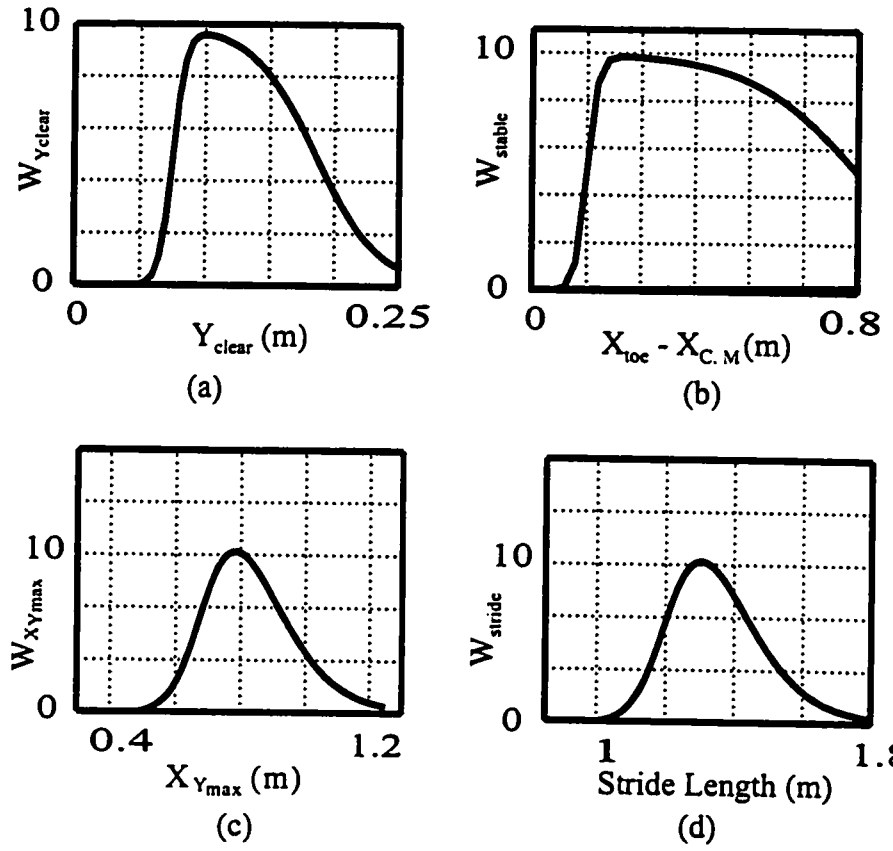

Figure 5.5: **Weighting factors for trajectory characteristics. Factor profiles shown are maximized when (a) Y_{clear} is 0.1 m, (b) $X_{toe} - X_{C.M.}$ is 0.2 m, (c) $X_{Y_{max}}$ is 0.8 m, and (d) stride length is 1.25 m. The obstacle was assumed to be just behind $X_{Y_{max}}$.**

of mass is posterior to, and at a certain distance from foot landing. The velocity of the center of mass will affect control of landing stability in the subsequent step.

5.2.5 Objective Function Generation

To describe how well any given swing trajectory over an obstacle meets the characteristics defined above, it is necessary to generate a quality metric (or objective function) by which the overall trajectory characteristics can be ranked. Two approaches for defining such an objective function were investigated. The first approach (referred to

as Method A) was to define a weighting function for each of the four trajectory characteristics described above, and then obtain an overall scalar metric for the trajectory as the product of the weights for each characteristic. The second approach (Method B) was to fit a third order polynomial to the experimentally measured average toe trajectory, and compute the objective function value as the sum-of-squared-errors between the optimization model results and the polynomial fit to the average experimental foot trajectory. The comparision of the two methods could show that how good the four posulated objectives in method A produced the experimental toe trajectories. Method A, however, carried the advantage of considering the ceneter of mass location with respect to the toe of the swing limb.

The weighting functions used to quantify each of the four trajectory characteristics for Method A of the leading limb, are shown in Figure 5.5. These weighting functions were designed in a somewhat intuitive manner, although there is a logical rationale for their profiles. Figure 5.5a shows that a toe clearance of 0.1 m is most desirable, with lower clearance being severely penalized, while greater clearance is simply less efficient. Figure 5.5b weights the stability of the landing; a distance of 0.2 m was deemed optimal, with a shorter distance being severely penalized, while a longer distance is satisfactory but somewhat less desirable. Figure 5.5c weights the maximum toe elevation as a function of the distance to the obstacle (for an obstacle at 0.78 m from toe-off). Ideally, the maximum toe elevation occurs over the obstacle, with an increasing penalty for large elevations early or late in the trajectory. Figure 5.5d weights the step length, based on a nominal desired step length of 1.25 m. For any given trajectory, these four weighting functions are used to provide four weighting factors for that trajectory. The product of these weighting factors yields a quality metric that is used to rank the trajectory, the negative of which is the objective function value to be minimized.

5.2.6 Optimization

The goal of the optimization was to find a vector of parameter values describing the temporal muscle activation profiles and initial conditions that resulted in a trajectory for which the objective function was minimal. The general form of the minimization problem solved was:

$$\begin{aligned} \text{minimize} \quad & f(X) = \{f_1(X),\, f_2(X),\, \ldots,\, f_k(X)\}^T \\ \text{subject to} \quad & g_j(X) \leq 0 \quad j = 1, \ldots, m \\ & X \in R^n \;\&\; f_i : R^n \longrightarrow R \quad i = 1, \ldots, k \end{aligned} \tag{5.3}$$

where $X = (x_1, x_2, , x_n)$ is an n-dimensional vector of decision variables (muscle pulse parameters and initial conditions), $f_i(X) = f_i(x_1, x_2, \ldots, x_n)$, $i = 1, \ldots, k$ (the four weighting functions of Figure 5.5), and $g_j(X) = g_j(x_1, x_2, \ldots, x_n)$, $j = 1, \ldots, m$ (muscle force and pulse duration upper and lower limits) are real-valued non-linear functions [69]. Each constraint was added as penalty a function. In this way, both direct unconstrained methods and secant methods could be formulated using same constraint functions. The added constraints were:

- Muscle forces must have positive values (i.e. tensile).
- The maximum stress for each muscle cannot exceed $35 kg/cm^2$ [83].
- The minimum pulse duration is 60 ms (time taken for muscle twitch).

The constraint vector, $\{\lambda\}$, is:

$$\lambda_i = \frac{100}{1 + exp((p_i - b_i) \times s)} \qquad i = 1, \cdots, 8 \tag{5.4}$$

where the control parameter vector, $\{p\}$, is:

$$\{p\} = \{t_{bs}, t_{rs}, t_{bd}, t_{rd}, \sigma_b, \sigma_r, -\sigma_b, -\sigma_r\} \tag{5.5}$$

where t_{bs}, t_{bd}, and σ_b are the start time (ms), duration (ms), and tension (kg/cm^2) of biceps femoris. t_{rs}, t_{rd}, and σ_r are the start time (ms), duration (ms), and tension (kg/cm^2) of rectus femoris. The upper/lower bound vector, $\{b\}$, is defined as:

$$\{b\} = \{0, 0, 60, 60, 35, 35, -35, -35\} \tag{5.6}$$

The kinetic constraint, λ_9 is:

$$\lambda_9 = \frac{|f_{rectus} + f_{biceps}|}{1000} \tag{5.7}$$

where f_{rectus} and f_{biceps} are the force pulse magnitude for rectus and biceps femoris muscles (N).

The final objective function, M_f, is:

$$M_f = \sum_{i=1}^{9} \lambda_i + W_t \tag{5.8}$$

where in method A, $W_t = \prod_{i=1}^{n} W_i$ (n is the number of weighting functions W). In method B, W_t is the sum-of-squared-errors.

The exponential functions for each constraint were designed to ensure that the penalty function would become active only at points close to the limits of the constraint function. The kinetic constraint was divided by a large value (1000) to ensure that any stress minimization could be performed only after other objectives were generally satisfied.

Two direct search procedures were investigated: the non-linear simplex method [56], and a multi-directional search algorithm [79]. The BFGS secant update method [26] was also examined. Direct search methods were found to be more stable for this work, since secant methods require gradient information and are based on approximating and updating the Hessian matrix (matrix of second derivatives), while direct search methods do not use gradient information. This attribute of direct search methods is important, since the model requires simultaneous numerical integration

of the equations of motion, and the analytical calculation of partial derivatives is not possible. While finite difference approximations could be used, the accuracy with which the objective function values could be calculated was limited by accumulating errors in the numerical integration of the equations of motion; this made the finite difference approximations unreliable, and resulted in instability in the optimization. Ultimately for the simulation of the trailing limb, the simplex method was used, while for the leading limb optimization the method was improved by using a multi-directional search algorithm from reference [79].

A disadvantage of numerical optimization methods is the computational effort required, which is directly related to the number of iterations required to find the final solution, and thus depends on the problem size. However, on observing the effect of the control inputs on each of the trajectory objectives, it became evident that general trends could be tabulated (Table 5.1). This table was used to guide the optimization towards the field of attraction of the global minimum, as our problem included several local minima. This separation of objectives and their causality not only assisted us in better understanding the problem, but also resulted in faster convergence by driving the problem towards the field of attraction of the global minimum. Note that as the desired objectives were known (the weighting functions and their maxima in Figure 5.5) the desired or minimum was known.

5.3 Results

The simulation was performed for both the trailing limb (when the obstacle is encountered in early swing) and leading limb (when the obstacle is encountered in mid to late swing). The focus of this study was on the effect of each objective and the selected control inputs on the swing limb trajectory over the obstacle. Each optimization is validated by its closeness of fit to either the objective functions which are based on experimental observations [63] (see methods section d) or the polynomial fit to the average spatial kinematic toe trajectory taken from reference [63].

		Y_{toe}	X_{Ymax}	X_{toe}-X_{CM}
biceps femoris	Peak force ↑	↑	↓	↓
	Start time ↑	↓	↑	↑
rectus femoris	Peak force ↑	↓	↓	↑
	Start time ↑	↑	↑	↓

Table 5.1: **Sample rule base used for guidance of the optimization procedure towards the global minimum. The table demonstrates the effect of start time and force pulse amplitude of the two bi-articular muscles on the toe clearance over the obstacle (Y_{clear}), location of maximum toe elevation ($X_{Y_{max}}$), and the measure of landing stability ($X_{toe} - X_{C.M.}$). The upward arrow indicates increase in value of each quantity shown.**

To reduce the number of initial conditions that should be included as control inputs in the optimization problem, a sensitivity analysis was performed to find the relative effect of the initial velocities on toe clearance. Five values of stance limb velocity at toe-off between -1 and -3 rad/s were evaluated, as well as 20 values (over 0 to 5 rad/s) for the swing thigh angular velocity, 20 values (over -4 to -1 rad/s) for the swing shank angular velocity, and 3 values (over 0 to 5 rad/s) for the swing foot. The results of this analysis revealed that stance limb initial velocity dominantly influenced stride duration with little effect on toe clearance. The hip and knee angular velocities of the swing limb, however, had a significant effect on the toe swing toe elevation. Hence the optimization study focused on these two angular velocities as well as the active torques of the bi-articular muscles. All other parameters and anthropometric data were set to values given in reference [83].

The obstacle location from toe-off was varied such that the swing limb encounters the obstacle either in early swing or mid to late swing. We step over the obstacle first with the lead limb followed by the trailing limb. The first series of simulations with the obstacle stepped over in early swing corresponds to the trailing limb while the second series corresponds to the leading limb. The simulation results are described next.

5.3.1 Trailing limb stepping over obstacles

The initial states (angular velocities and displacements at toe-off) were set to typical values of normal locomotion [83] and the bi-articular muscle forces were optimized. To investigate the relative importance of the stride length and landing stability objectives, three combinations of objectives were examined by computing the objective function as the product of *i*) objectives (a), (b), (c), and (d) in Figure 5.5, *ii*) objectives (a), (b), and (c), *iii*) objectives (a) and (c). The obstacle distance was set to 25 cm from toe-off, with an obstacle height of 15 cm. In general, it was found that removing either the stride length objective (d) or stability objective (b) had little effect on the optimization result in the sense that a stable landing is achieved in either case.

However, removing both resulted in unstable landing, although the other two objectives were achieved (Figure 5.6). The optimization model shown in Figure 5.6a has a toe clearance of 10 cm and the location of maximum toe clearance is at 25 cm (The objective weighting function reached 100% of its maximum). However, the stability margin (the measure of landing stability as shown in Figure 5.4) was -13 cm. The three objectives in the model shown in 5.6b have values of 9 cm for toe clearance, 27 cm for the location of maximum toe clearance, and 15.5 cm for the stability margin. The desired value for the stability margin was chosen to be 15 cm and that for the location of maximum toe elevation at 25 cm from toe- off. The objective weighting function reached 91.4% of its maximum.

Using three objectives (obstacle clearance, location of maximum toe elevation, and landing stability, i.e. *ii*) above) the effect of obstacle location was investigated. The 15 cm obstacle was located at 15, 25, and 35 cm from the toe-off location of the swing limb. The results for 15 and 25 cm distances are shown in Figure 5.7 and optimal muscle force parameters are tabulated in Table 5.2. The kinematic characteristics found for the models in Figure 5.7a and 5.7b respectively are as follows: toe clearance 9 cm and 8.5 cm (target 10 cm), location of maximum toe elevation 27 cm (target 25 cm) and 17 cm (target 15 cm) from toe-off, with a stability margin 15.5 cm and 16 cm (target 15 cm). The objective weighting functions reached 91.4% and 89% of their maximum. From Figure 5.7 it is evident that a successful swing is achieved for both obstacle distances, although the nearer obstacle results in a shorter stride. Table 5.2 indicates greater muscle effort required when the obstacle is encountered earlier in the swing (at 15 cm). Biceps femoris effort increases to get the toe rising more rapidly while rectus femoris pulses earlier and somewhat stronger in order to limit the toe clearance over the obstacle to the desired value, place the location of maximum toe elevation over the obstacle, and extend the swing knee to provide landing stability.

When the obstacle distance was increased to 35 cm (pushing it more towards mid swing) obstacle clearance and landing stability could not be satisfied simultaneously; several local minima were found, corresponding to compromised maximum

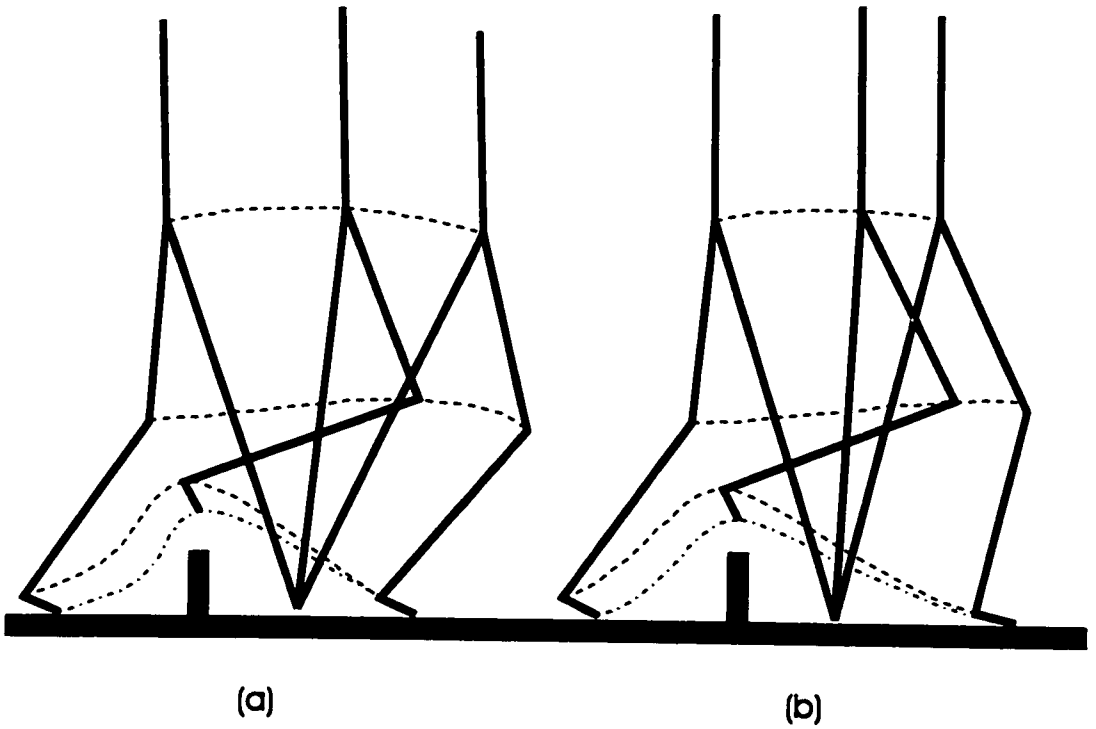

Figure 5.6: **Stick diagrams for trailing limb stepping over an obstacle when (a) only the objective functions for toe clearance over the obstacle (Y_{clear}) and the location of maximum toe elevation ($X_{Y_{max}}$) are used, (b) three objectives (except the stride length objective) are used. For each stick diagram stance limb, trunk, swing thigh, leg, and foot are shown. The dashed lines represent the joint and toe trajectories. The stick diagrams shown represent toe-off, mid-swing at maximum toe elevation, and end of swing (landing). Note the unstable landing of simulation (a) where the center of mass is ahead of the leading toe position.**

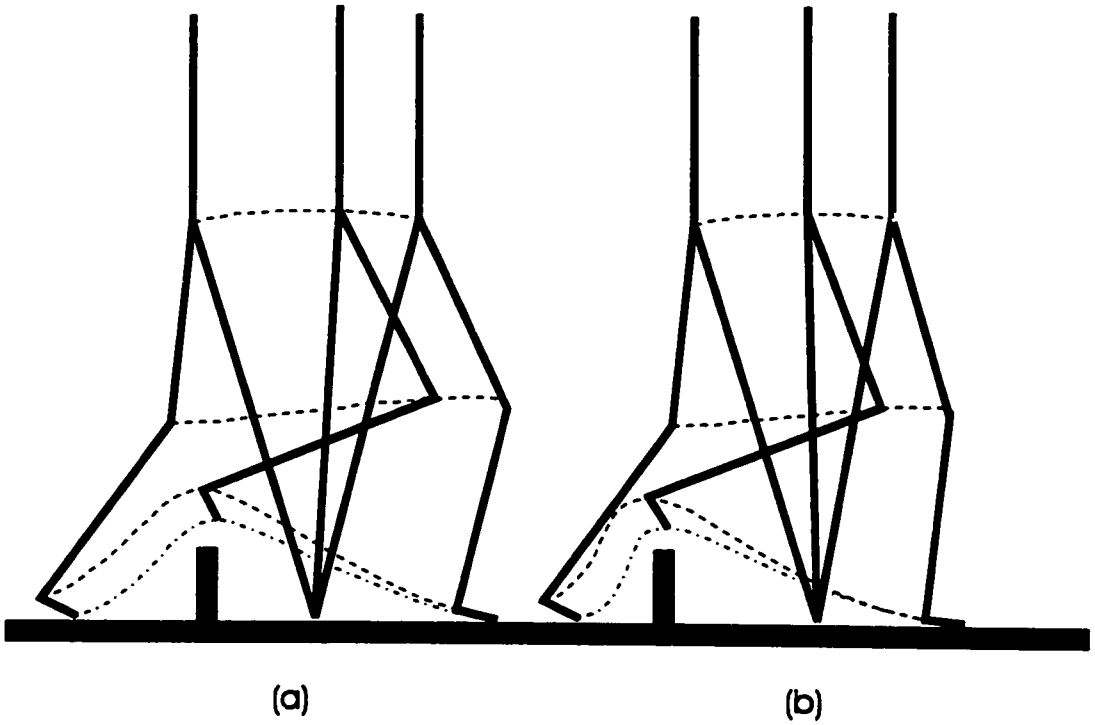

Figure 5.7: Stick diagrams for trailing limb stepping over an obstacle for: (a) three objectives except the stride length objective are used, and the distant between toe-off location and the obstacle is 25 cm; (b) three objectives except stride length objective are used and the distance between toe-off location and the obstacle is 15 cm. For each stick diagram stance limb, trunk, swing thigh, leg, and foot are shown. The dashed lines represent the joint and toe trajectories. The stick diagrams shown represent toe-off, mid-swing at maximum toe elevation, and end of swing (landing). Both simulations satisfied all three objectives by optimizing peak force and start time for rectus femoris and biceps femoris.

Toe-off to Obstacle Distance (cm)	Muscle Force Parameters					
	Magnitude (N)		Start Time (s)		Duration* (s)	
	BF.[1]	RF.[2]	BF.[1]	RF.[2]	BF.[1]	RF.[2]
25	305	992	.01	.18	0.1	0.1
15	488	1055	.01	.10	0.1	0.1

[1]BF. Biceps Femoris [2]RF. Rectus Femoris * Duration fixed during simulation

Table 5.2: **Control inputs for the trailing limb stepping over obstacles: (a) when all objectives except stride length objective is used and obstacle is located at 15 cm from toe-off location; (b) when obstacle is located at 25 cm from toe-off location. The control inputs that are not shown were kept constant.**

toe height location and landing stability. The rectus femoris force was also found to reach the maximum physiological limit set, although even without this upper limit, a stable landing could not be achieved. However, when the stability objective was removed for this obstacle location, the rectus femoris force decreased significantly. This demonstrates that rectus femoris plays a major role in satisfying the landing stability objective in this configuration.

From the above scenarios, it is possible to characterize the general effect of each control input on the objectives. Table 5.1 shows the effect of four of the control inputs on three of the objectives. For instance, increasing the amplitude of the biceps femoris force resulted in increasing the toe clearance, while the location of the maximum toe clearance moved backwards, and the distance between the center of mass and toe at landing (indicator of stable landing) reduced. Such tables were used to guide the optimization algorithm towards the field of attraction of the global minimum. This approach was found to be very successful in directing the optimization method

towards the global solution. Since method A was successful in achieving the objectives for the trailing limb trajectory, method B was not explored.

5.3.2 Leading limb stepping over obstacle

The experimental angular displacements and velocities for normal gait were used to initiate the swing. Single pulse activity for each muscle group was considered, and the parameters of the non-linear dampers were set to partially cover the function of biceps femoris activation during late swing. Using these initial conditions and applying all four objectives, it was not possible to both clear the obstacle and have a stable landing with single pulse bi-articular muscles. Figure 5.8a shows one locally minimum solution in which landing stability and step length are satisfied, but the foot failed to clear the obstacle. Relaxing the physiological constraint on maximum muscle force was by itself insufficient to clear the obstacle. By both removing the location of maximum toe clearance objective and relaxing the physiological constraint on maximum muscle force (i.e removing the objective related to the efficiency), the obstacle could be cleared. However, the resultant toe trajectory (Figure 5.8b) was very different from any experimentally observed trajectories. We found that by just removing an objective, the resultant optimized trajectory either failed to clear the obstacle, or was markedly different from experimental trajectory (Figure 5.8b). Therefore the problem is not with the chosen objective criteria, but rather with insufficient control inputs.

The initial angular velocities at toe-off are the result of the active control of muscles during the double support phase, and the values used above corresponded to those for normal walking. The angular velocities of the swing limb hip and knee were therefore included as control inputs to be optimized, together with the bi-articular muscle force inputs. The resultant trajectory is shown in Figure 5.8c and clearly achieves all four objectives. However, the toe trajectory is different from that found by a polynomial fit to the experimentally measured data (shown by the dashed line in Figure 5.8c), and the knee joint can be seen to move backwards at the end of the swing phase, which was not observed in experimental data [63]. The solution values of the initial conditions

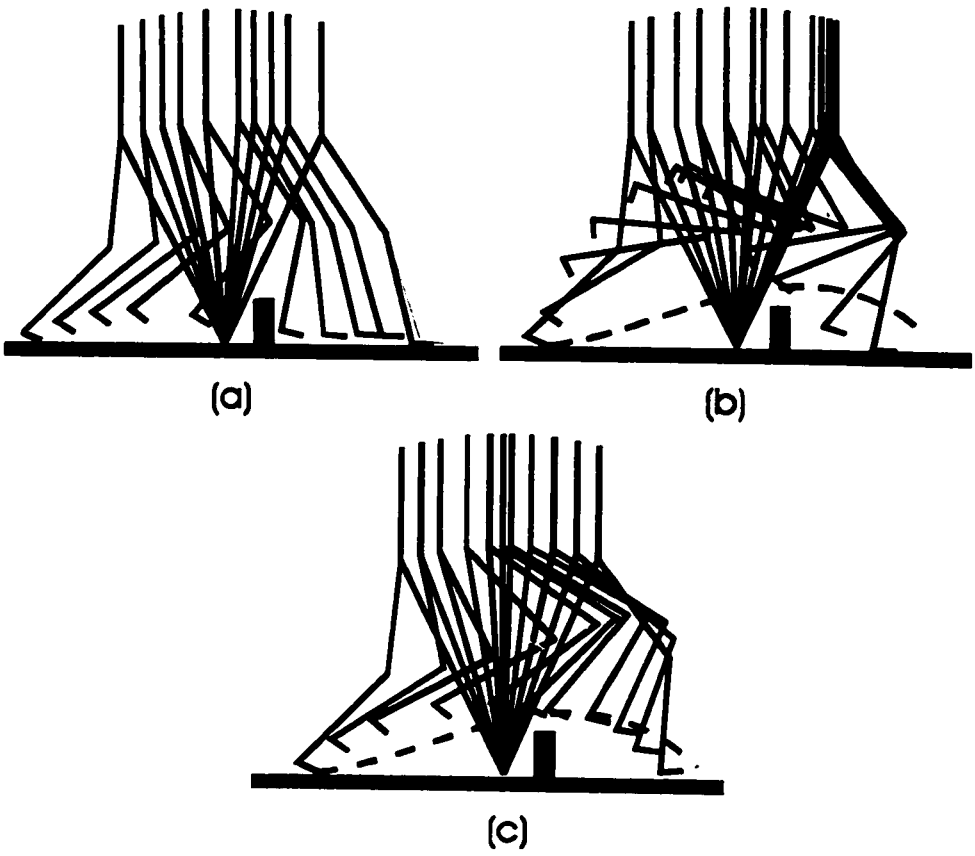

Figure 5.8: Stick diagrams of solution trajectories for the leading limb: (a) when only bi-articular muscle forces are optimized. Note that stride length and landing stability objectives are satisfied while toe clearance over obstacle and the location of maximum toe elevation objectives are not; (b) when location of maximum toe clearance objective and physiological constraint on maximum muscle force are relaxed. Note the trajectory differs markedly from the experimentally observed data (shown by the dashed line); (c) when angular velocities of the swing hip and knee at toe-off are also optimized. Each individual objective is satisfied, although the trajectory differs from the least squares polynomial fit to experimentally observed data (shown by the dashed line). Each instant of the stick diagram includes the stance limb, trunk, swing thigh, leg, and foot. The time interval between each two consecutive stick figures is 45ms (except for the last three instances of (b) where the time interval is 20 ms).

and muscle parameters are given in Table 5.3 (Method A). The optimization results in a toe clearance of 11.3 cm (target 10 cm), the location of maximum toe clearance at 72 cm (target 78 cm), a swing length of 128 cm (target 125 cm), and a stability margin of 28 cm (target 20 cm). The multiplication of the objective weighting functions reached 81% of its maximum. For the purpose of comparison, Method B was also used to determine the initial conditions and muscle parameter values that resulted in the toe trajectory matching the experimental trajectory (a least squares third order polynomial fit to experimental data) as closely as possible (with a resultant RMS error of 0.84 cm). The optimization resulted in a toe clearance of 14 cm, the location of maximum toe clearance at 82 cm, a swing length of 126 cm, and a stability margin of 13 cm. The resultant control input values are given in Table 5.3. The initial velocities are clearly too large for both methods, with the exception of the knee velocity for Method B (3 rad/s for the hip and -3 rad/s for the knee is typical). The much lower biceps femoris force required for Method A is primarily due to the much higher initial knee velocity. Also, there is no co-contraction in the solution using Method B, while this is significant in the solution using Method A. The low stability margin for Method B indicates the closeness of the hip to the leading toe at landing.

5.4 Discussion

Our goal was to use multi-objective optimization approach to understand what the CNS is trying to control during adaptive locomotion over uneven terrain and how it achieves that using the many options available. Both the successes and failures of the simulations have been illuminating in this respect.

Consider first the issue of what the CNS is trying to control. Both methods of arriving at the objective function require that several objectives be simultaneously satisfied. In the first method (A) the objectives are explicitly identified, while in the second method (B) matching of the end point trajectory indirectly includes not only the objectives in the first method but also probably others (except the stability

Method	Muscle Force Parameters						Angular Velocity at Toe-off (rad/s)	
	Magnitude (N)		Start Time (s)		Duration (s)			
	BF.[1]	RF.[2]	BF.[1]	RF.[2]	BF.[1]	RF.[2]	Hip	Knee
(A)	408	252	.29	.35	.16	.3	5.5	-5.7
(B)	808	105	.10	.20	.07	.05	6.4	-3

[1]BF. Biceps Femoris [2]RF. Rectus Femoris

Table 5.3: **Control inputs for the leading limb stepping over obstacles. A comparison of methods A and B shows that the latter method favorably produces smaller knee initial angular velocity, minimal co-contraction and shorter duration of rectus femoris activity. For the angular velocities at toe-off positive signs indicates hip flexor velocity while negative sign indicates swing knee flexor velocity.**

criteria). The only attempt in the literature that we are aware of, which has used a single criterion optimization method to generate limb trajectory over obstacles, has not been very successful [15]. Patla and Rietdyk [63] have described how tripping and slipping are avoided during this adaptive locomotor behavior, and identified key kinematic measures that capture this control. Based on this experimental evidence and interpretation we have outlined the multi-objectives that have to be met. Success of both methods of generating objective weighting functions in producing the appropriate trailing and leading limb trajectory over the obstacles in this apprach, clearly show that the CNS is not optimizing a single objective, but rather several objectives.

When one of the two objectives related to stable landing is removed, the resultant trailing limb trajectory is still found to be adequate. This suggests that control of limb trajectory over obstacles encountered during early swing is relatively simpler since fewer objectives have to be satisfied. In contrast, when we compare the simulations for the leading limb (obstacle encountered in the late swing phase) we find that both methods (A and B) can lead to an adequate global solution. However, neither the knee trajectory (Method A, Figure 5.8c) nor the stability margin (Method B) was close to experimental values. This indicates that when an obstacle is stepped over during late swing, the objectives included are necessary but not sufficient; further objectives such as landing velocity (related to avoidance of slipping) may have to be considered.

Next we turn our attention to how the CNS achieves its goal of satisfying multiple objectives. The large number of muscles involved in the control of locomotor behavior theoretically provides the CNS with a large number of options. We have chosen to focus on a subset of key control inputs that were based on the experimental data available in the literature. Research has shown, for example, that rotational power at the knee and not the hip joint is key to swing limb flexion [50], and this is reflected in the dominant modulation of the biceps femoris activity during the early swing phase [63]. In contrast, rotational work done at the hip joint rather than at the knee joint following limb elevation, is critical for stable landing [61] and is reflected in rectus

femoris activity during the late swing phase [63]. It is for this reason that we have focused on single pulse activity of these two bi-articular muscles. Appropriate separation of the activity of these two muscles in the simulation, with earlier biceps femoris activity followed by rectus femoris activity, supports the experimental evidence. That activity of rectus femoris is related to control of stability during landing is confirmed when removal of the stable landing objective leads to reduction in its activity. Rectus femoris also contributes to positioning the maximum toe clearance over the obstacle. Therefore, it is active even without the stable landing objective, although to a lesser extent.

For the leading limb, inclusion of single articular muscles in the model might not have reduced the significance of the initial conditions at toe-off. The major deficiency in the optimization of the leading limb was locating the maximum toe clearance over the obstacle. This could be achieved by modifying initial conditions and not by active control during swing phase. However, such possibility needs to be investigated in more detail.

While CNS control exerted during the swing phase alone through the activation of these two bi-articular muscles is adequate for the trailing limb, it was not enough for the leading limb. Initial conditions at toe-off had to be included as additional control inputs. Empirical work has shown that hip hiking achieved through translational work at the hip joint is an important additional contributor to swing limb elevation [61]. Our biomechanical modelling work has shown that effective hip elevation is in part due to the forces initiated during the double support phase, and this can be captured in the hip and knee joint angular velocities at toe-off. Thus successful simulation of lead limb trajectory over an obstacle when hip and knee joint angular velocities are included as input parameters supports experimental evidence.

The criteria chosen to rate the quality of any particular swing trajectory are not exclusive, nor are the shapes of the weighting functions used to describe their relative distribution. As previously stated, all four criteria are required for successful leading limb trajectories over obstacles. While adjusting the strength and distribution of

the weighting functions may refine the optimized trajectories, the number of control inputs or objectives cannot be reduced.

Finally we note an observation made on static optimization models which were mostly concerned with partitioning the joint torque, calculated from inverse dynamics, to muscle forces spanning that joint. Collins [16] and Buchanan and Shreeve [13]. (for wrist and elbow) showed that the choice of many kinetic cost functions used in the literature had minimum effect on the optimization results. Collins [16] suggested the use of more than one criterion for optimization, while Buchanan and Shreeve pointed out the strong dependence of muscle coordination on the number of degrees of freedom at the elbow and the shoulder joint that are satisfied [13]. In line with these suggestions, we feel a better optimization model should include both kinetic and kinematic criteria. In the long run, a forward approach including kinematic objectives (as opposed to an inverse dynamics approach) combined with kinetic objectives can provide better insight to the solution to the redundancy problem in both skeletal system and the muscles.

5.5 Conclusions

A multi-objective optimization approach based on kinematics objectives has been presented. This optimization approach demonstrates that the use of biceps femoris and rectus femoris is adequate for stepping over obstacles when encountered in early swing. However, if the obstacle is encountered in late or mid-swing, then additional active control prior to the toe-off (role of initial conditions at toe-off) become important. The manual guidance of optimization, using tables such as Table 5.1, provides a fast means of converging to a global minimum and avoiding local minima. A fuzzy logic approach using the sample rule base (Table 5.1) can automate the manual guidance process, and is a promising tool for finding the global minimum. Finally, in order to find better solutions to the redundancy problem in skeletal system and muscle actuators, optimization approaches have to evolve their objectives to include both

multi-objective kinematic criteria and dynamics of the movement.

Chapter 6

Neuro-Fuzzy-Genetic Optimization: Models of the Proactive (feed-forward) Control System

A human ambulator continuously develops and modifies the relationship between the external world and the movement dynamics of its own components through the use of various sensory systems. For a novice ambulator, an obstacle in the path is hit frequently when first encountered. This may be due to the lack of internal representation of the obstacle and/or the limb movements required to avoid it. Through several exposures and trials, coordination of limb movements to avoid the obstacle is learned. This skill is developed with practice and multiple exposures to similar situations, and limb coordination becomes more stereotypical and automatic.

The objective of this work is to develop a connectionist representation of a novice ambulator who after performing several trials, learns to associate visual inputs of the obstacle size and location with respect to the limbs. The ambulator then learns to produce the muscle forces and joint velocities required to step over the obstacle. This is done within a feed-forward network of neurons.

6.1 Motivation

The purpose of developing this model is twofold: first to develop a more powerful tool for addressing the biomechanical and motor control issues involved in stepping over obstacles, and second to develop learning algorithms that could be expanded to include a whole range of activities in addition to obstacle avoidance strategies.

Results of many experiments show that the strategies used by humans to step over an obstacle may vary from person to person, as well as between two trials made by the same person. When the performance of stepping over a single sized obstacle at a certain location is desired, numerical optimization models usually lead to a unique optimal solution. A more desirable learning method however, is to be able to provide a pool of possible strategies (or a pool of some of the possible solutions to the optimization problem). This characteristic could be achieved with the use of genetic programming which is used in this chapter. We use this characteristic to continue our investigation on the strategies used for stepping over obstacles. The questions we wish to address are as follows:

1. How does active control of muscle forces during the double support phase affect the requirements of active control during the swing phase?

2. Why does the human ambulator favor a 60% obstacle location to stride length ratio when the leading limb steps over the obstacle?

3. Does genetic optimization confirm the experimentally observed correlation between hip elevation energy and obstacle height [63]?

4. When is the use of active control during swing phase most crucial?

In the previous chapter, we used optimization routines to find an optimized combination of muscle forces and joint velocities at the start of the swing phase, used to perform the obstacle avoidance task while satisfying certain objectives. In this chapter neural weightings and activation functions are determined and used to enable the

ambulator to step over any height obstacle at various locations, without requiring a separate optimization for each new set of sensory inputs. Here, the model is not concerned with optimal performance over a single sized obstacle (fixed behavior); rather, it is concerned with a satisfactory performance over a range of obstacle sizes (adaptive behavior).

Often the goal of the ambulator is not to excel in the independent performance of a single task, such as stepping over an obstacle. We seek to improve the performance of this task within a more general framework; that is, the specific requirements of the external world. A better learning model of stepping over obstacles should keep venues open for further expansion and inclusion of its superset of behaviors. A combination of the expert system and adaptability is required for specific tasks as well as for more general decision making problems (Figure 6.1). For instance, based on learning and adaptation, an expert system for the task of stepping over an obstacle could be developed. However, this expert system must function within the obstacle avoidance network, which is another expert system because its parameters have also been learned and adapted to the more general requirements for the external world; such as, should the ambulator step over the obstacle or steer clear? These blocks have different responsibilities with different input and outputs, but may have the same structure that has been copied repeatedly. The immediate advantage of such a repeatable network is that its functionality and decision making capabilities can be expanded and adjusted to the requirements of the external world. We follow the assumption that the goal of learning in the intelligent system is to adapt the parameters to produce more generalized rules for a more robust system, parallel to developing certain specific skills.

6.2 Related Research

In the optimization chapter we reviewed the literature for the use of optimization routines for obstacle avoidance strategies and solving redundancy problems in muscle

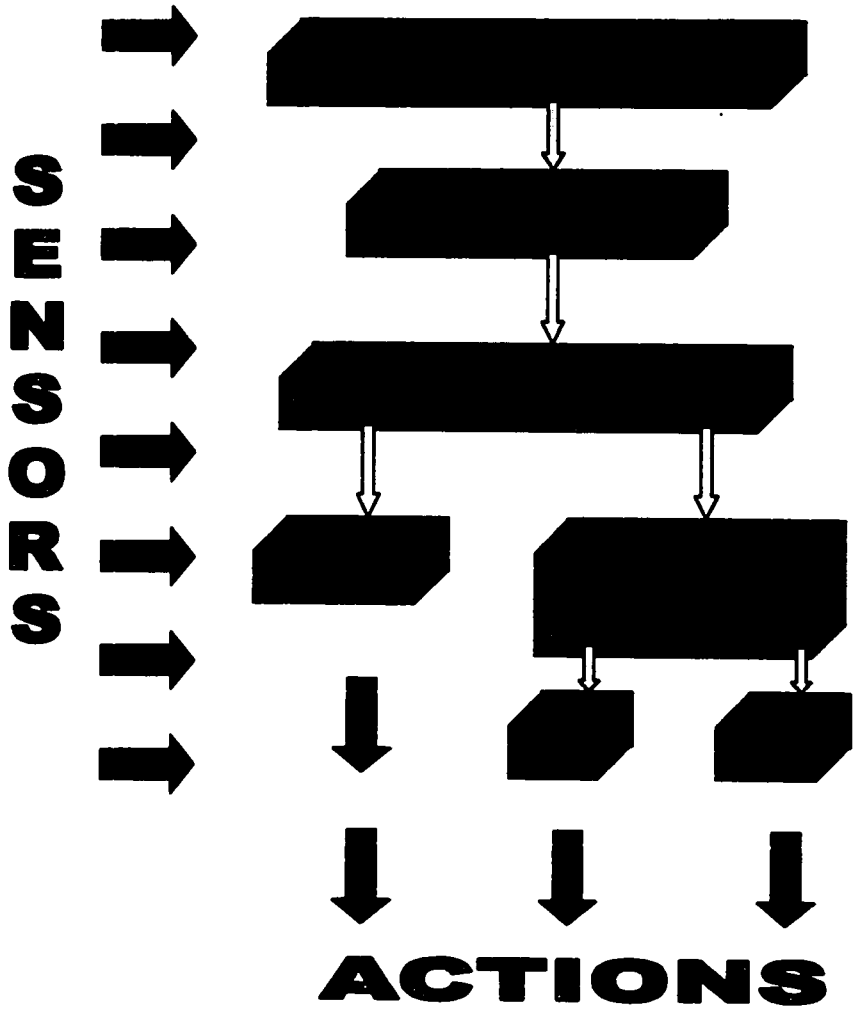

Figure 6.1: A simplified model for locomotion based on subsumption architecture [12]. All layers shown receive all the sensory information, however, they use this information selectively.

actuators spanning one or several joints. In this section we review some of the other research that has inspired this work, and are most related to the methodology used here.

Brooks [12] proposed that instead of building systems that intend to cover the complete range of activities, one should follow an incremental path from simple to complex behaviors. Each parallel behavior shown in Figure 6.1 is a complete subsystem in itself, featuring sensing, reasoning, and acting. Each parallel behavior represents a layer of control. Each layer can monitor and influence the behavior of the layer below it. Once such behavior is adapted, it remains unchanged and covers a particular aspect of the whole system's behavior. In Brooks' proposed subsumption architecture, not all sensors need to feed into a central representation. At the same time, however, such information may still be used by the robot. Other layers of control may use the results to achieve their own goal independent of how other layers may use them. Angle and Brooks [4] applied this architecture to a six-legged robot named Attila. Each leg had three degrees of freedom, an active whisker, a gyro-stabilized pan-tilt head carrying a range finder and a CCD camera, 10 onboard processors, and over 150 sensors. Our hypothesis fits well in the subsumption architecture. Each of the parallel behaviors shown is a superset level in which its structure is a copy of the obstacle avoidance level. Their outputs, as shown, ultimately influence the actuators via the obstacle avoidance level (element of motivation as described in our hypothesis).

Beer [7] proposed that planning, as typically formulated in AI, is fundamentally intractable in real life situations. The approach that he took was similar to that of Brooks except in "the choice of agent (physical robot vs. simulated insect), control scheme (network of augmented finite state machines vs. neural networks), and degree of biological inspiration". Beer's work showed that relatively simple networks of neurons are capable of producing the required motion of a hexapod. He simulated the central pattern generators (CPG) of an insect and obtained a variety of insects walking patterns. His control system simulated insects' behaviors including locomotion,

wandering, edge following, and feeding. It was capable of organizing its behavioral receptors in a variety of ways to meet environmental demands. Beer differentiated between adaptation and learning, but did not include learning in his simulation. The *biologically inspired* controllers of the insect were fine tuned by trial and error.

Edelman [24], in his theory of neuronal group selection, argues that the world does not come pre-labeled in particular categories that are directly represented in the brain. Rather, an animal must form appropriate categories itself, and constantly update them as it confronts the external world. He hypothesized that groups of neurons undergo a selection process similar to that of populations of organisms during evolution. Simulations with his DARWIN software produced a simple organism capable of adaptively interacting with its environment [66].

The work concerned with evolution of behavior widely uses genetic algorithms (GA). One example is the work of Lewis, Fagg, and Becky [47] who used genetic algorithms for stage development of the CPG of a hexapod robot. Their goal was to evolve a biologically inspired neural network to generate a sequence of signals that can drive the legs of the hexapod robot to produce consistent forward locomotion along the body axis. Their approach required careful selection of an intermediate on the way to a goal set. Hence, they designed a biologically inspired objective function satisfying a three-stage evolution process: formation of limb oscillators, coordination of oscillations, and coordination of limbs. The promising results of their work encouraged us to use similar tools for simulation of stepping over obstacles.

6.3 Neural Control of Locomotion

Locomotion is a complex motor task and requires continuous, active control. The role of reactive and proactive control (similar to feedback and feed-forward control), sensory redundancy and confliction, control levels (spinal level, brain stem, and cortex), and substrates such as the cerebellum and basal ganglia is briefly discussed in Appendix C. Obviously, the complete picture of the neural control system is not known.

Even with the existing hypotheses for the functions and roles of neural substrates (see Figure 6.3 in Appendix C), modelling such a system is problematic. Therefore, we started developing our model based on the simplest innate behaviors. We first considered fixed action patterns as a series of stereotyped movements. Then we add a learning ability to the system, in order to make the fixed action patterns adaptive.

A simplified model of the neural organization for fixed action patterns consists of three main blocks (Figure 6.2). The fixed action patterns are typically activated by specific stimuli, called *sign stimuli.* One of the responsibilities of the sensory analyzer is to extract the sign stimuli and their intensity from a series of exposed sensory inputs. This information is directed to the command system. The command system triggers preprogrammed stereotypical motor acts, which are performed by motor pattern generators. These three components are the minimum required for the simplest preprogrammed motor acts. In a simplified analogy, when a human steps over an obstacle, certain features of the obstacle (e.g. height, location, and width) are extracted by the sensory analyzer. It may further perform a rough quantification of these features (e.g. visual observation of a small obstacle). Based on this information, the command system triggers a preprogrammed activation pattern (e.g. activation pattern for biceps femoris). The simplified diagram of the hierarchy of the locomotor control system from that presented by Patla (Figure 6.3) includes two levels of control: supraspinal and spinal. The blocks representing the visual system and somatosensory cortex perform the role of the sensory analyzer (Figure 6.2). The command system is presented by the motor cortex, which is known to be responsible for planning movements. The pattern generators in the spinal neurons are then responsible for motor pattern generation. Addition of learning, however, requires two more blocks.

At least two additional centers are required for learning. The cerebellum (as discussed in Appendix C) participates in motor learning. The storage of this knowledge is presented by another block. It is important to note that this block may not represent any specific substrate. Reflexive memory (forms of perceptual and motor learning that are exhibited by alterations in the performance of tasks), which is of our concern

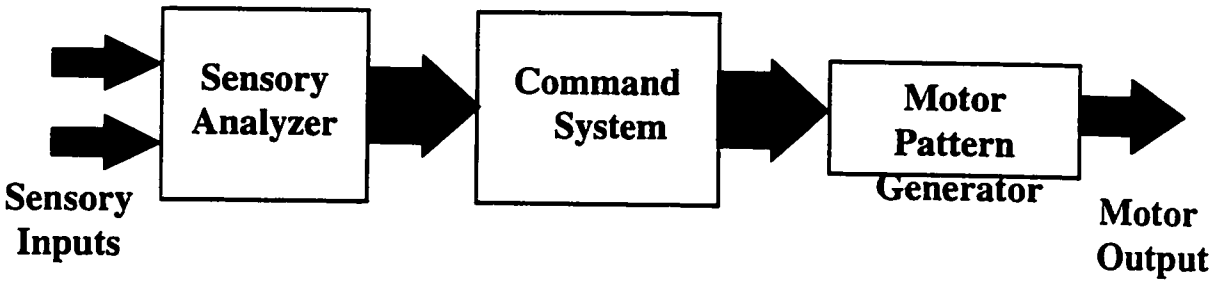

Figure 6.2: **Simplified model of neural organizations for fixed action patterns [43].**

in this work, may be stored in various locations. Learning affects all three blocks of Figure 6.2. Perception of an obstacle can be modified by learning. For the ambulator, the sense of dimension and location of the obstacle is continuously modified and refined. As well, motor plans and motor pattern outputs are also continuously prone to modification and refinement. Therefore, the learning blocks communicate with all levels of control. They not only gather all the afferent and efferent copies (sensory and motor act information), but also synapse to various substrates in order to influence their performance. The learning center (cerebellum) is connected to all other blocks (as shown in Figure 6.3).

Several experiments have shown a human ambulator begins to modify its normal gait a few steps before reaching the obstacle [62]. Although we only model the swing phase of locomotion, the initial joint velocities at toe-off, produced by muscle forces prior to the swing phase of stepping over obstacles, represent the effect of the previous modifications. In addition, previous research and our own modelling work (as will be discussed in chapter 7) suggest that the swing phase is primarily under feed-forward control. Therefore, only feed-forward control is considered in this chapter.

In the following section we develop our model by borrowing and combining a neural network model, fuzzy logic control, genetic optimization, and reinforcement learning. Throughout this chapter we have made an effort to create an analogy between this model and the blocks of the control system shown in Figure 6.3. The analogy we

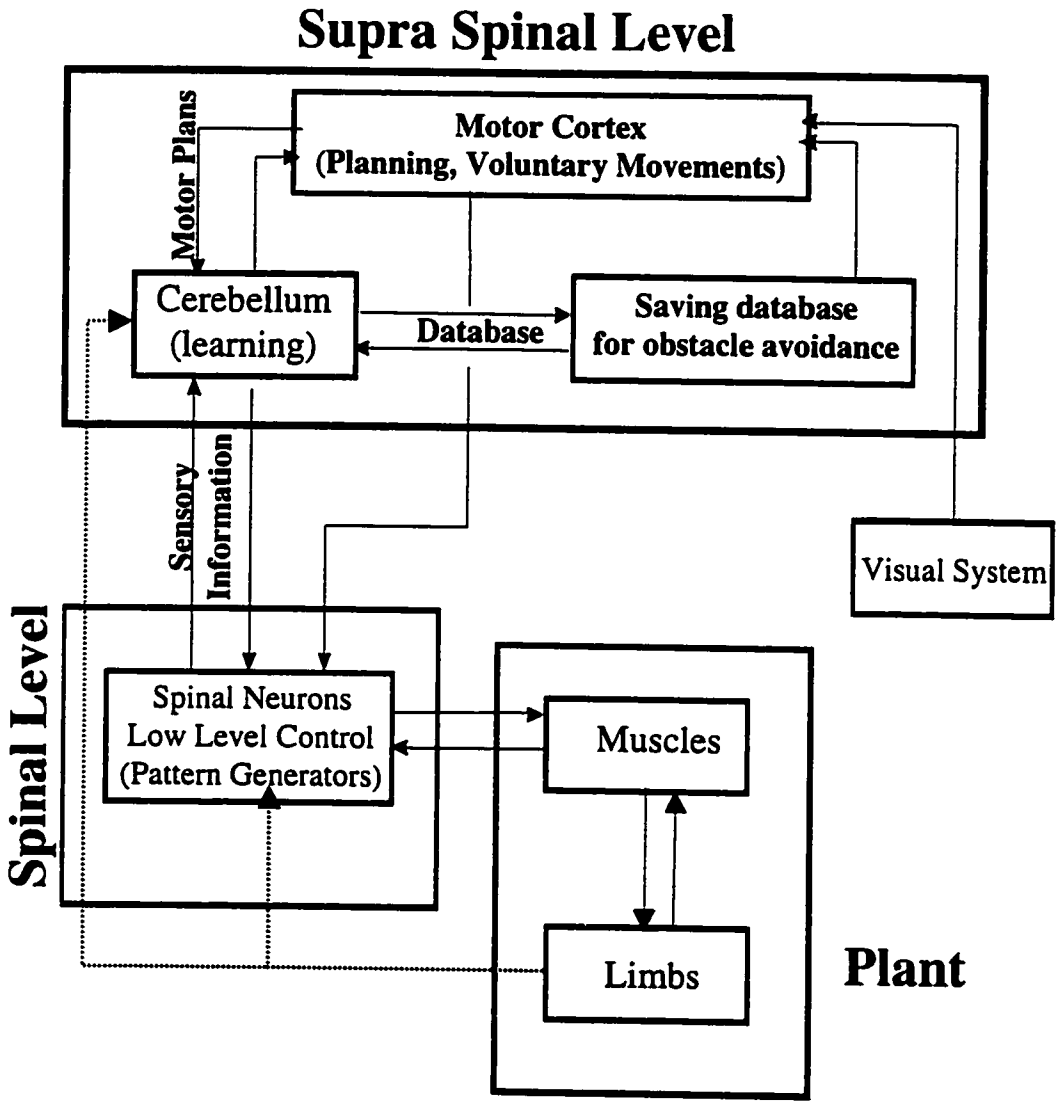

Figure 6.3: **Simplified diagram of the hierarchy of the locomotor control system.**

have made is concerned with the functionality of each block, for the functions that we have just described. (Of course each substrate has far more responsibilities than those considered.). Each block is represented by layers of neurons; however, neither the function nor the structure of the neurons in each substrate has relevance to biological neurons. The type and functions of the neurons are chosen to model a neuro-fuzzy system, as has been developed in the literature [40]. The combination of genetic algorithm and reinforcement learning is novel in the current work.

The three blocks shown in Figure 6.2 relate in spirit to the idea of the fuzzy inference systems. Fuzzy inference is based on a logical system which is closer to human cognition than conventional logic. Its logic captures the approximate nature of cognition within the real world. Fuzzy logic describes the world with linguistic labels (e.g. small, large). The heart of fuzzy expert systems is their linguistic control rules, which are based on an expert knowledge and define the world as a set of if-then rules. Fuzzy inference consists of three mechanisms which somewhat perform functions of the three blocks in Figure 6.2. (Appendix D details some fuzzy architectures): 1) A *fuzzification interface* which transforms crisp sensory input values into degrees of match with linguistic values. The sensory inputs get linguistic values (e.g. small, medium, or large obstacle). 2) A *knowledge base* which includes a series of rules and performs the inference operations on the rules (e.g. if antecedent then consequent). 3) A *defuzzification mechanism* which transforms the fuzzy results to the crisp output values.

Similar to behaviors which are mediated through networks of neurons [43], fuzzy logic could also be embedded through a connectionist model (Appendix E). Based on the cellular connectionism view, individual neurons are situated together in functional groups and connect to one another in a precise manner [80]. Fuzzy logic can be viewed as a parallel neural network where each neuron represents a fuzzy membership function and each synaptic connection represents a weight for a fuzzy rule. The fuzzification, knowledge base, and defuzzification layers are analogous to the blocks in Figure 6.3 (excluding the cerebellum).

Application of the neuro-fuzzy network resolves the problem of defining a connectionist model consisting of individual blocks of Figure 6.3. There is no quantitative information about the input-output relation of the blocks. The information at hand is the visual input of the obstacle and limb locations, and some kinematics measures of body location during and after the swing. If we were to design a feed-forward multi-layer neural network to model stepping over obstacle behavior, the role and physical function of the intermediate (hidden) layers (Appendix E) would not have been known. Application of the neuro-fuzzy network (also known as the adaptive network [40]), is a remedy to this problem. In a neuro-fuzzy network, each layer has a certain function which can define an input-output set.

6.4 The Model

The simulation model used in this work includes a neuro-fuzzy architecture which receives two reference sensory inputs (obstacle height and location). This then generates the required initial velocities at toe-off and the required bi-articular muscle pulses. The neuro-fuzzy network's outputs are applied to a link segment planar model of the human lower limbs (plant). The rule-base (weights) of the neuro-fuzzy architecture is trained by a reinforcement learning architecture, while its membership functions are set by genetic optimization. Figure 6.4 illustrates the model. The details of this model are as follows:

6.4.1 The Simulation Plant

The simulation plant consists of a five degree of freedom planar link-segment model (Figure 6.5). The inputs to this link-segment model include initial angular velocities at toe-off and single pulses of bi-articular muscle forces (please refer to the optimization section 5.2 for the justification of these choices). The anthropometric data (e.g., segment weights, lengths, center of masses) were taken from [83] for a human weighing 60 kg. The initial angular displacements at toe-off were as follows (Figure 6.5):

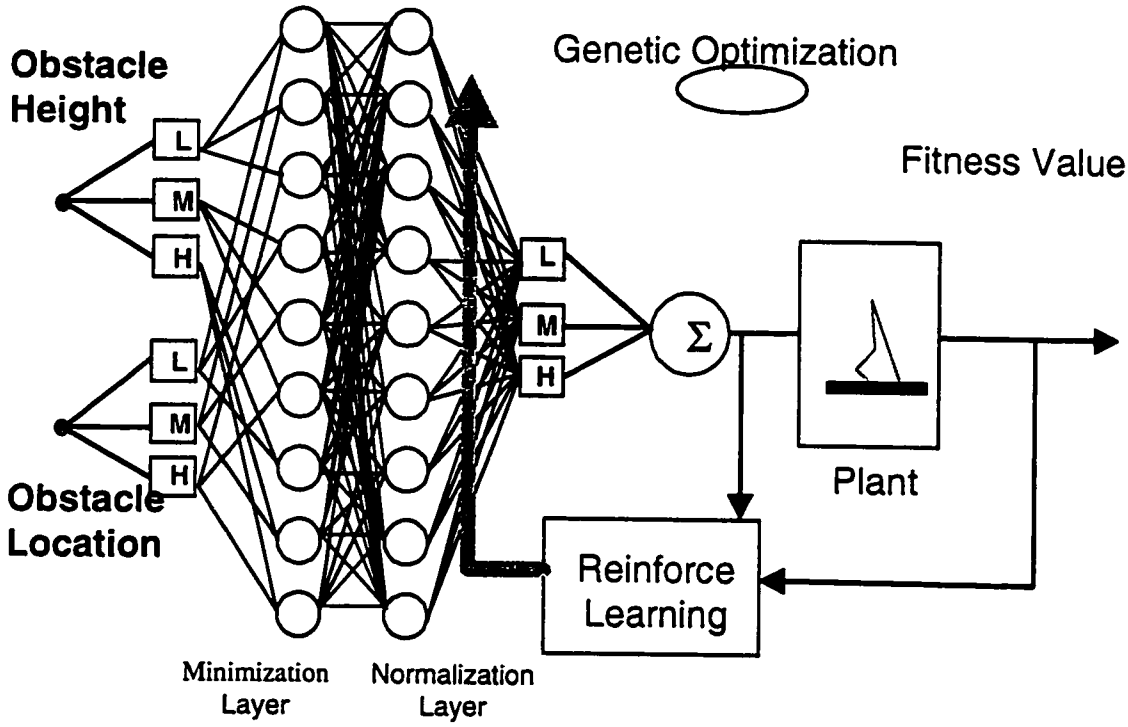

Figure 6.4: **The neuro-fuzzy network with its learning paths. The square nodes refer to the adaptive neurons.**

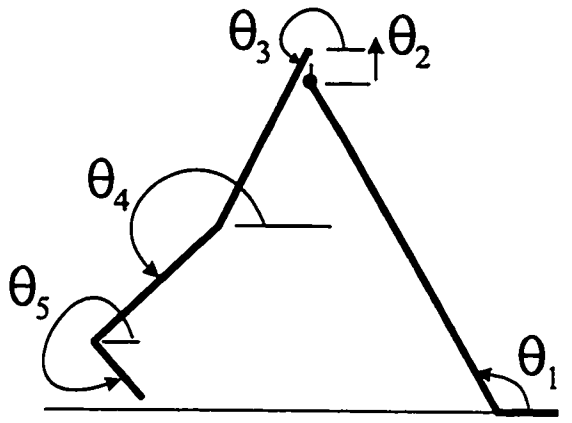

Figure 6.5: **The 5 degrees of freedom model used in the simulation.**

$$\hat{\theta} = \{\theta_1, 0, 4.63, 4.19, 5.76\}\ rad \tag{6.1}$$

where θ_1 was found from the constraint that the swing toe should be at ground level at toe-off.

Each muscle pulse was characterized by five parameters. These parameters were defined in the previous chapter (see Figure 5.2). We kept two of these parameters constant during these simulations: rise time was set at 60 ms, and half relaxation time was set at 100 ms.

The output of the link-segment model is the kinematics of the trajectory. Of the kinematic parameters; toe clearance over the obstacle, location of maximum toe clearance, and landing stability (see Figure 5.4) were calculated and used for developing the fitness value for the genetic optimization. This will be described later.

6.4.2 The Neuro-Fuzzy Architecture

The neuro-fuzzy network (Figure 6.4) is a superset of feed-forward networks. It is similar to a multi-layer feed-forward network [68], except each node performs a particular function on the incoming signal. The choice of the node activation function

depends on the input-output relation that the layer or the node is to carry out. In Figure 6.4, the functions of each of the five layers are as follows (we also make an attempt to create an analogy between the layers and the blocks of Figures 6.3 and D.3):

Reference Inputs

The reference inputs include the sensory inputs captured by vision (obstacle location and height in our case). The crisp value of these references are given by the vector $\hat{x} = \{x_1, x_2\}$ (Figure 6.4).

Layer 1: Sensory Membership Layer

This layer performs the fuzzification on the sensory inputs (similar to the fuzzification interface in Figure D.3). In other words, the degree of membership of each sensory feature (obstacle height, and location) in each of the linguistic sets (small, medium, large) are determined. This can also be translated to determining the activation pattern for each sensory feature (analogous to the sensory feature analyzer block in Figure 6.3). Each neuron in this layer is an adaptive (shown by square) neuron (as defined in Appendix D). Each of these neurons is associated with a linguistic label. In our case, the linguistic labels for obstacle height are: $\{low, medium, high\}$ and for location are: $\{earlyswing, midswing, lateswing\}$. The activation function of neuron i in layer 1 is:

$$O_{1i} = \mu_{L_i}(x) \tag{6.2}$$

where μ_{L_i} denotes the membership function of neuron i corresponding to the linguistic label L, as a function of the input x. The number of the neurons in this layer is the sum of the linguistic labels of all the reference inputs. The activation functions may be any of the usual shapes: triangular, trapezoidal, or bell-shaped (Figure 6.6). Each of these functions are defined by a set of variable parameters called

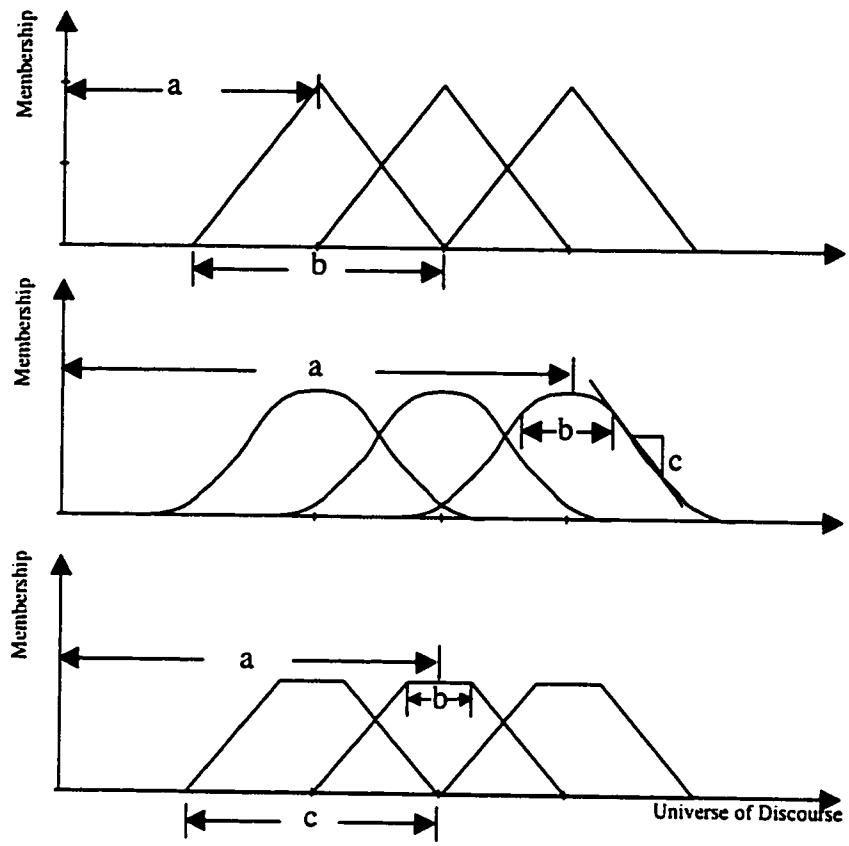

Figure 6.6: **Three types of membership functions: a) Triangular consisting of two defining parameters, b) bell-shape consisting of three defining parameters, and c) trapezoidal consisting of three defining parameters.**

premise parameters [40]. For example, for the bell shaped membership function, the parameters $[a_i, b_i, c_i]$ define $\mu_{L_i}(x)$ as:

$$\mu_{L_i}(x) = \frac{1}{1 + [(\frac{x-c_i}{a_i}^2)]^{b_i}} \tag{6.3}$$

Layer 2: Minimization Layer

This layer is part of the decision making block in the fuzzy algorithm (Figure D.4). Each neuron in this layer represents the firing strength of a rule. These are fixed action (shown by circle) neurons. They perform a minimization operation (see Appendix

D) between the incoming signals. Other operators (such as multiplication) may also be used as activation functions. The number of neurons in this layer is equal to the number of fuzzy subsets (rule-base). In our case we usually had two reference sensory inputs, and each sensory input included three linguistic sets. The number of fuzzy subsets therefore was 3^2.

The function of this together with layers 3 and 4 would be analogous to that of the motor cortex block (motor planning) in Figure 6.3 and the command system in Figure 6.2. These blocks use their previous knowledge (stored in the knowledge base in Figures D.3 and 6.3) to plan the required motor actions from the received sensory information.

Layer 3: Normalization Layer

This layer is also part of the decision making block in Figure D.3. These are *circle* (fixed action) neurons. The i^{th} neuron calculates the ratio of the i^{th} rule's firing (in layer 2) to the sum of all the rules' firing strengths. The connection strengths between layers 2 and 3 are all unity. The output of the i^{th} neuron in layer 3 is therefore given as:

$$O_{3i} = \frac{O_{2i}}{\sum_{j=1}^{n} O_{2j}} \tag{6.4}$$

where n is the number of neurons in layer 2. The number of nodes in this layer is equal to the number of fuzzy subsets (rules).

Layer 4: Action Membership Layer

This layer calculates fuzzy values of the network outputs (actions). These are *square* neurons (adaptive). The number of neurons in this layer is equal to the number of linguistic labels of the network outputs (actions). The structure of this layer is different from ANFIS [40] in that the number of neurons is not necessarily equal to the number of fuzzy subsets. The activation function of the neurons in this layer

is analogous to the centroid of the area method for triangular memberships (see Appendix D). As usual, each triangle will have two parameters (the base and the mean value of the triangle membership function). The neurons of layers 3 and 4 are fully connected. Each of the connections implements a rule-base. Therefore, for each of the layer 4 neurons, only one of their output connection's strengths must be equal to 1, and the rest must be equal to zero. However, we have modified this binary representation, and this will be discussed in the reinforcement learning section. In our case, the network contains 9 outputs (start time, duration, and magnitude of the biceps femoris and rectus femoris pulses, as well as hip elevation velocity, hip flexor velocity, and knee flexor velocity at toe-off). Each of these outputs usually comprised three linguistic sets $\{low, medium, high\}$. However, in some of the simulations (as will be discussed in the results section) we increased the number to 4 or 6 linguistic sets to produce a more continuous output.

Layer 5: Summation Layer

This layer performs the defuzzification process (defuzzification interface in Figure D.3). It calculates the crisp value of each output (action) by performing the maximum operation ("OR" function) on its linguistic sets (see Appendix D). The number of neurons in this layer is equal to the number of outputs. The strength of all of the connections between layers 4 and 5 is equal to 1. However, the linguistic neurons in layer 4 are only connected to their corresponding output. The output of the j^{th} neuron in layer 5 is given as:

$$O_{5j} = \sum_{i=1}^{n_k} O_{4_{n_k}} \tag{6.5}$$

where n_k is the number of linguistic labels for the k^{th} output.

This layer represents the spinal pattern generators in Figure 6.3. The summation layer is analogous to the motor neurons in the spinal level. However, the direct spinal level sensory feedback (afferent feedback) is not modeled in this work.

6.4.3 Learning

The remaining block to be discussed in Figure 6.3 is that referring to the learning center (we have called it cerebellum, although we acknowledge that cerebellum is not the only learning center in the human). As shown, this block communicates with all other blocks. It receives sensory information from the sensory analyzer, motor plans from the motor cortex, motor actions (efferent copies) from the spinal level, and finally information regarding the state of the limbs (with respect to the obstacle and the segments) after performing the swing. It also communicates with the knowledge base. Learning modifies both the synaptic strengths (strength of the connections) and the signal transmission properties of the neurons.

In a standard feed-forward neural network, learning is usually implemented by modifying the connection strengths and thresholds of the neurons. In adaptive networks, learning is also performed on the square neurons such that their activation function would be modified not only by a threshold value but by two or three parameter sets (e.g. the bell-curved activation has three parameter sets).

As noted in the literature review, some researchers have used global search algorithms for training neural networks. For example, Lewis et al. [47] used genetic algorithms to train the neural network of a six legged robot, while Kim et al. [44, 81] used genetic algorithms to train rules and membership functions in a neuro-fuzzy network. Others have used hybrid models of optimization to develop rules and modify membership functions of fuzzy networks [40].

This work is somewhat similar to that of Kim et al. [44]; although there are several significant differences:

- Kim et al. [44] used genetic optimization for training both the weights and the memberships of the neuro-fuzzy network. This work utilizes reinforcement learning for training the weights, while genetic algorithms are used to train the adaptive neuron's membership (activation) functions.

- The connection strengths (the rule-base of the neuro-fuzzy network) were presented by binary values (in other words, a rule is either off or on). In the proposed model, the strength of the connection has an approximate value (in other words a rule may be partially on).

- Simulations of the above models were performed on the Cart-Pole system. This work performs the simulations on a five degree of freedom planar link segment model of the lower limbs.

Genetic Algorithms

The highly parallel and robust technique of genetic programming (Appendix F) was used to optimize the membership parameters for the square neurons. Figure 6.7 illustrates how the neuro-fuzzy network, simulation plant, and the genetic algorithm are connected. The genetic pool (Figure 6.7) usually consisted of 200 individuals (genotypes or strings of binary characters). Each parameter of any linguistic set of the network outputs was represented by an 8 bit binary fixed length string. Therefore, for 9 network outputs, each including 4 linguistic sets, with each linguistic set being defined by 2 parameters, a $9 \times 4 \times 2 \times 8$ bit binary string was assigned. The standard genetic algorithm with only mutation and crossover operators was used. Selection was performed using the standard Baker's SUS algorithm (see Appendix F). Usually a 2 point crossover was performed at the rate of 60%. The mutation rate was maintained constant at the rate of 0.1%.

The algorithm always started with similar membership shapes distributed uniformly within the universe of discourse (Figure 6.8). The genetic optimization routine then changed the parameters of each linguistic set belonging to the various network outputs (actions) in order to maximize a fitness value. The fitness value was maximized when the toe clearance over an obstacle reached 10 cm, and the location of maximum toe elevation was equal to the corresponding network reference input. Additionally, for some simulations, the stability margin (Figure 5.4) was also considered in calculating the fitness value. The desired stability margin was set to 0.2 m.

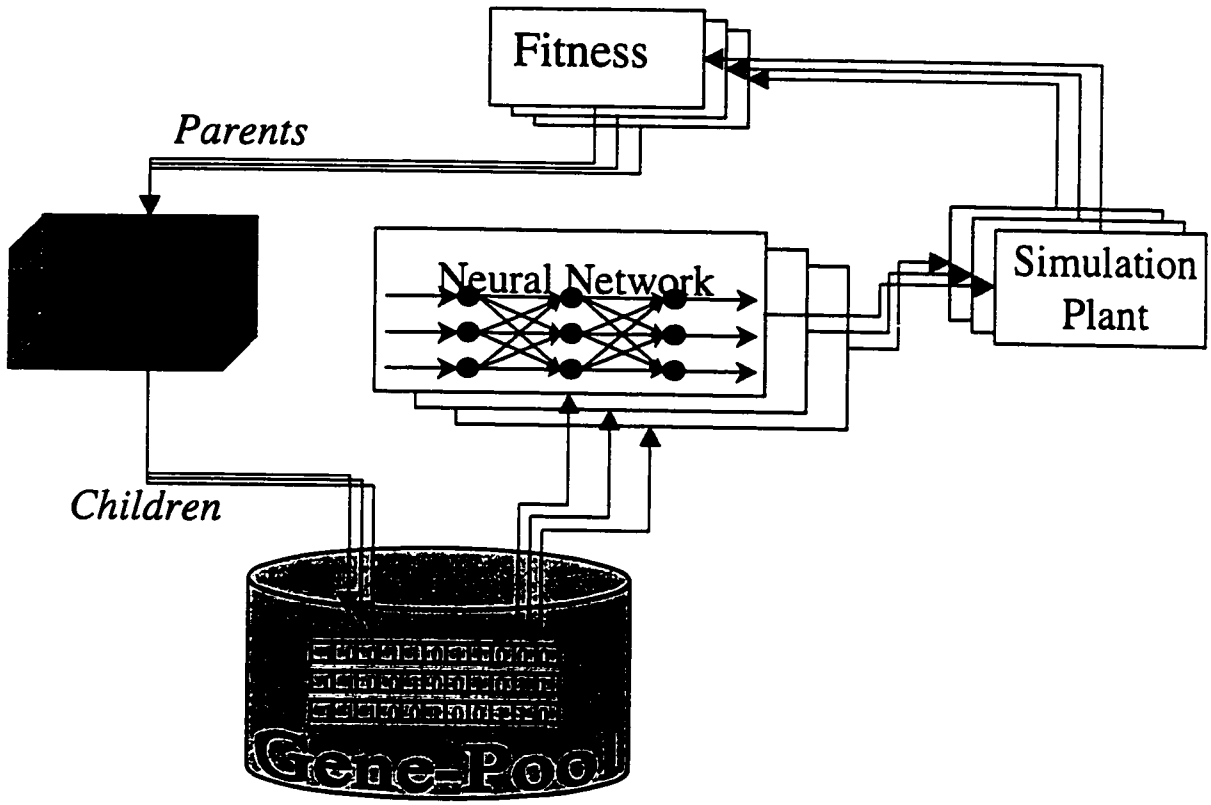

Figure 6.7: **Illustrative relation between the genetic pool, the network, and the plant. For details please see Appendix F.**

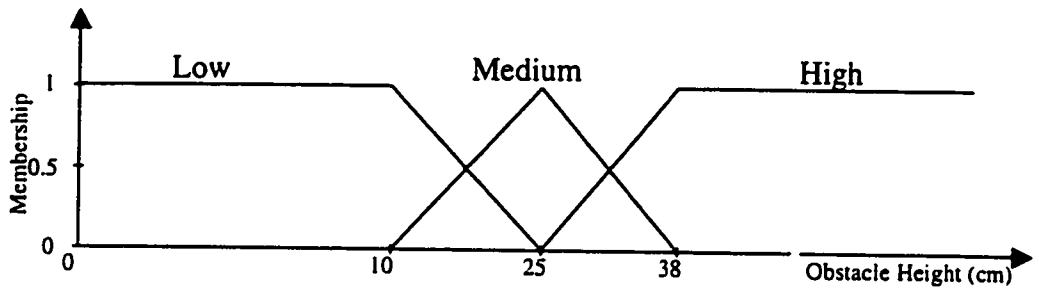

Figure 6.8: **Uniform memership function over the universe of discourse.**

Typically the fitness value, F_{total}, was:

$$F_{total} = 2000 - F_{clearance} - F_{location} - F_{stability} \tag{6.6}$$

$$F_{clearance} = |Y_{clear} - .1| \times 1000 \tag{6.7}$$

where Y_{clear} is the toe clearance over the obstacle as shown in Figure 5.4,

$$F_{location} = |(X_{Y_{max}} - X_{obst})| \times 1000 \tag{6.8}$$

where X_{obst} is the obstacle-toeoff distance, and

$$F_{stability} = |X_{toe} - X_{C.M.} - .2| \times 1000 \tag{6.9}$$

where $X_{toe} - X_{C.M.}$ is the stability margin shown in Figure 5.4. All the units are in meters.

For each simulation, the genetic optimization continued for 30 generations. The program would also terminate when either the fitness value, F_{total}, had reached 90% of its maximum, or the pool had lost its diversity.

Reinforcement Learning

The connections between the normalization layer (layer 3) and the action membership layer (layer 4) represent the rule-base of the neuro-fuzzy architecture. Each of the neurons in the normalization level represent an antecedent of an if-then rule. The consequent of rules are then defined by neurons of the layer 4. Figure 6.9 shows one of the neurons in layer 3 representing an antecedent, connected to three neurons of layer 4 representing the linguistic sets of one network output. Based on the concept of a fuzzy associative memory matrix (Figure D.2 in Appendix D), one of the represented connections can be 1 and the others must be zero. For example the two following rules should not exist simultaneously:

IF a1 AND b1 THEN z is SMALL
IF a1 AND b1 THEN z is LARGE

Kim et al. [44] let the genetic algorithm take care of learning the rule-base. In the present work, the rule-base is learned by a reinforcement architecture. Each trial on the link segment model provides the system with one set of the network's actual input-output mapping. This is potentially a rule that could be used to affect at least one of the weighted connections between layers 3 and 4. To reduce the dimension of the genetic search, each plant simulation is used to reinforce one of the rules. The procedure is as follows (Figure 6.9): The inputs and outputs of the plant are fuzzified by passing through their original membership functions. The *maximum operation* is performed on the linguistic sets to find the maximal membership of the input-output mapping . The linguistic labels corresponding to the maximal memberships are put together in the form of an if-then rule as shown in Figure 6.9.

The natural interpretation of this rule in the network (Figure 6.9B) would be that the weights corresponding to the output neuron with the linguistic label *medium* is set to 1, while the weights corresponding to the output neurons with linguistic labels *low* and *high* would be set to zero. However, there is a potential problem with this form of rule adjustments; a slight change in inputs x and y may not transform them

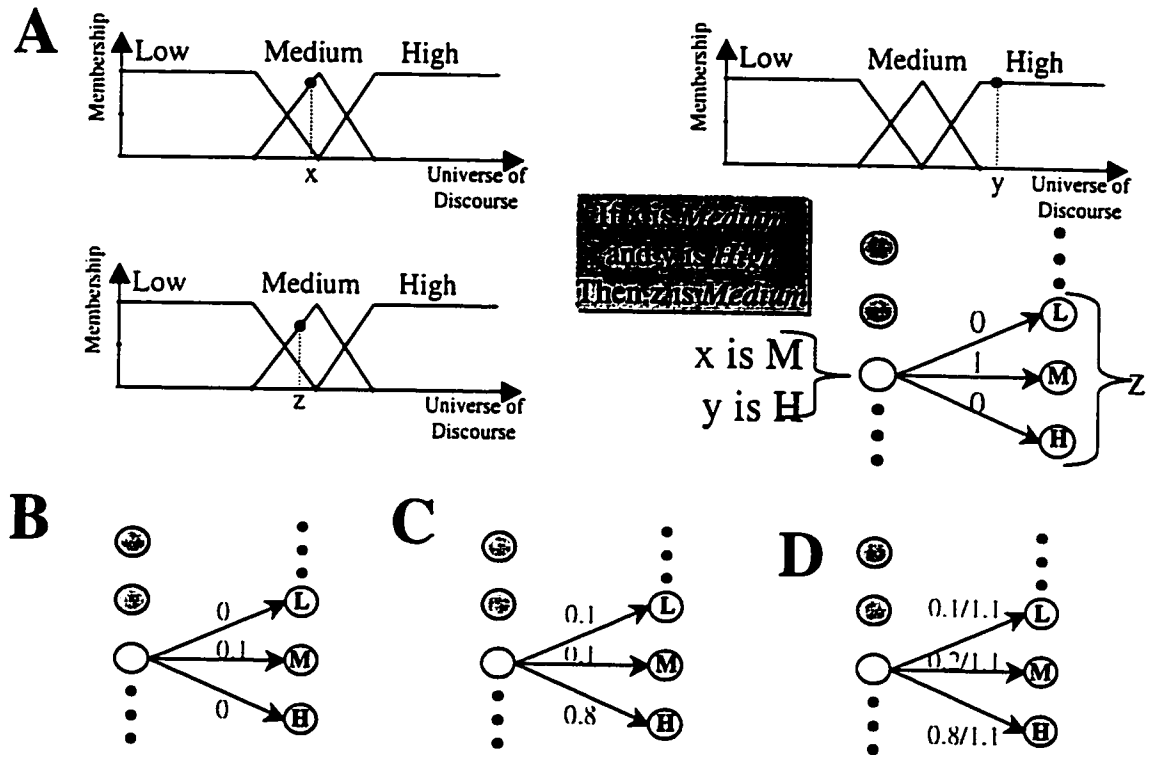

Figure 6.9: **Training of weights by reinforcement learning. A) based on maximal membership the references x and y and the network output z are assigned with a linguistic set. The rules then will turn the corresponding weight on. B) In modified reinforcement learning to the rule chosen by the trial performed, a reward of 0.1 is assigned. C)A specific example of the reinforced learning after 10 different trials. D) The distribution of the reward after the 11^{th} trial.**

to a new linguistic set, although it may cause a change in the output z membership values. In other words, two set of inputs with identical linguistic labels could be mapped to two different outputs. Figure 6.9C illustrates a remedy to such situations. Instead of rewarding the connection corresponding to a rule by 1, the connection is rewarded by 0.1 each time the network corresponds to the rule. However, the effect of each rule on the network is reduced as the number of the trials increases. This is done by normalizing the linguistic sets to 1 after each trial (see Figure 6.9). The reward system defined in this way is rule specific, and therefore introduces more than one baseline for reinforcement learning.

Genetic learning does not interfere with reinforcement learning of the rules. As mentioned, the reward system uses the original uniform membership distributions, and not those modified by the genetic operations. This approach is necessary because the memberships defined by the genotypes vary significantly during the evolutionary process. On the other hand the reinforcement learning has to be started from the very first trials (we begin by assuming that we have absolutely no knowledge about the rule-base) and cannot wait for the evolutionary process to become more stable.

The use of original uniform memberships has another advantage; it enforces the genetic optimization to modify the membership parameters around a center baseline (the original memberships). We can therefore always expect that the membership labeled *large* corresponds to a higher range in the universe of discourse than the membership labeled *medium*.

Eventually, after the genetic optimization converges to the solution, we can then modify the reinforcement learning to look at the memberships of the best individual in the pool, instead of the original memberships. This further improves results. We refer to this stage as "skilled learning".

6.4.4 Selection of Model Parameters

In the design of the neuro-fuzzy-genetic architecture, several parameters need to be determined. In the neuro-fuzzy part, these parameters include: the number of lin-

guistic sets for each input and output, the type of linguistic sets for each input or output, and the defuzzification method. In addition, for genetic learning, several parameters need to be determined. These parameters include: the size of the genetic pool, the number of binary bits for the linguistic set, the number of crossover sites, the crossover and mutation rates, the selection pressure, and the termination criteria. For the numerical integration of the link-segment model, the maximum allowable error at each time step plays a crucial role in the speed and accuracy of the simulation.

Various types of linguistic sets (Figure 6.6) introduce different numbers of free parameters. For example, the bell-shaped curve has a smooth shape. Although more flexibility in defining each linguistic set can be obtained by the bell-shaped curve we chose to use the triangular shape, since this has one less parameter, and therefore the linguistic set for each output would be several bits shorter. This has a drastic effect on the length of each genotype in the pool, and thus, reduces the computational load.

Increasing the number of linguistic sets for each input-output resulted in more detailed knowledge of each universe of discourse. This increase also resulted in producing more if-then rules in a more precise manner, such that each rule had smaller boundaries with better-defined elements. This parameter affected reinforcement learning (finding the weights for the rule-base) the most and made it more effective. However, increasing one linguistic set for one of the inputs, exponentially increased the size of the network. In the network shown in Figure 6.4 the addition of a linguistic set for input x results in one extra connection to layer 1, three new neurons and connections for layer 2, three new neurons and 63 new connections in layer 3, and 36 more connections in layer 4. Note that this illustrates a network for only one output, while the actual network used included nine outputs. Therefore, all of the above numbers are multiplied by a factor of 9.

Defuzzification methods usually affect the transient response in feedback control systems. Of the two methods for the mean-of-maximum and the centroid-of-area (Figure D.4), the latter yields to better steady state responses, while the former yields to better transient responses [46]. The transient response for the maximum criterion

method is better than the centroid-of-area method, however, it is not superior to that of the mean-of-maximum method. As the architecture designed in this chapter was meant for the steady state response, the centroid-of-area was found to be the most suitable method.

The number of the genotypes in the genetic pool affects the degree of parallelism in the search routine. The larger the population number, the less there is the chance of the pool losing its diversion. Hence, the chances of premature convergence to a local non-fit solution would be reduced. However, as each genotype holds information regarding one set of network parameters, by increasing the number of genotypes in a pool, the number of computations required for one generation will be proportionally increased. Each evaluation of the networks requires simultaneous integration of the link-segment plant model. As well, transfer of information between genotypes gets more difficult when the population increases. Therefore, a balance should be met with the necessary diversity, the convergence speed, and the computational loads required. Each problem has its own specific favor in this matter. In this work, by several trials, it was found that the pool size between 100 to 500 were most suitable.

The number of binary bits assigned to each linguistic set defines the grid over the whole universe. An 8 bit binary string divides the universe of $\{0, 4\}$ to 256 grids of length $1/256$ each. Therefore, the resolution in the solution space increases with the number of bits in the individual binary strings. This effect combined with the size of the universe will determine how fine/coarse the network operates over the solution space.

The number of crossover sites and the crossover rate combined with selection pressure determine the rate at which the pool converges. The number of crossover sites must be based on the length of the building blocks for each genotype. For a highly epistatic representation (when too many elements are dependent on other elements, e.g. parity problem) the higher number of crossover sites in a gene is not desirable. In this situation, unless a unique set of binary values are found simultaneously, no substantial fitness improvement can be achieved [18]. By increasing the crossover rate,

the fitness of an individual string compared to the pool becomes less important. In other words, the possibility of destroying an individual with best fitness increases in favor of giving more faith to the average fitness of the pool and the schemata (building blocks carried by that gene). The mutation rate is another means of producing diversity in the pool. It becomes more important as the pool size reduces and/or the selection of the fittest pressure increases. The value chosen here (0.1%) was suggested in [18].

The selection pressure depends on the selection algorithm and how the fitness function is scaled. The standard SUS selection algorithm aims at selecting the individuals with higher than average fitness. However, an exponential scaling of the fitness function can change the topology of the surface that the genetic program is climbing on. This exponential fitness may create a bias towards the original peaks and increase the probability of immature convergence by widening the distance between the fittest individuals and the rest of the pool at each generation. A low selection pressure, on the other hand, results in very slow convergence, if any, and a higher computational load. It follows that a linear scaling with a not very large pool (between 100 and 200 population) works best for this problem.

Finally, the termination criteria are mostly dependent on the search goal. For an optimization looking for one best solution, the termination criteria might be reaching certain fitnesses. The diversity of the solutions and their range was important for us to ascertain. Clearly, in many instances this problem had more than one solution. Therefore, we believed that the better termination function would look at both 90% of genotypes having more than a certain fitness ($RMS < 5\ cm$), and limit the optimization to 30 generations (the justification for selecting these termination criteria will be shown later).

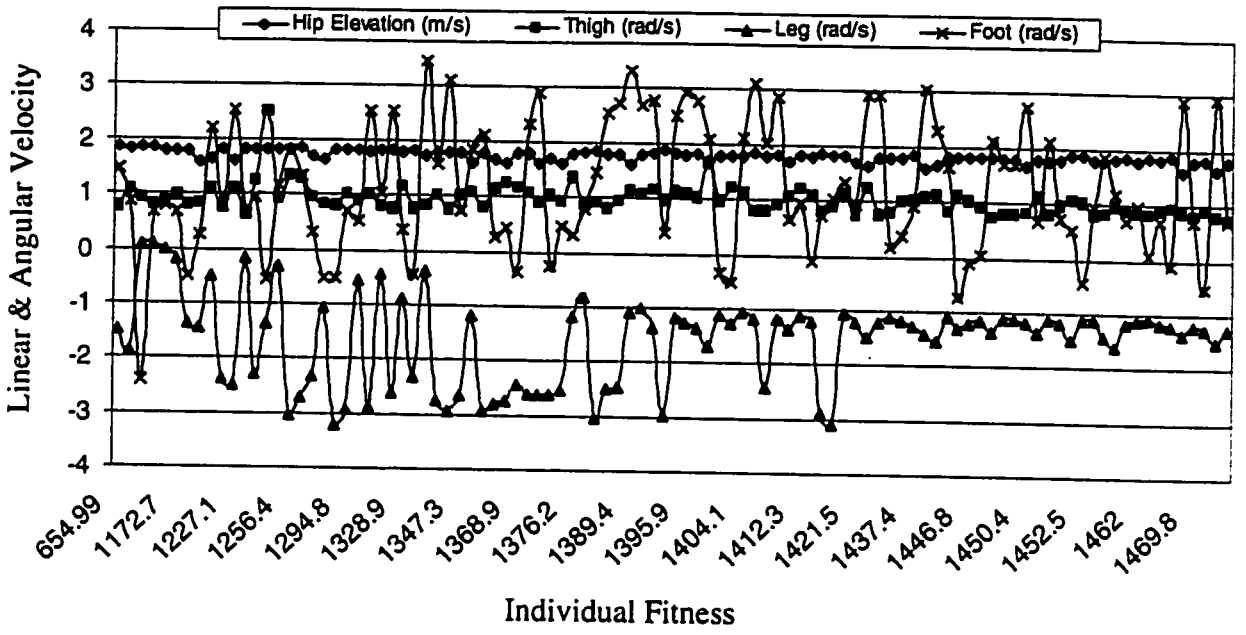

Figure 6.10: **With the increase of fitness in the genetic population, the range of variation of all except foot velocity at toe-off converge to a certain level.**

6.5 Results

6.5.1 Sensitivity of the Final Pool to the Foot Angular Velocity at Toe- off

The genetic optimization was performed on a five degree of freedom link-segment model (Figure 6.5). The goal was to find the sets of initial velocities at toe-off (linear stance hip, angular swing thigh, angular swing leg, and angular foot) that produce at least 95% of the maximum possible fitness value. This would correspond to less than 5 cm error in satisfying both objectives of a 10 cm toe clearance over the obstacle, and locating the maximum toe clearance over the obstacle (see Equation 6.6). The genetic pool included 100 genotypes and the simulation was terminated when the average fitness of the pool was more than 95% of the maximum possible fitness.

Several simulations for different values of the reference inputs (obstacle location with respect to the toe-off and obstacle height) to the neuro-fuzzy model were per-

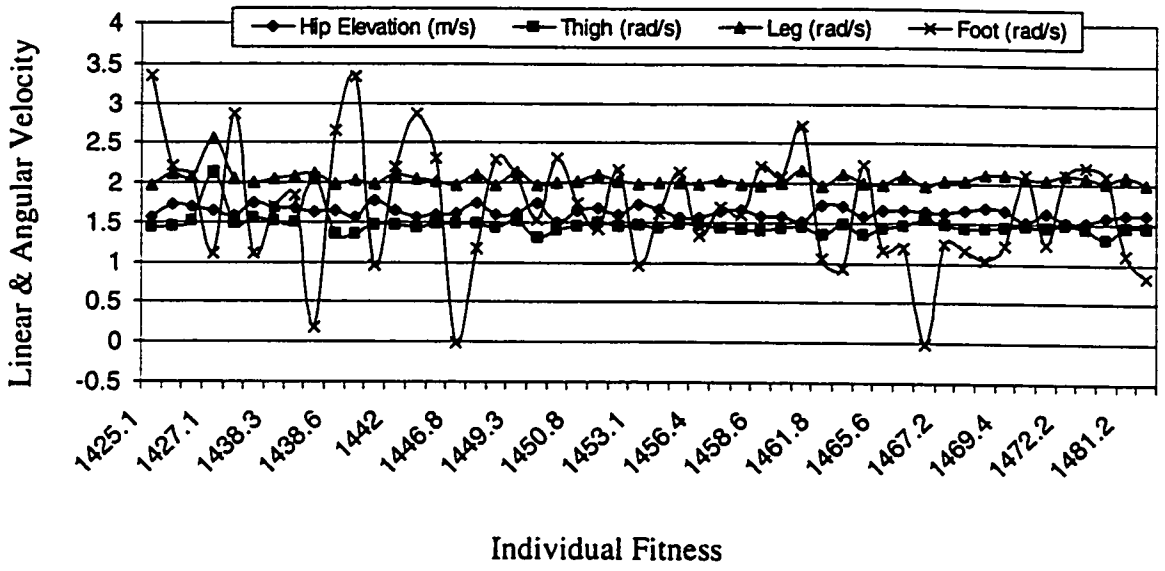

Figure 6.11: **The fittest genotypes are not sensitive to the foot velocity at toe-off.**

formed. A typical result for an obstacle height of 20 cm located at 30 cm from toe-off, and sorted by the fitness of the genotypes in the pool, is shown in Figure 6.10. As the fitness value increases, all of the initial velocities (except the foot angular velocity) converged to a baseline value. Even in the fittest genotypes (Figure 6.11) there is a significant range for the foot segment initial velocities. This indicates that the final solution is less sensitive to the foot segment angular velocity at toe-off compared to the other three initial velocities studied. Based on this result, the rest of the simulations were performed with the foot segment fixed to the leg at a 90 degree angle.

6.5.2 The Effect of the Number of Criteria Used in the Design of the Fitness Function

The number of individual genes in the pool was increased to 500. When the two criteria: location of maximum toe elevation and toe clearance, were used to design the objective function, physically unacceptable solutions were found in the pool. Figure

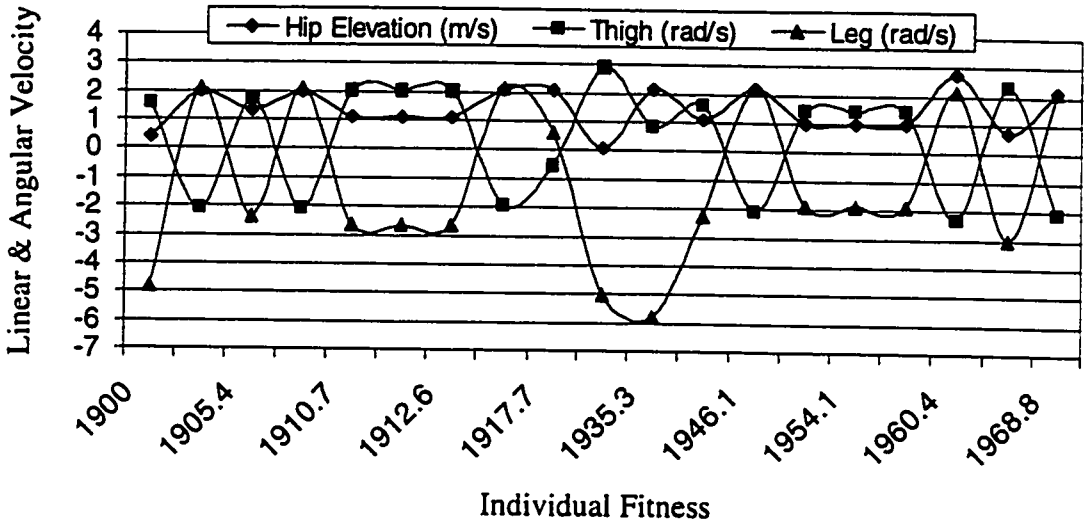

Figure 6.12: **Two solutions with opposite signs exist for the thigh and hip initial velocities.**

6.12 shows two ranges of solutions with opposite signs for the swing leg and thigh angular velocities. However, the solution range corresponding to the backward swing of the thigh and the forward swing leg angular velocities at toe-off are not physically acceptable (Table 6.1, rows 1 and 2).

Two remedies were considered: a) addition of a new constraint that limits the movements of the swing limbs at toe-off, b) addition of a new objective to the fitness function. The former remedy would limit some of the possible movements, while the latter would create more realistic landings. Therefore, the landing stability criterion was added for evaluating the fitness function (Figure 5.4). A 20 cm distance between the stance hip and the swing toe at landing was considered optimal.

Simulations(Table 6.1, row 3) with the added stable landing criterion showed that the undesirable solution was removed from the final pool. A comparison between rows 2 and row 3 of the table demonstrates a significant reduction in the hip elevation velocity at toe-off. This lower velocity caused significant loss of altitude of the hip at landing, which in turn was a physically unacceptable solution. To avoid this, the amount of loss of altitude of the swing hip was constrained. Since the addition

V_{he}	ω_t	ω_l	Y_{clear}	Xy_{max}	X_{stable}	Fitness
0.749	2.304	-3.038	0.319	0.310		1961.0
2.123	-2.118	2.165	0.299	0.315		1968.8
0.580	3.777	-4.307	0.305	0.296	0.202	1990.3
2.184	1.940	-0.753	0.293	0.576	0.176	1679.7

Table 6.1: **The change of initial velocities with the addition of stability criteria and the hip elevation constraint.**

of a spring and damper to reduce the loss of altitude of the hip (an anatomically justifiable solution) would cause extra computational effort for the variable step size simultaneous integration of the link segment model, it was decided to add a constraint to the fitness function: for each centimeter loss of hip altitude in excess of 10 cm, the fitness function was penalized by 3 cm. Simulation with the added constraint to avoid loss of hip altitude (Table 6.1, row 4) showed that the hip elevation velocity was increased significantly in the pool of solutions. This was combined with lower leg backward velocity. The major compromise was the reduction in the fitness value.

The results (row 4 of Table 6.1) show that this reduction of the fitness function was due to the increased error in locating the maximum toe elevation during the swing phase. Therefore, without active control, it was not possible to produce an efficient swing for the obstacle located at 30 cm from the toe-off location. Note that the step length at the beginning of the swing was set to 45 cm. The above configuration,

therefore, refers to a condition that the obstacle had encountered during early swing. In other words, the trailing limb was stepping over the obstacle. The effect of the obstacle location on the fitness function is described next.

6.5.3 The Effect of the Obstacle Distance from Toe-off Location

The obstacle height was set to 10 cm while the obstacle location was varied along the stride length. Each simulation was performed on a genetic pool of 200 individuals. At least two simulations for each obstacle location were performed.

The progression of the average fitness, with generations at various obstacle-toeoff distances, (Figure 6.13) shows that most of the improvement on average fitness is usually achieved by generation 30. Therefore 30 generations were chosen as the landmark for termination of the simulations. Only the simulations in which the pool did not converge before 30 generations were used for plotting the results.

The maximum fitness was obtained for a obstacle-toeoff distance of 55 cm (Figure 6.14,A). For a symmetrical swing over the obstacle, this distance corresponds to approximately 60% of obstacle-toeoff distance to stride length ratio (O/S ratio). As discussed in previous chapters, this ratio is usually observed in young subjects stepping over small and medium-sized obstacles. Also evident is that as the obstacle is encountered earlier in the swing (obstacle-toeoff distance less than 55 cm), the maximum fitness of the pools reduces. The same trend, although less significant, occurs when the obstacle is encountered later in the swing (obstacle-toeoff distance greater than 55 cm).

The average fitness of the pools also favored obstacle placement around $50-60\%$ of the stride length (Figure 6.14, B) although not as pronounced as the maximum fitness (Figure 6.14, A). Obtaining a high fitness value became more difficult as the obstacle was encountered earlier in the swing or in late swing. From these results we can conclude that for an obstacle placed at mid-swing, less additional active control

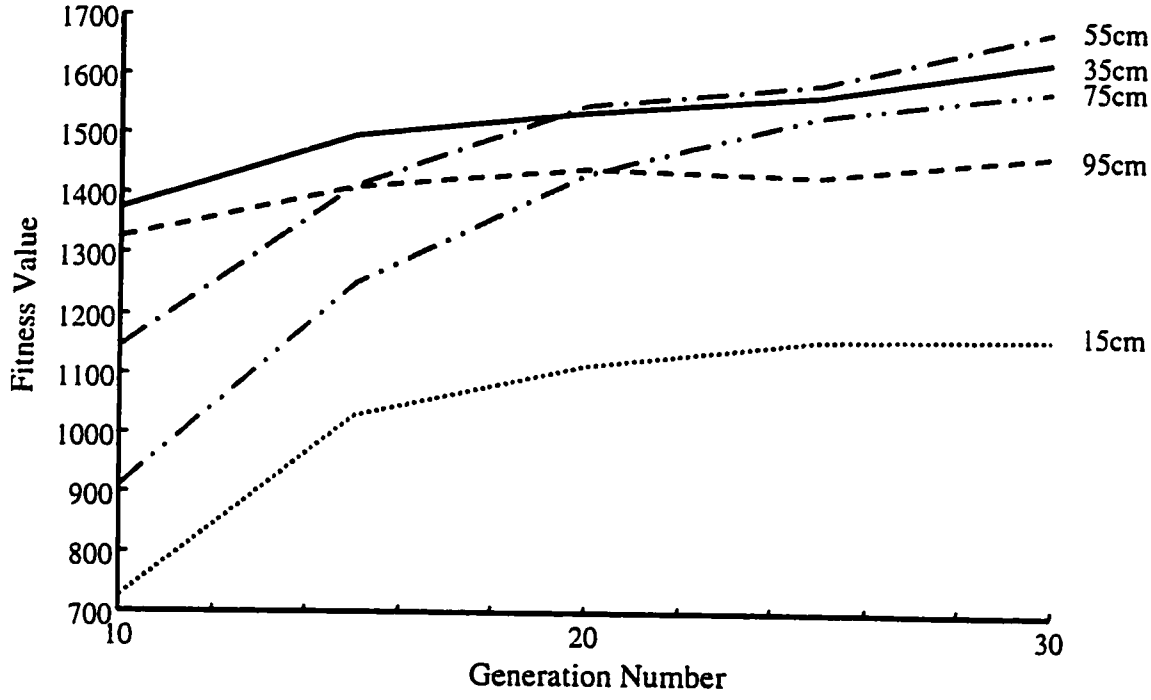

Figure 6.13: **The progression of average fitness with generations for various obstacle-toeoff distances.**

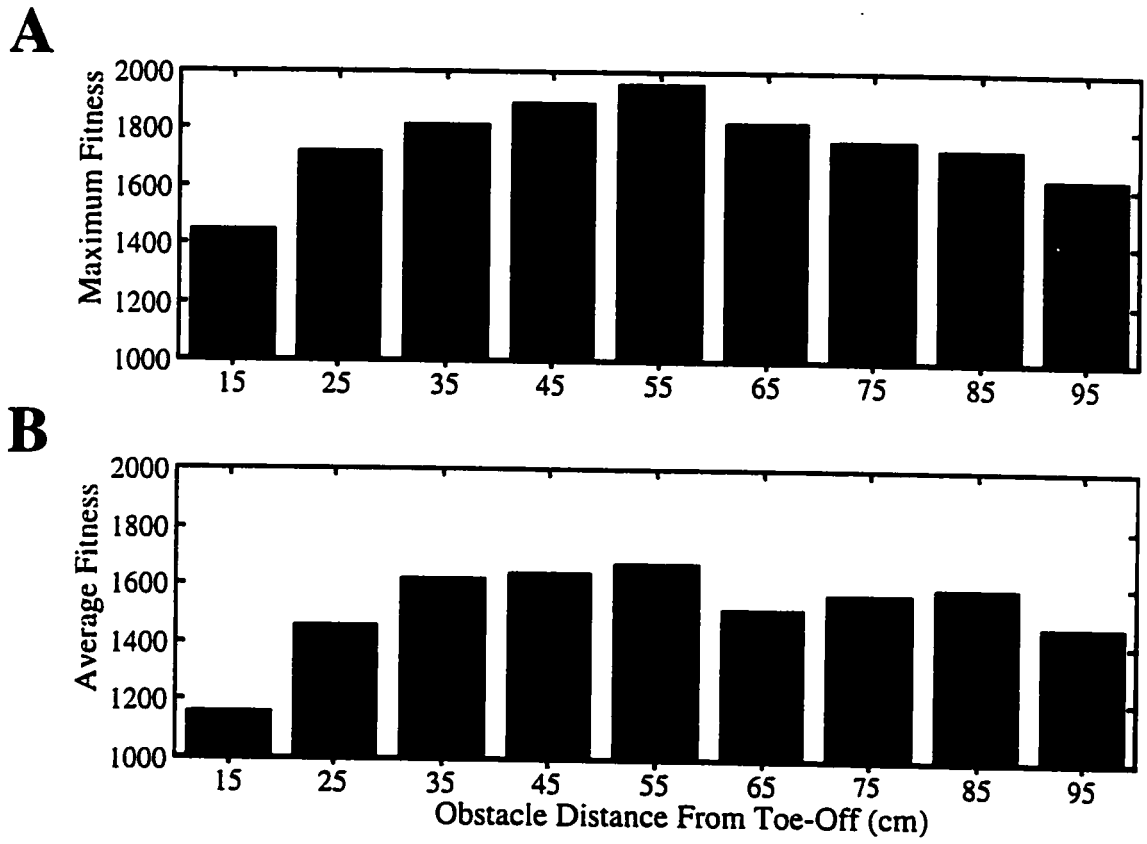

Figure 6.14: **Maximum fitness (A) and average fitness (B) of the gene pool after 30 generations as a function of the obstacle-toeoff distance.**

No.	V_{he}	ω_t	ω_l	Stride	Y_{max}	Y_{clear}	XY_{max}	X_{stable}	Fitness
1	2.92	1.67	-0.44	1.49	0.57	0.24	0.76	0.20	1350.66
2	2.16	1.92	-0.44	1.22	0.34	0.17	0.59	0.23	1446.83
3	2.19	1.88	-1.17	1.11	0.40	0.19	0.54	0.06	1426.87
4	1.41	1.07	-1.24	0.60	0.21	0.19	0.31	-0.18	1414.36
5	1.54	2.12	-0.49	0.95	0.20	0.12	0.49	0.18	1283.84

Table 6.2: **The results for a typical solution pool for 15 cm obstacle-toeoff distance with a 10 cm obstacle on pathway.**

is required to achieve the objectives of safe clearance of the obstacle (safe landing and efficient swing).

6.5.4 The Effect of Initial Velocities on Each of the Objectives

A closer look at the results obtained from one of the solution pools shows why a higher fitness value was not achieved for the trailing limb (Table 6.2). For this simulation the obstacle-toeoff distance was set to 15 cm, and the obstacle height was 10 cm. Row 1 of the table indicates a solution where high hip elevation velocity (2.92 m/s) was used with lower backward velocity of the leg (-0.44 rad/s). For this solution, landing stability was achieved while the toe cleared the obstacle by 14 cm (desired solution was 10 cm). The obstacle-toeoff distance ($X_{y_{max}}$) was very far from the desired value of 15 cm, causing an inefficient swing (maximum toe clearance was 57 cm).

Row 2 demonstrates a solution in which hip elevation velocity at toeoff (V_{he})

was reduced to 2.16 m/s from the 2.92 m/s in row 1. The obstacle-toeoff distance ($X_{y_{max}}$) came closer to the desired value, while the maximum toe clearance dropped significantly. This denotes the high influence of the hip elevation velocity on the maximum toe elevation and its location. Comparison of row 5 to rows 1 and 2 shows that the observed change in maximum toe elevation is not due to the change in the thigh forward velocity. In row 5, while thigh forward velocity remained relatively high, a reduction in hip elevation velocity caused a lower maximum toe elevation and location.

Comparison of rows 3 and 4 with rows 1, 2, and 5 demonstrates the dominant influence of the leg backward velocity on the stability criterion. By increasing the backward velocity of the leg by almost 1 rad/s, a stable landing was largely compromised. The effect of thigh forward velocity on stable landing seems to be less than leg backward velocity, and more than hip elevation velocity. Row 4 demonstrates a condition in which both toe clearance and location of maximum toe clearance objectives were accomplished, however the combination failed due to an unstable landing.

6.5.5 Failure Analysis

As an alternative method for comparison of the pools, a failure analysis over the populations of genotypes was performed. The percent genotypes resulting from failure to clear the obstacle ($Y_{clear} < 0$) and/or unstable landing ($X_{stable} < 0$) was plotted for various generations, as well as for various obstacle-toeoff distances.

A typical simulation for a pool with 200 individuals in the population, and an obstacle height of 10 cm positioned 55 cm from toe-off, is shown in Figure 6.15. As expected, the failure rate was reduced from 60% in the fifth generation to less than 2% in the 30^{th} generation. The reduction in failure rate denotes the convergence to a fit population. The low failure rate after 30 generations shows that satisfactory convergence in the pool is produced. Further generations would improve the results insignificantly. The range of population fitnesses based on each of the criteria after 30 generations shows moderate variations in each of the criteria (Figure 6.16).

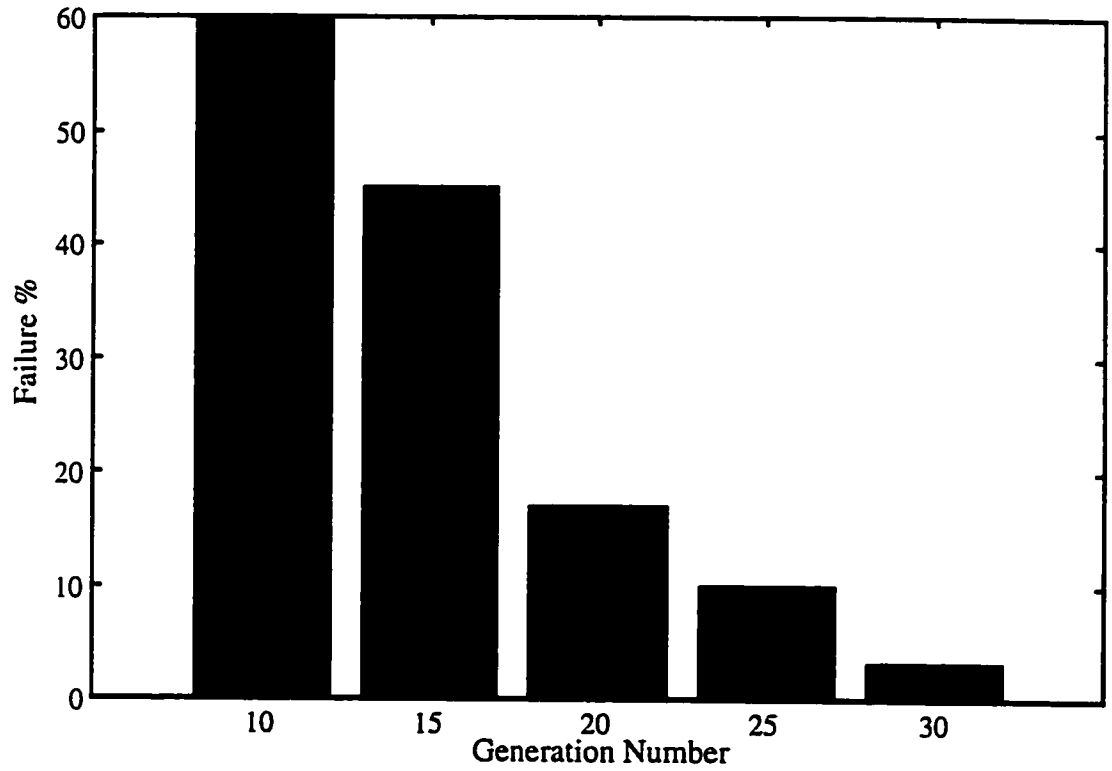

Figure 6.15: **A typical reduction in the failure ratio for a pool with 200 individuals in the population, obstacle height of 10 cm, positioned 55 cm from the toe-off, as a function of generation number.**

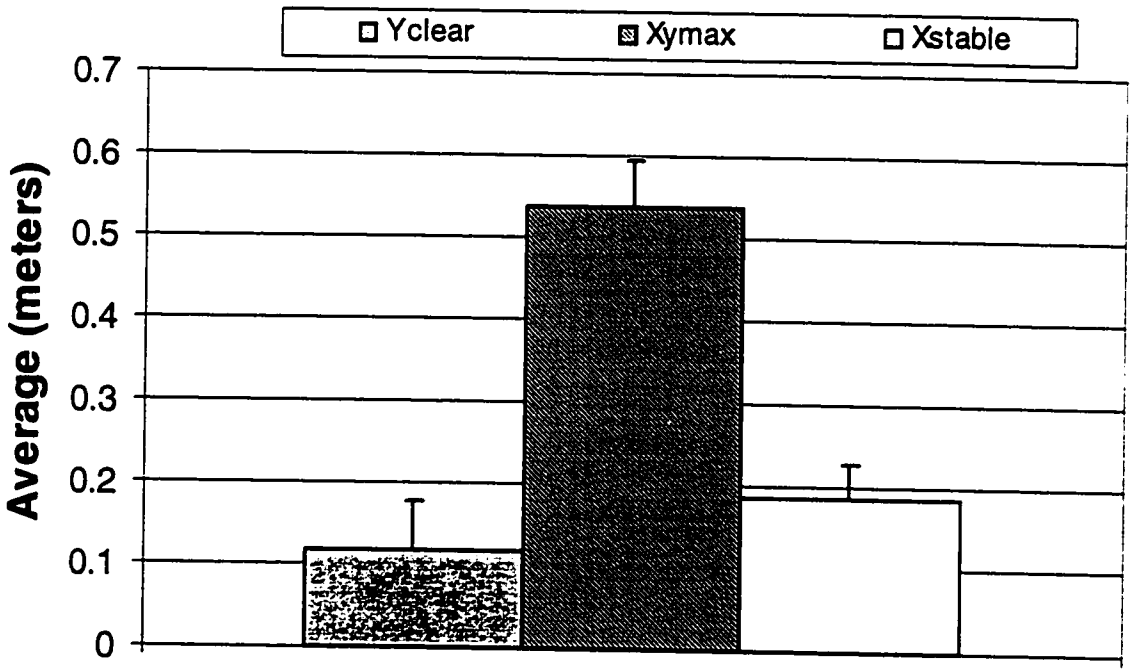

Figure 6.16: **The range of population fitness after 30 generations for an obstacle height of 15 cm and obstacle-toeoff distance of 55 cm from toe-off.**

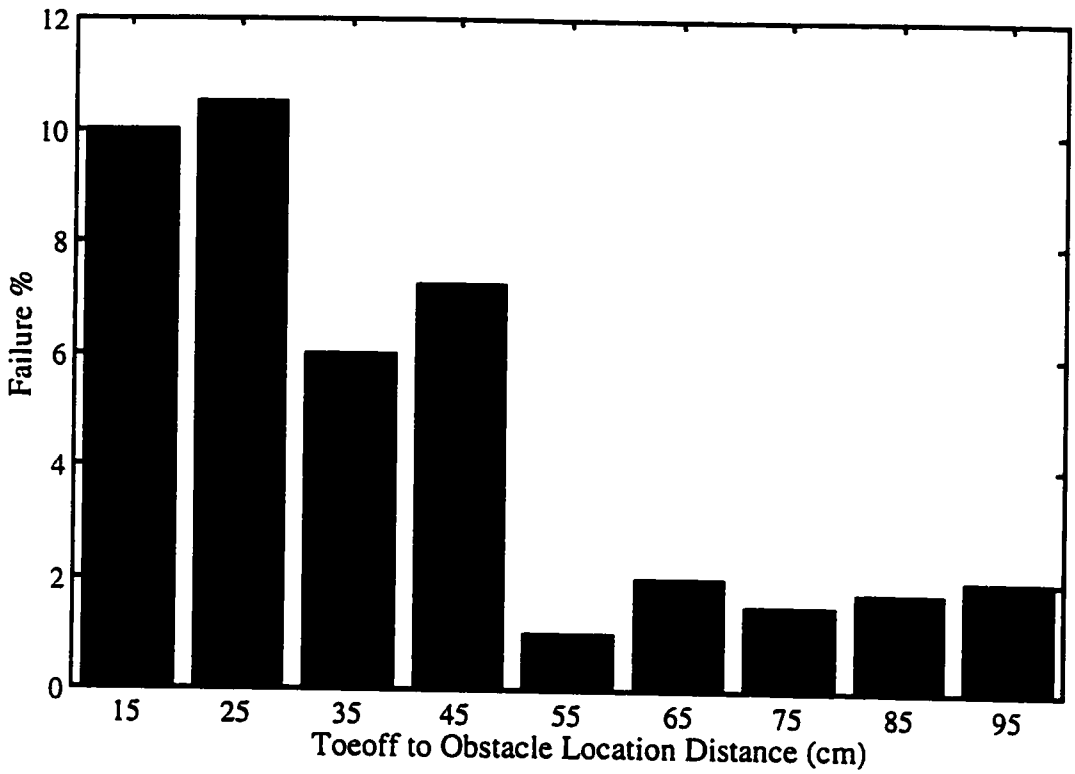

Figure 6.17: **The failure rate in clearing a 15 cm obstacle with increasing obstacle-toeoff distance in generation 30.**

The failure rate of generation 30 was studied for various obstacle locations (Figure 6.17). Although an obvious trend with increasing the obstacle-location distance was not observed, one can easily conclude that the average failure rate for the trailing limb is in general higher than what is observed for the leading limb. For the trailing limb the failure rate was usually over 6%, while for the leading limb it was reduced to less than 2%.

6.5.6 The Effect of Obstacle Height

Hip elevation velocity at toe-off is highly correlated with the obstacle height. The obstacle-toeoff distance was fixed at 55 cm, and several simulations were performed with various sized (10, 15, 20, 25, 30, and 35 cm) obstacles. All the individuals that demonstrated a fitness of more than 1900 (out of maximum fitness of 2000)

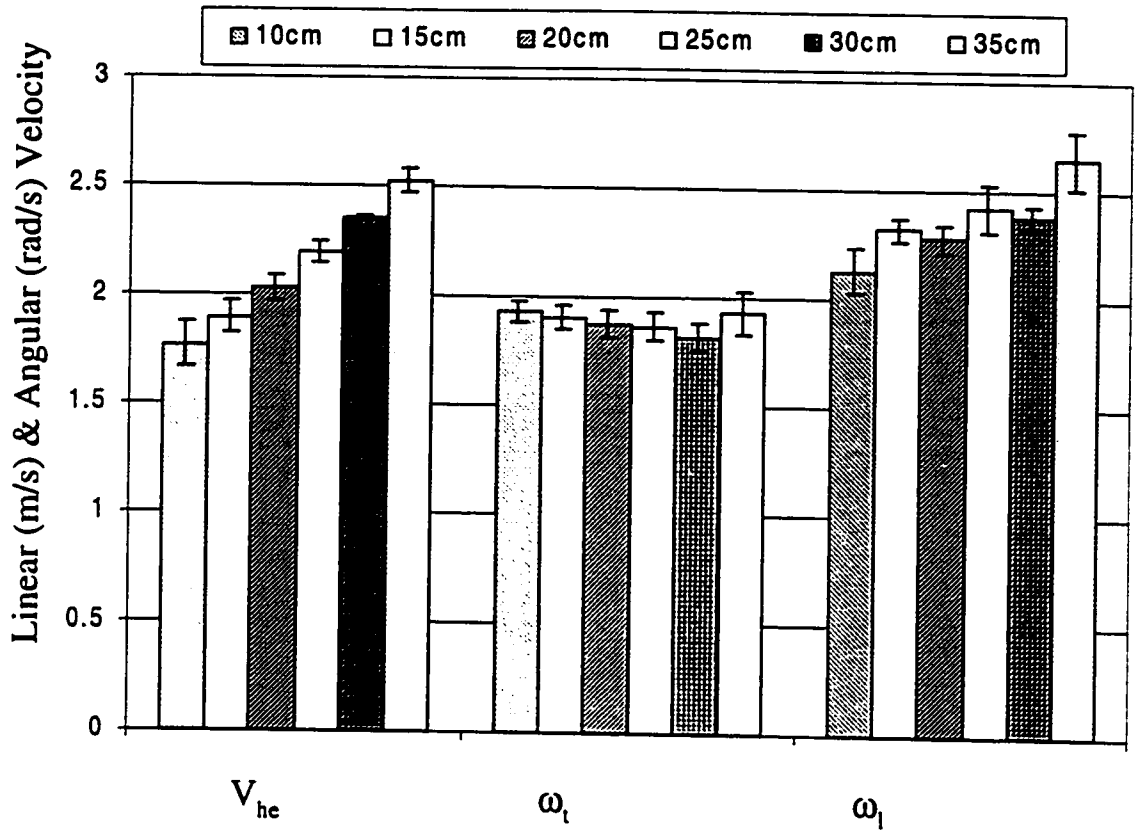

Figure 6.18: **The average value and standard deviation of the initial conditions at toe-off (hip elevation velocity v_{he}, thigh angular velocity, ω_t, and leg angular velocity, ω_l) for 6 obstacle heights (at 55 cm obstacle-toeoff distance) in generation 30.**

were collected (in the case of the 35 cm obstacle, all the fitnesses larger than 1850 were collected). The average value and the standard deviation of each of the initial conditions were calculated (Figure 6.18). The hip elevation velocity at toe-off showed maximum correlation with obstacle height. However, no correlation between obstacle height and hip flexion was found, and, little correlation was observed between knee flexion velocity ($(\dot{\theta}_3 - \dot{\theta}_4)$ in Figure 6.5) and obstacle height.

A plot of the three objectives versus the above 5 obstacle heights showed that the toe clearance remained close to the desired value (10 cm) while the stability margin remained close to the desired value of 20 cm (Figure 6.19). The location of maximum

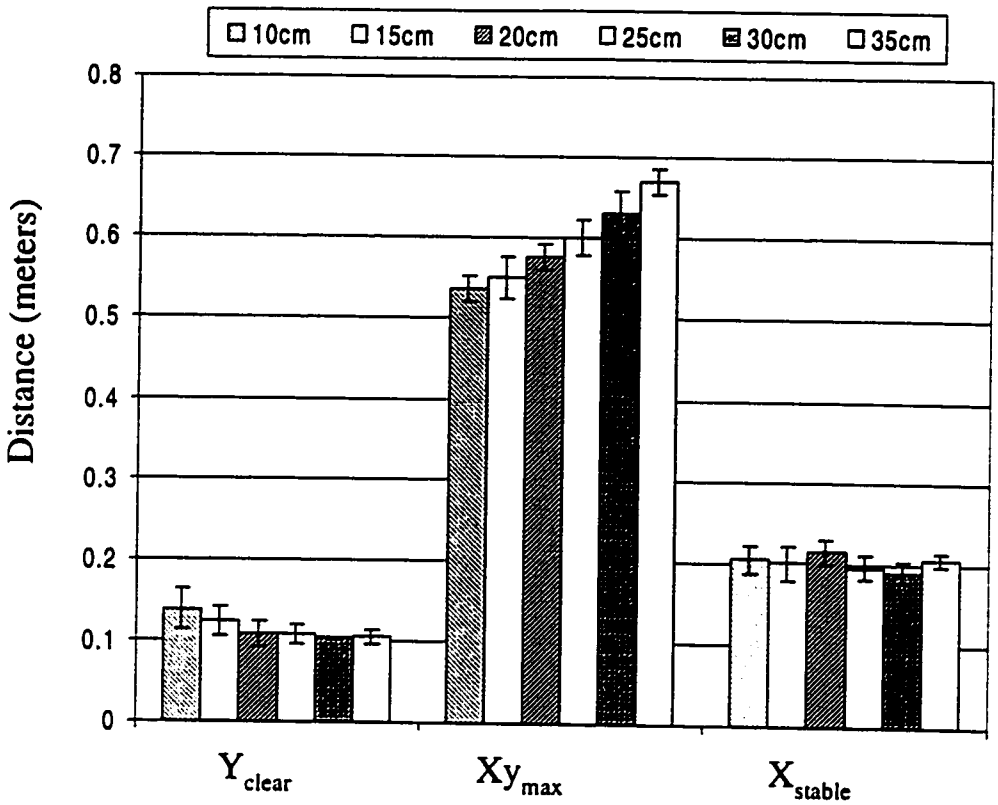

Figure 6.19: **The range of values for the 3 objectives (toe clearance, Y_{clear}, location of maximum toe elevation, $X_{y_{max}}$, stability margin X_{stable}) for 6 obstacle heights, in generation 30.**

toe elevation, however, demonstrated an increasing trend with obstacle height. For the largest obstacle (35 cm), the average location of maximum toe elevation was closer to 65 cm. The increasing trend was similar to that of hip elevation velocity at toe-off. The results clearly confirm the sensitivity analysis of the previous subsection, suggesting that knee flexor velocity at toe-off is mostly concerned with stable landing, while the hip elevation velocity at toe-off is mostly responsible for the control of the maximum toe elevation and its location (indicators of movement efficiency).

6.5.7 The Effect of Bi-Articular Muscle Forces

The single pulse activities of the two bi-articular muscles, biceps femoris and rectus femoris, were modelled as shown in Figure 5.2. For each muscle pulse, three parameters were varied: pulse magnitude (f_p), pulse start time (t_s), and pulse duration (t_d). The rise time and half relaxation time were set at 60ms and 100ms respectively.

The results of the simulation, for an obstacle height of 20 cm and an obstacle-toeoff distance of 15 cm (trailing limb), are shown in Figure 6.20. Similar objectives to the previous simulations were to be satisfied ($Y_{clear} = 10cm, X_{Y_{max}} = 15cm, X_{stable} = 20cm$. Figure 5.4). The plots are arranged based on the individuals with the fitness of more than 1800/2000 in the pool. The simulation was performed for 30 generations.

Clearly, the maximum and average fitness values obtained for this pull is larger than the one obtained by simulation with only initial velocities at toe-off (see Figure 6.14 for 15 cm obstacle-toeoff distance). In Figure 6.20 the biceps activity usually started before the rectus acivity (biceps_ts vs. rectus_ts) while the rectus ativity lasted longer (biceps_td vs. rectus_td). The pulse magnitude for the rectus was slightly higher than that for the biceps. Many of the solutions in the pool included co-contraction between the two muscles (overlap between the area bordered by biceps_ts and biceps_td, and the area bordered by rectus_ts and rectus_td denotes the amount of co-contraction). Note that, in this model, for equal muscle pulse magnitudes, co-contraction would result in a net extensor torque on both hip and knee joints. Clearly, the pool shows that more than one solution exists.

The results of the simulation, for an obstacle height of 20 cm and the obstacle-toeoff distance of 55 cm (lead limb), are shown in Figure 6.21. Similar objectives to the previous simulations were to be satisfied ($Y_{clear} = 10cm, X_{Y_{max}} = 55cm, X_{stable} = 20cm$). The plots are arranged based on the individuals with the fitness of more than 1900/2000 in the pool. The simulation continued for 30 generations.

In the pool shown in Figure 6.21, the fitness values over 1900 increased significantly compared to the pool for the 15 cm obstacle-toeoff distance (shown in Figure 6.20. Rectus femoris activity (rectus_ts) often started prior to biceps femoris (biceps_ts).

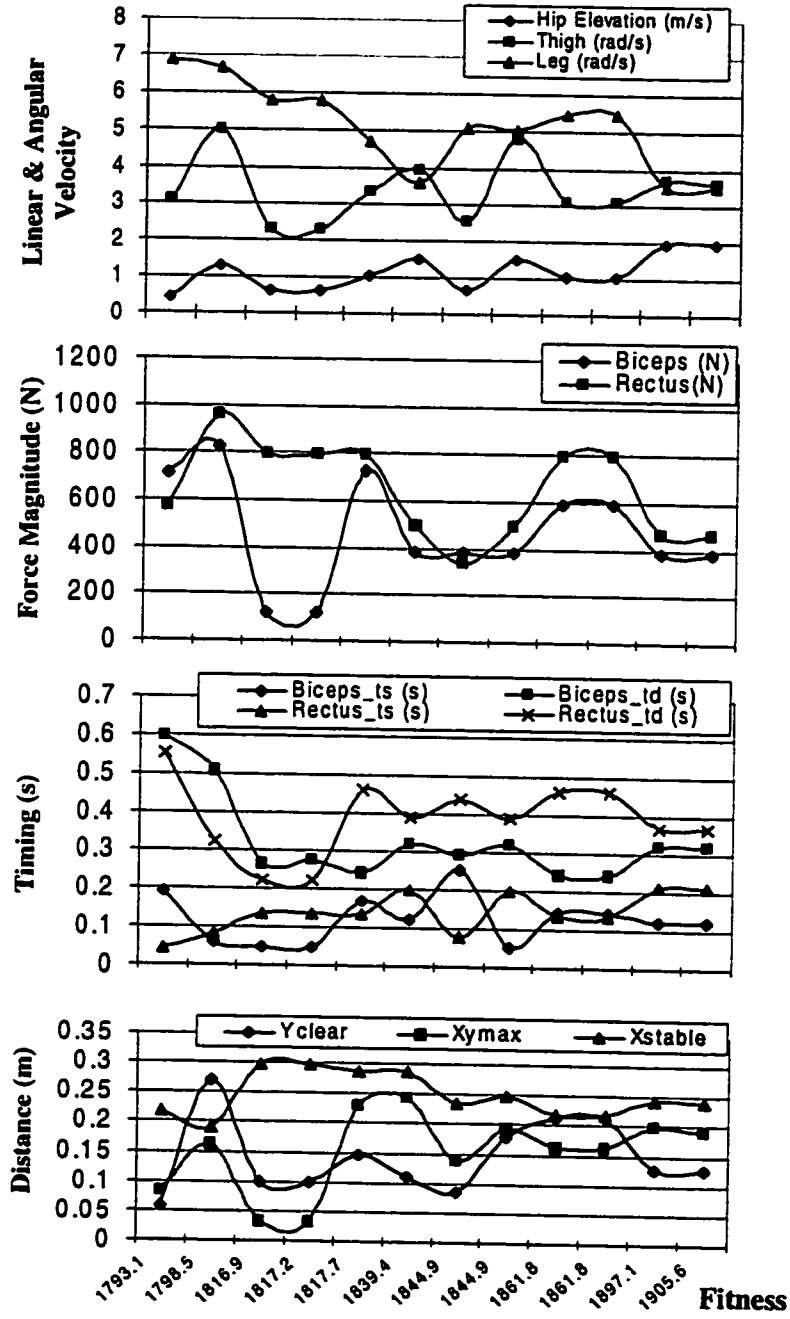

Figure 6.20: **Initial velocities, muscle pulse magnitudes, timings, and the fitness criteria for reference inputs of 20 cm obstacle height and 15 cm toeoff-obstacle distance.**

Also, some of the solutions showed no muscle activity (consistent with the simulation with initial velocities only).

6.5.8 Adaptive Locomotion

An important question yet to be addressed is how successful can the neuro-fuzzy network operate over a range of untrained obstacle heights? The neuro-fuzzy network was trained such that reinforcement learning continued with random reference inputs (visual data) for the first two generations. After that, reinforcement learning of the network weights (rule-base) was terminated and genetic learning on the linguistic sets of the network outputs (the initial velocities at toe-off) continued for 28 more generations. Genetic optimization was performed with only one pair of reference values (obstacle height of 10 cm and obstacle-toeoff distance of 55 cm). After the network was trained, its performance on a range of obstacle heights (5 cm to 40 cm) was examined (Figure 6.22). For the simulation shown, only three linguistic sets (small, medium, and high obstacle; short, medium, and long toeoff-obstacle distance; and low, medium, and high for each of the three control inputs) were used to train the network.

The neuro-fuzzy network showed a satisfactory performance over a range of obstacle heights (Figure 6.22). A typical figure for one of the genes with a high fitness of 1800/2000 shows that the network learned how to increase the hip elevation with increasing obstacle height. The trend observed was consistent in most of the pool with fitness values over 1800/2000. The average failing rate over three simulated pools was 20%. Additional training and increasing the number of linguistic sets from 3 to 5, resulted in better fitness values for the network trained obstacle height (15 cm), and also its neighborhood heights (10 cm and 20 cm). However, the network usually failed to produce a satisfactory performance over obstacle heights far from the trained height.

Genetic learning of a neuro-fuzzy network exposed to two sizes of reference obstacles (10 and 30 cm obstacle height, 55 cm toeoff-obstacle distance), and initial

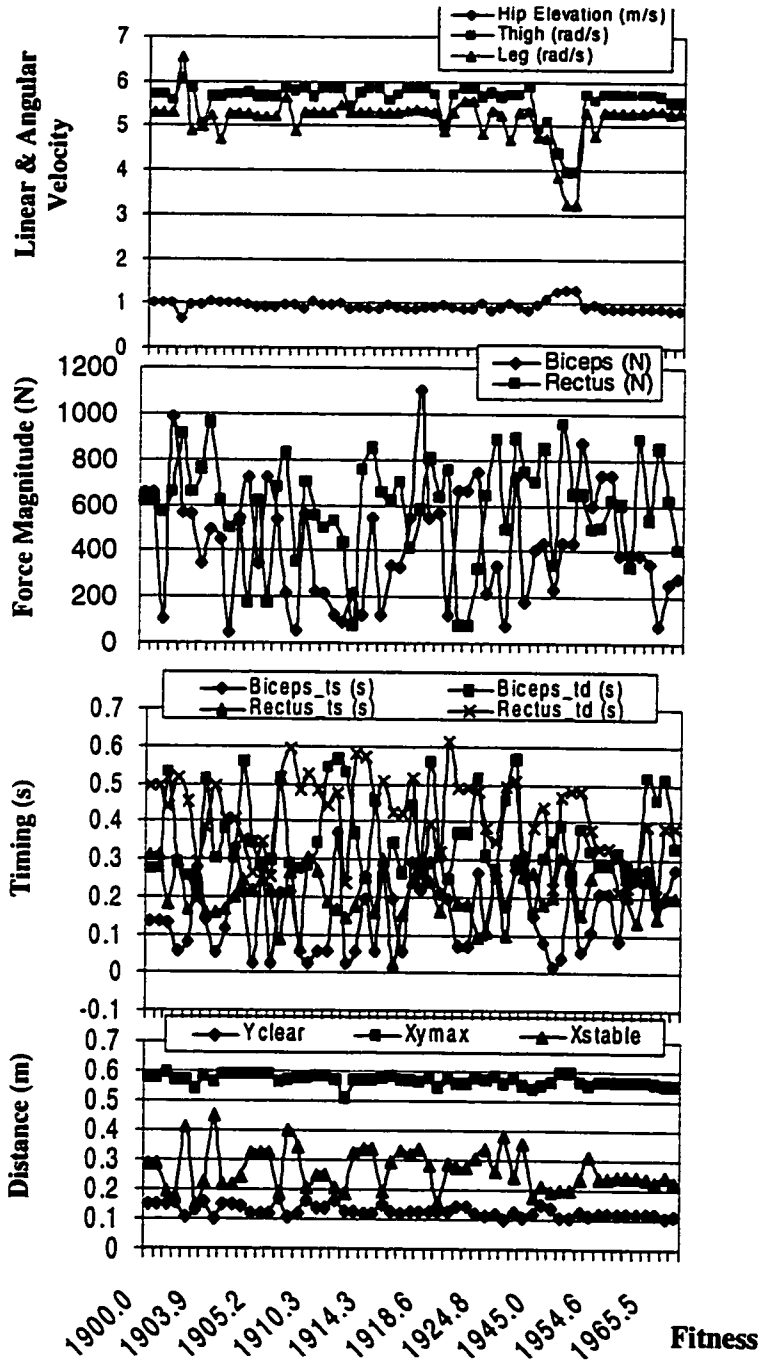

Figure 6.21: **Initial velocities, muscle pulse magnitudes, timings, and the fitness criteria for reference inputs of 20 cm obstacle height and 55 cm toeoff-obstacle distance.**

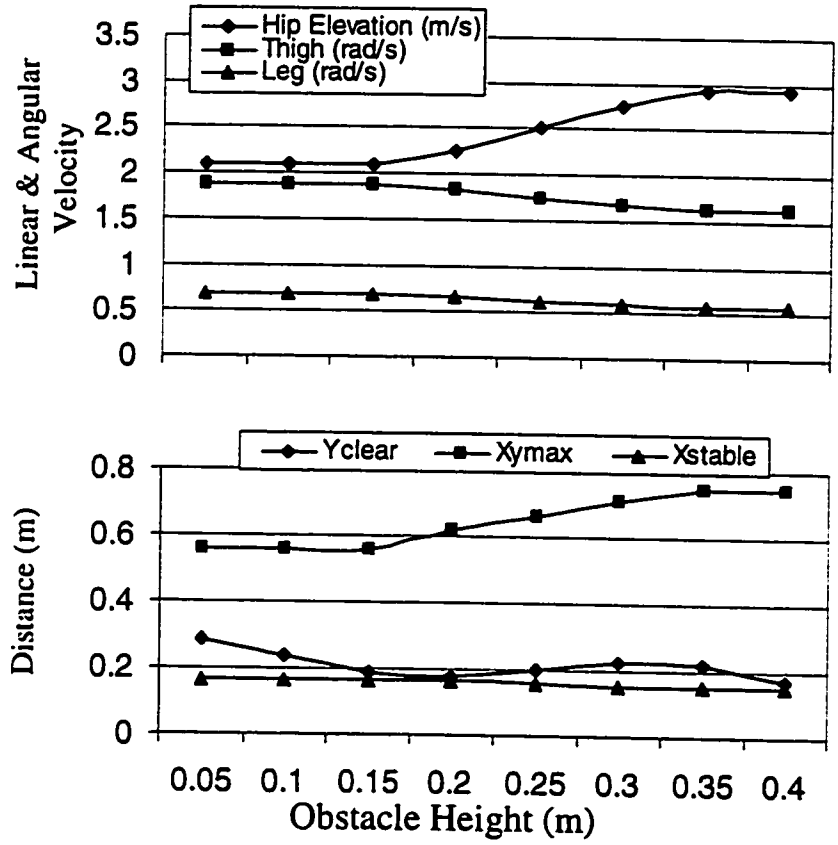

Figure 6.22: **A neuro-fuzzy network which was trained with an reference obstacle height of 15 cm and toeoff-obstacle distance of 55 cm was successfully used for stepping over various obstacle heights.**

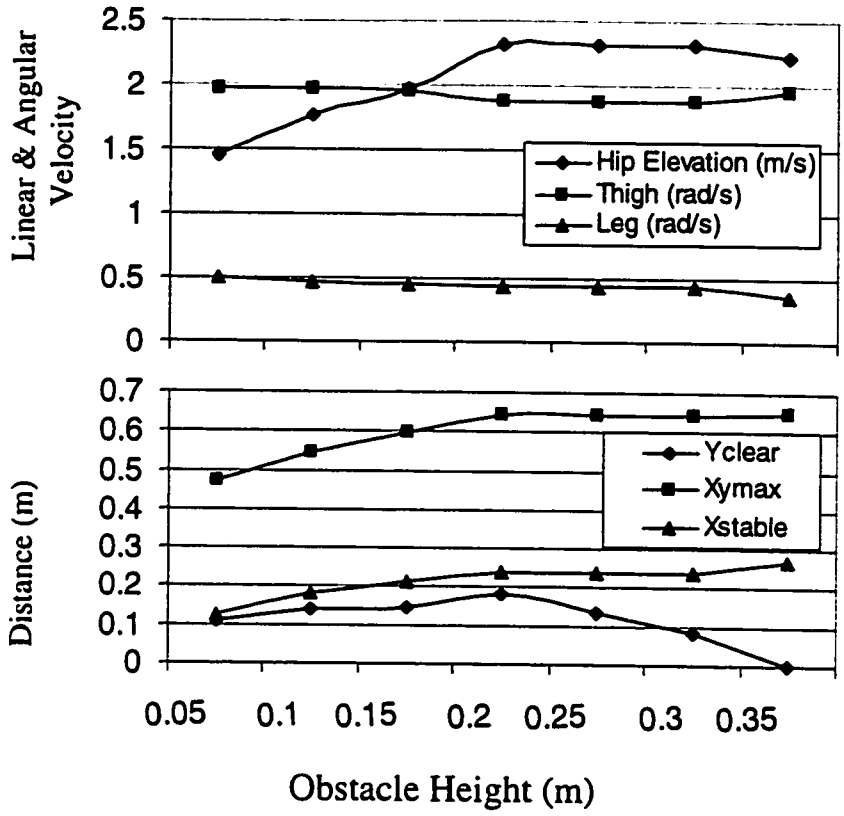

Figure 6.23: **A neuro-fuzzy network which was trained with two reference obstacle heights (10 cm and 30 cm) and the toeoff-obstacle distance 55 cm, was successfully used for other obstacle heights.**

reinforcement learning (2 generations) that showed an improvement in the failure rate (10.1% after 30 generations). The simulations were performed with 5 linguistic sets for each reference input (obstacle height and location) and 3 linguistic sets for each network output (toe-off velocities). In general, the fitness of the pool was better conditioned than the simulation where only one reference obstacle was used to train the pool. Most of the individual genes in the pool showed satisfactory performance when interpolating, and relatively poor performance when extrapolating the size of an obstacle. Figure 6.23 shows that except for the 35 cm obstacle, performance was satisfactory. Also evident is that hip elevation velocity at toe-off was most correlated with the size of the obstacle.

6.6 Discussion

Genetic optimization was found to be more robust than the gradient descent and direct optimization methods used in the optimization chapter. The large search space, the nonlinear interaction of the free parameters, and the existence of local minima in the search space were some of the reasons that made genetic optimization a more attractive approach for this work.

In many cases, the program accomodated several solutions to the problem. The characteristic of finding a population of solutions rather than one optimum solution is consistent with human behavior, demonstrating a choice of strategies in performing a task such as stepping over an obstacle. These characteristics turned the approach into an effective tool for analyzing the sensitivity of the solution to the control parameters and/or their range of effectiveness.

One interesting result of this work is the use of genetic optimization for sensitivity analysis of the control variables. The development of a pool of solutions, which satisfy certain criteria (Figure 6.11), showed the sensitivities of each of the initial velocities in the final solution pool. The results indicated that foot and/or ankle angular velocities were not crucial for achieving the desired trajectory. The ankle angular velocity at toe-off was produced by active muscle forces, (especially the plantarflexors), during the double support phase. In Chapter 3, however, we concluded that ankle push-off is the major potential contributor to the swing hip elevation velocity and ankle plantarflexor velocity at toe off. The addition of these two results suggests that the primary responsibility of the plantarflexor activity, observed during the double support phase, is to increase the swing hip elevation velocity. There is no advantage to increasing ankle angular velocity in the system.

The initial simulations were conducted using a minimal number of control parameters without any limiting constraint. Additional fitness criteria and new constraints were provided systematically to eliminate physiologically and anatomically unacceptable solutions (Table 6.1). The approach of starting the simulation with a limited number of free parameters, rather than introducing all the available control parame-

ters, proved to be beneficial in providing a better understanding of the system. Using this approach it was found that active control during the swing phase was more crucial for the trailing limb than for the leading limb (Figures 6.15). This approach also showed that for the leading limb, less active control during swing and more planning during the double support phase was required. These insights could not been achieved if the simulation had started with several active muscle forces.

It has been shown that the stepping strategy is planned a few steps before reaching the obstacle [33]. This suggests that for the leading limb, the muscle forces during the double support phase (producing initial velocities at toe-off) may be at least as important as the active control during the swing phase. Other experiments, in which the subjects were tripped over unexpected obstacles, further strengthen this hypothesis. These experiments showed that the subject failure rate dramatically reduces when the unexpected obstacle is seen one step ahead, suggesting that active control is not the first line of protection for a safe landing. Also, based on the calculations in chapter 7, the very short available response time (ART) for reacting to a body perturbation (usually in the range of 60ms), indicates that some proactive mechanisms, in addition to the active control during the swing phase, is necessary to ensure safe locomotion (see also [19, 25, 33]).

With respect to the above discussion, the requirement of using minimal active control during the swing phase could be very advantageous to the safety and perhaps the efficiency of the movement. Initial velocities at toe-off (produced by active muscle forces during the double support phase) were found to best satisfy the objectives when the obstacle is encountered at mid swing ($50-60\%$ obstacle location to stride length ratio). The experimental data obtained from young subjects stepping over obstacles at their normal pace [33] (see also the results in chapter 7) were consistent with this result. When the obstacle was encountered in mid swing, minimal active control was necessary to satisfy the efficiency and safe trajectory objectives. The use of minimal active force during this phase has certain advantages. When the CNS does not rely on active muscle forces to produce a satisfactory toe trajectory, it can use these resources

to produce a faster recovery strategy in the case of an unexpected perturbation to the body center of mass (such as an unexpected trip over an obstacle). The importance of the above statement is better revealed when considering the very short available response time for reactive response to a mechanical perturbation (Chapter 7).

Hip elevation velocity plays a major role in both placing the maximum toe elevation over the obstacle (Figure 6.18), and producing the required toe clearance (Figure 6.19) over a range of obstacle heights. Hip flexor velocity at toe-off seems to be more correlated with stride length, and has a dominant control over stable landing (Table 6.2). As concluded from Chapter 2, the hip elevation velocity at toe-off is more energy efficient than the active knee and hip flexor torque during the swing phase of stepping over an obstacle.

From these results it can be suggested that for the trailing limb, hip elevation velocity at toe-off is not the dominant contributor to the toe elevation. It is important to note that hip elevation velocity also has a dominant effect on locating the maximum toe elevation during the swing phase. As the size of the obstacle increases, the hip elevation velocity at toe-off moves the location of the maximum toe elevation towards late swing. The optimization program then starts to reduce the effect of hip elevation velocity. The lost toe elevation due to this correction is compensated by increasing the knee flexor velocity. However, the additional knee flexion velocity will result in a lower stability margin. Thus the potential failure rate increases for the trailing limb pools (Figure 6.17). As such, when obstacles are encountered during early swing (trailing limb stepping over the obstacle), the relative importance of the hip elevation strategy reduces. Therefore, we could expect to see more contribution from active knee torques for the trailing limb. In fact, the experimental observations reporting the high energy correlation of the hip elevation strategy with the obstacle height were done for the leading limb and not for the trailing limb [63].

The observations on the trailing limb in this chapter complement the results of the optimization chapter. The results reconfirm that initial velocities at toe-off are important for the leading limb to step over the obstacle. In the previous chapter,

it was shown that bi-articular muscles could not achieve a successful swing over the obstacle without modifying the initial conditions. The bi-articular muscles, however, were found to be sufficient for the trailing limb to clear the obstacles and to achieve a stable landing. The added result to this scenario was that the initial velocities at toe-off by themselves are not sufficient to produce an acceptable trajectory.

Adaptive locomotion over various sized obstacles was achieved by exposing the model to only one or two different obstacle sizes, after the second generation. It is important to note that the design of the network (the number of the linguistic sets, the universe of discourse, and the membership shape) has an affect on the results obtained for adaptive locomotion. The purpose of this section was to demonstrate that such a goal is achievable with this network. The complete training of the network could include the number of linguistic sets for each variable. Similar to feed-forward neural networks, the neuro-fuzzy network can fall into the danger of memorizing data points, instead of generalizing the complete behavior. This problem will be more significant when the muscle actuators are added to the control input sets.

The adaptive network introduced in this work represents the stepping block in Figure 6.1. The same structure could also be used for the other blocks, except the input-output definitions would need to be modified.

Research has shown that the two bi-articular muscles, rectus femoris and biceps femoris, have significant activity during the swing phase of obstructed gait [50, 63]. Biceps femoris has two peaks of activity. The first peak starts prior to heel contact and continues during early swing. The early activity of biceps femoris plays a critical role in elevating the limb over the obstacle. The second pulse of activity of the biceps is modeled by the nonlinear damper and spring. The forces exerted by these springs and dampers model both the passive forces arising at the joint limits, and the second burst of activity in biceps femoris during late swing. The activity of the rectus femoris generally occurs after clearing the obstacle, and is used to provide a stable landing and an adequate step length.

The addition of bi-articular muscles resulted in achieving higher fitness values for

the trailing limb, compared to the simulations that only included initial velocities at toe-off as control inputs. This suggests that for the trailing limb, the use of active control during the swing phase is necessary and could be achieved by bi-articular muscles. The early activation of biceps femoris is consistent with experimental findings [50, 63]. However, the genetic pool offered more than one solution, some including co-contraction. Co-contraction indicates the possibility of the existence of another optimization criterion such as joint stiffness in the human ambulator. It could also indicate the contribution of single articular muscles on the hip and knee joints during the swing phase. Therefore, the observed co-contraction may have substituted for the single articular muscle activity which was not modeled in this work.

As expected for the leading limb, the addition of bi-articular muscles introduced redundancy in the solution space. We have already observed that for the leading limb, initial velocities at toe-off by themselves produce high fitness values. The addition of bi-articular muscles increased the number of possible solutions. The use of these muscles reduced the need for higher initial velocities. Therefore, they affect both metabolic cost and joint stiffness. Also for higher obstacles, the initial velocities at toe-off were not sufficient to fully optimize the swing (see Figure 6.19). Application of the bi-articular muscles could assist on this matter also.

Similar to a human ambulator, the development of pools of solutions ensures that the model can adapt to potential changes in the environment. The addition of muscle forces in both cases of trailing and leading limb stepping over the obstacle provided islands of solutions. It is important to note that these islands are not inclusive; they represent only a portion of the possible solutions, not all the possible solutions. Therefore, these values may not include all the range of solutions used by humans. On the other hand, several other characteristics, specific to humans, are not included in producing these pools. Some of the limitations of this work, in regards to this matter, are as follows:

- Only one typical anthropometric data set [83] was used for the link segment model. The possibility of the influence of other anthropometric parameters

(e.g. leg length to obstacle size ratio) was not considered.

- The requirements for lateral balance may impose some limitations on the use of the hip elevation strategy. These requirements were not modeled in this work.
- The simulations were performed for normal speeds of stepping over obstacles. The effect of varying the speed and active control of the stance ankle during the swing phase was not considered.
- Addition of uni-articular muscles, increases the number of possible solutions. This may result in more desirable solutions (specially for the trailing limb) because of reduction in co-contraction.
- Experiments that compare the energy correlation of trailing limb's various strategies to the obstacle height can shed more light on the direction of this research.

Chapter 7

Estimating Available Response Time following a Trip over an Obstacle

In previous chapters, modelling has been used to gain an understanding of the *proactive* balance control strategies where the muscle actuation try to provide safe toe clearance over the obstacle and a safe landing [19]. In this chapter, the modelling approach is applied to gain insight to *reactive* balance control strategies during locomotion. Specifically, the recovery from an unsuccessful step over an obstacle (tripping) is considered here.

7.1 Introduction

Tripping is one of the major causes of falls during locomotion. Controlling the balance of the body after a trip is a complex motor task. It involves control of several body segments subjected to relatively large dynamic forces and torques.

The study of unexpected perturbations during locomotion has provided some insights to the neural mechanism and sensory interactions responsible for reactive response to a trip to regain balance of the body. These studies were usually based on

electrical stimulation of cutaneous receptors for the lower limbs during locomotion of cats or humans. This method enables researchers to control both timing and amplitude of the stimulation. The latency of the reactive responses measured have generally shown that the first line of defense to an unexpected perturbation is of reflex type (a stereotypical reactive response which is not voluntary). However, the responses are not monosynaptic (stereotypical reflexes characterized by latency of between 25 and 60 ms; they form a feedback loop from sensory receptors directly to motoneurons that activate the muscle fibers). Rather, responses are polysynaptic (they include intermediate neurons in the loop from sensory receptors to motorneurons). Polysynaptic responses are usually characterized by latencies between 60 and 120 ms. The review from Dietz [19] nicely describes the nature of these responses.

The results of research with electrical stimulation also indicates that latency and amplitudes of reflexes depend on the phase of locomotion. Cats response to cutaneous stimulation by excitation of flexors during the swing phase, and excitation of extensors during the stance phase [21, 22, 27, 28, 65]. Humans also exhibit the same phase-dependent excitation pattern when exposed to cutaneous electrical stimuli [8, 23]. Yang and Stein [87] found a reversal of the response from excitatory to inhibitory within the swing phase of human locomotion. They attributed this response to the task of control of balance. The excitatory response of the tibialis anterior in early swing resulted in extra limb flexion, while the inhibitory response during late swing resulted in lowering the limbs. Both flexing the limbs during early swing and lowering the limbs during late swing are appropriate responses for regaining the balance of the body. These longer latency reflexes are dependent on the movement task [73] and the phase of the gait cycle [25].

Mechanical perturbation to the balance is more realistic than electrical stimulation. Dietz et al. [20] studied the responses to mechanical perturbation of balance during treadmill locomotion. They attached a cord to the swing limb and momentarily obstructed the swing leg motion. They found that the perturbation applied during late swing results in larger muscle excitations. Eng et al. [25] studied the

recovery from an actual trip during locomotion over ground. They observed an elevating strategy when the obstacle was encountered early in the swing (flexion of the swing limb and extension of the stance limb). They also observed the lowering strategy (extension of the swing limb and flexion of the stance limb) during late swing. Both these recovery strategies were attributed to the overriding concern of the CNS to the balance and stability. Rietdyk and Patla [67] tripped their subjects in a uni-limb support condition (stance limb support), and tri-limb support (stance limb support and arms resting on two parallel bars). They found that "the magnitudes of the EMG reflexive response to the trip were clearly modulated as a function of the threat to stability, not in a simple manner, but rather in a complex manner which optimized the recovery strategy". Their subjects also exhibited anticipatory adjustments which by the nature of the experimental protocol cannot be avoided.

The fact that during unexpected perturbations, reflexes are recruited suggests that the CNS cannot wait for a voluntary response. It is important for our overall understanding of the response strategy to determine the theoretical maximum response time available to the CNS.

We use a modelling approach to predict the available response time (ART). We define this as the time required for the body center of mass to move just ahead of the leading metatarsal-phalangeal (MP) joint after hitting an obstacle during the swing phase of locomotion (Figure 7.1). The modelling approach eliminates the element of anticipation to the trip. The model also provides some insight to the possibility of a voluntary response to the trip. As well, the quantitative effects of obstacle height, obstacle compliance, limb proximity to the obstacle, and phase of the swing over the obstacle are also investigated with respect to the ART.

7.2 Methodology

Experimental data were collected from subjects stepping over various size obstacles in the pathway. The 3-D kinematics of the motion were captured, the joint orientations

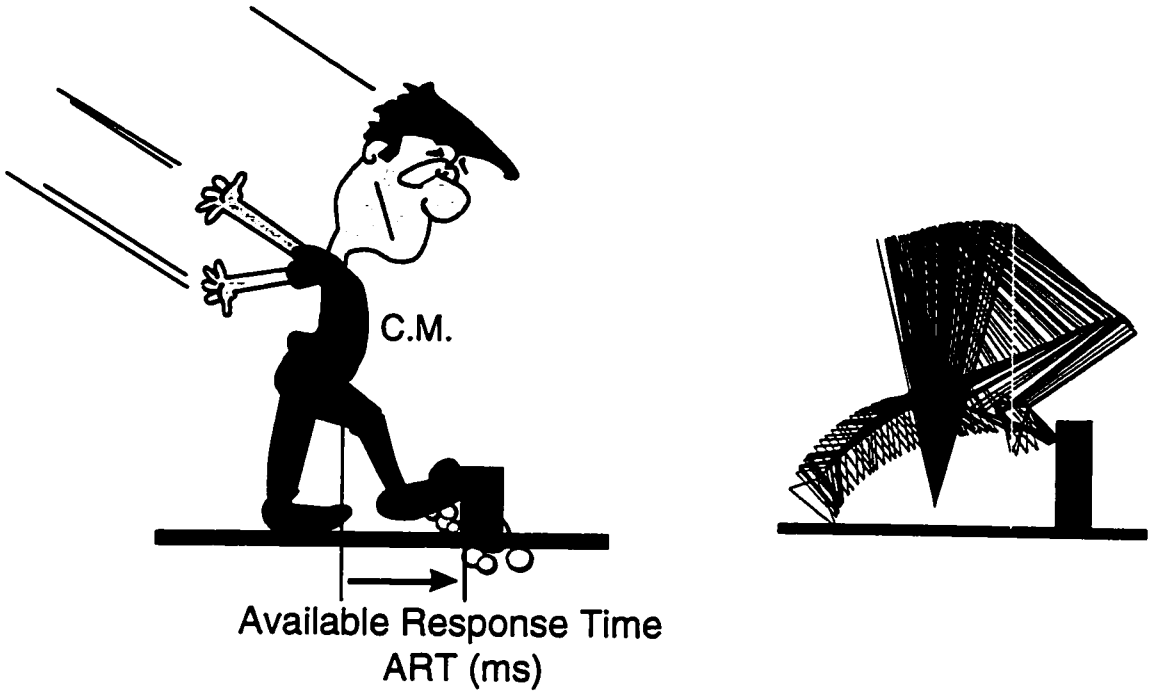

Figure 7.1: **Available Response Time (ART).**

and position were matched to a linkage model, and the joint torques were calculated. These torques were then used in a forward solution model to simulate the trip over unpredicted obstacles.

7.2.1 Experimental Protocol

Four healthy male subjects were asked to step over one of six different height obstacles ranging from 0.5 to 38 cm, placed halfway along a 12 m travel path. The obstacle was visible throughout the path, and the subjects were asked to walk at their natural speed. The height of the subjects ranged from 173 to 186 cm. The age of the subjects ranged from 28 to 35 years old. The weights of the subjects ranged from 65 to 78 kg. The The OPTOTRAK Motion Analysis system was used to capture the three-dimensional kinematics of the lower limbs. Twenty four infrared emmitive diode (IRED) markers were attached to eight segments of the lower limbs (three on each segment). These segments were: feet, legs, thighs, pelvis and trunk (Figure 7.2).

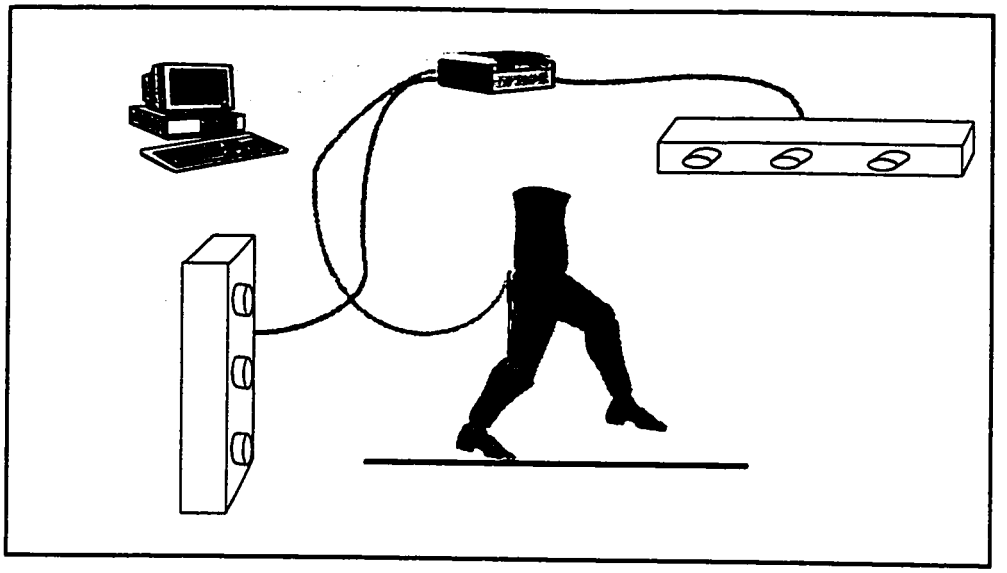

Figure 7.2: **Marker locations**

The markers were used to locate the principal axis, the position, and the orientation of the segments and joints. The eight segments had 48 degree of freedom (6 degree of freedom for each segment). The relative orientation of the principal axis (in the form of Xyz Euler rotation matrices) and the segment lengths were used to calculate the kinematics of the model that will be described in the next section. Manual and quadratic interpolations for any missed marker data were performed using KINGAIT software [39].

7.2.2 The Model

A six degree of freedom linkage model was developed to model the swing phase of stepping over an obstacle. The model included a prismatic joint (q_2) which accounted for the stance limb's joint interactions as shown in Figure 7.3. This also shows the generalized coordinates of the model. A symbolic program was written in MAPLE to derive the equations of motion using Lagrangian dynamics. The Denavit-Hartenberg convention [72] was used to define the joint coordinates (Appendix G).

The coordinate transformations from the principal axis of the 48 degree of freedom

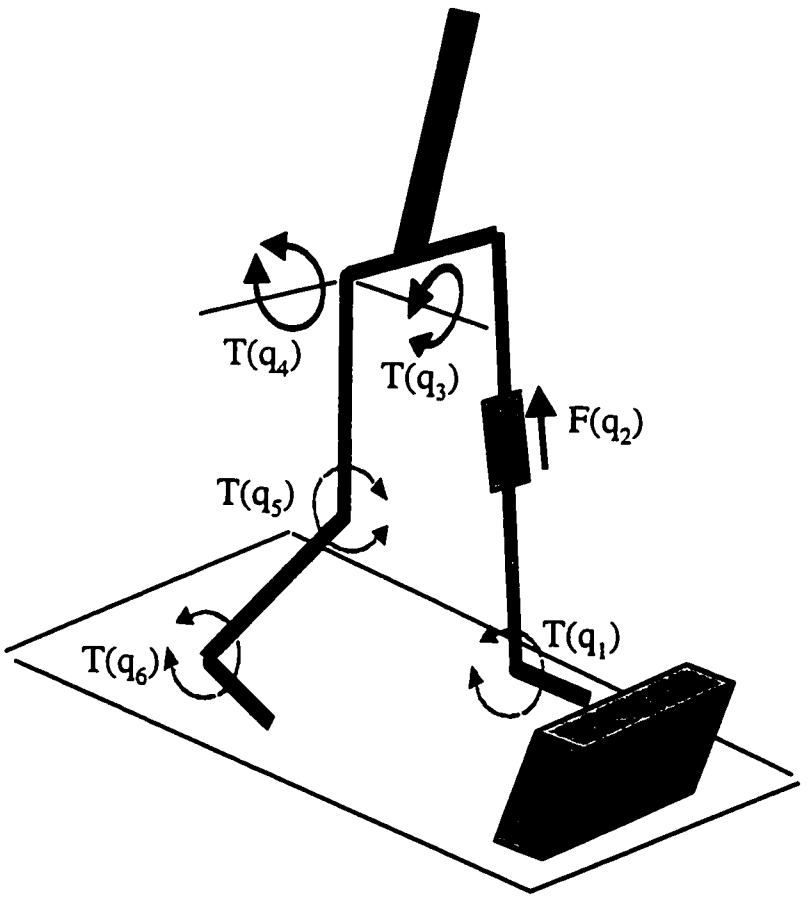

Figure 7.3: **Six degree of freedom model with prismatic joint.**

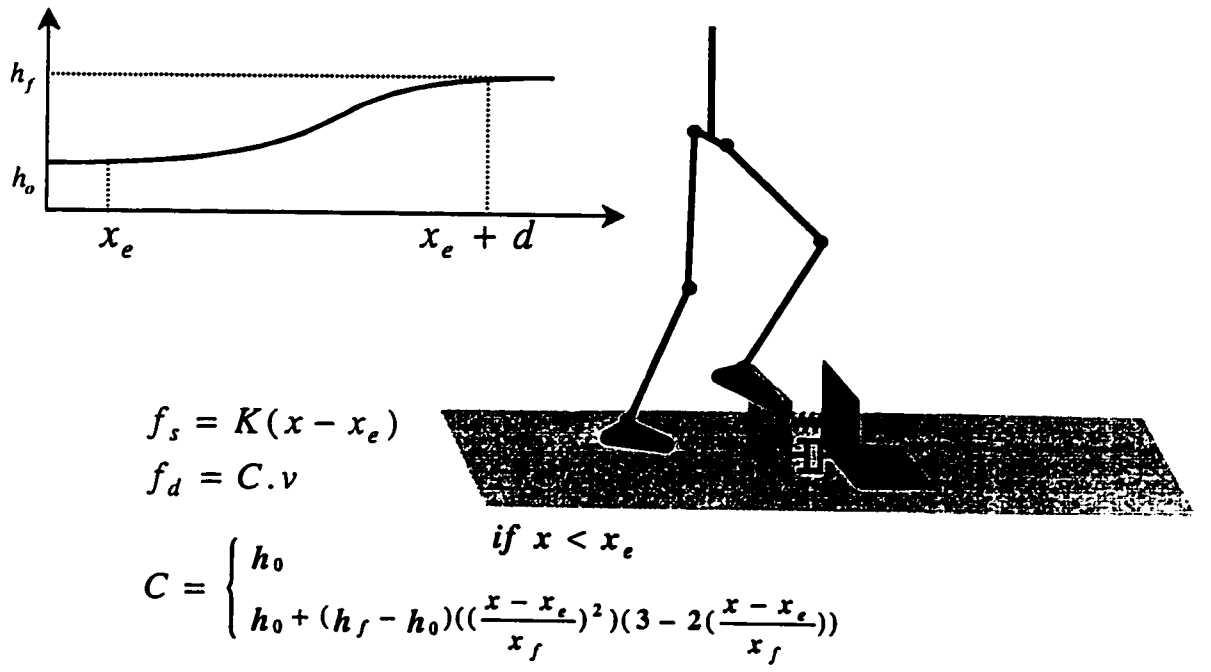

Figure 7.4: **Obstacle reaction force at impact.**

rigid body link segment model to the new 6 degree of freedom model was calculated.

Based on the calculated kinematics, the torques across the generalized coordinates of the 6 degree of freedom model (Figure 7.3) were calculated. The validity of the results was examined by reapplying these torques to the forward solution model, and deriving the kinematics of movement. The model kinematics were checked with that of the experimental data. The calculated and measured kinematics were in general agreement.

The calculated forces and torques over the generalized coordinates were applied to the forward solution model to find the trajectories before and after hitting an obstacle in the path. The simulated obstacle reaction force at impact was modeled by a linear spring and a non-linear damper. As shown in Figure 7.4, after the obstacle is hit ($x > x_e$), the spring force increases linearly ($F = K(x - x_e)$), where 1/k is the obstacle compliance. The damping coefficient is a function of $x - x_e$, and increases from h_0 to the final level of h_f as the obstacle is deformed from 0 to d cm.

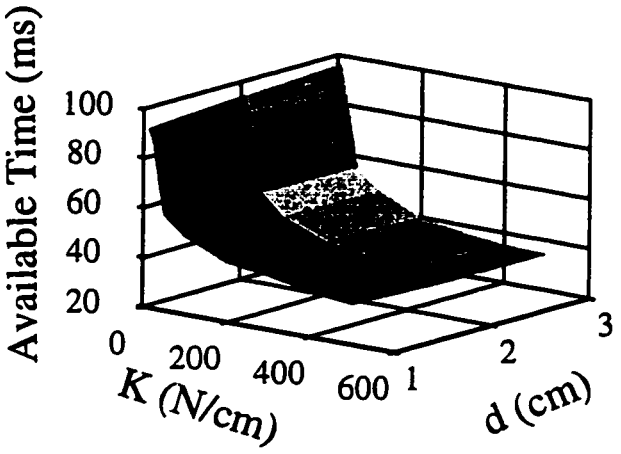

Figure 7.5: **The Effect of damping and compliance on the ART.**

As mentioned, this model was used to obtain some quantitative insight on the effects of obstacle height, limb proximity to the obstacle, and the phase of the swing on the *available response time.* In this study we refer to the location of the actual obstacle used in the experiments as *anticipated obstacle location*, and the obstacle's height is referred to as *anticipated obstacle height.* The location of the simulated obstacle which obstructs the toe trajectory in the simulation is referred to as the *impact location.*

7.3 Results

Both obstacle compliance and damping affect the ART. For the experimental trajectories, the effect of simulated obstacle compliance ($1/k$) and rate of energy absorbency (characterized by d in Figure 7.4) was examined. A typical plot for a trajectory over an obstacle height of 10 cm when the impact location is at the predicted obstacle location is shown in Figure 7.5. ART increases with increased obstacle compliance ($1/k$) and reduced rate of damping (d). However, the effect of the rate of damping was not as large when compared to the effects of compliance. ART ranged from 95 ms for compliant obstacles to 40 ms for rigid obstacles.

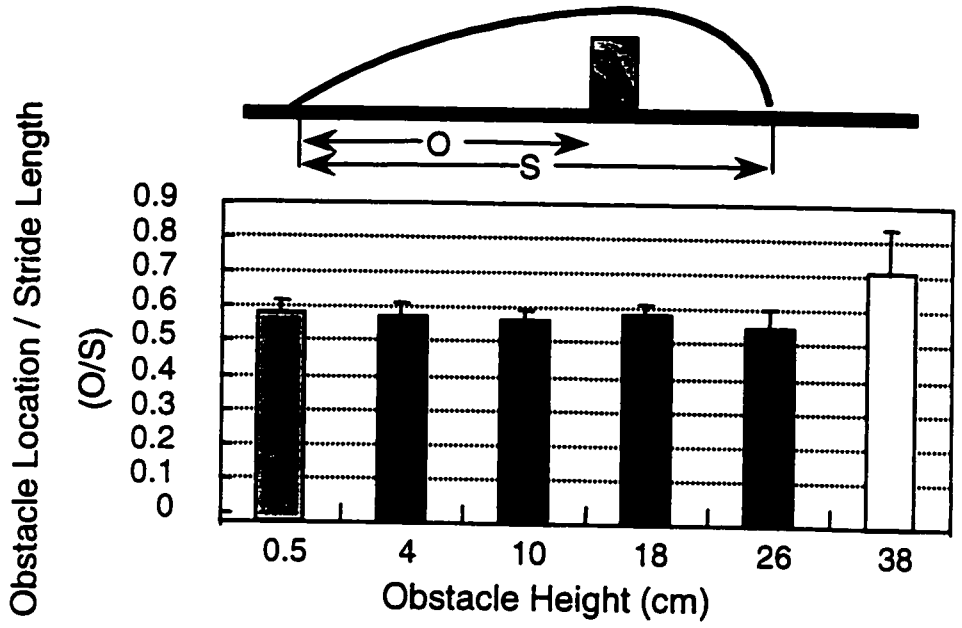

Figure 7.6: **Foot placement in young subjects.**

The ratio of obstacle location to stride length also affects the ART. The results of Patla and Reitdyk's [63] experiments demonstrated that the distance between the lead limb toe-off location and the obstacle (we call it obstacle location) is usually around 60% of the total stride length. In Figure 7.6, this ratio is referred to as the O/S ratio. The experimental results of the current work on young subjects confirm this finding (Figure 7.6). The results of our experiments show that for the small and medium size obstacles, the O/S ratio is normally within the range of 55% – 60%. However, for very high obstacles (38 cm obstacle) the O/S ratio increases to about 70% with a significant standard deviation.

In order to understand the above behavior, the model was examined by varying the simulated impact location along the stride length (Figure 7.7). Since the stride length found from experimental trials was constant, changing the impact location would indicate a change in the O/S ratio. The plot of available response time for a range of impact locations shows that when the obstacle is hit very early in the swing, ART goes over $180ms$. ART was minimum when impact location was around

mid swing, and ART was smaller for impact location in late swing compared to early swing. By increasing the O/S ratio from below 60% to above 70%, ART was increased by $25ms$. However, further increase to the O/S ratio from 70 to 80% did not affect ART.

ART increases with anticipation of the larger obstacle heights. This was examined by simulating the impact at anticipated obstacle locations for trajectories resulting from different obstacle heights (Figure 7.8). The increasing trend of ART was more distinguishable for the largest obstacles (26 and $38cm$). The standard deviation for these size obstacles was also increased. However it seems that only for the largest obstacles ($38cm$ height) the ART value was greater than $180ms$.

It is important to note that Figure 7.8 does not show "what happens to the ART when we trip over a larger obstacle". It shows "what happens to the ART when we are *expecting* to go over a larger obstacle, but we trip".

Even with removing the effect of the O/S ratio, the trend of increase of ART with anticipated obstacle height persists. The effect of the O/S ratio on anticipation of different size obstacles was removed by simulating the impact location at mid stride (Figure 7.9). ART reduced for all the anticipated obstacle heights from what was shown in Figure 7.8. However, a similar trend of increase in ART with anticipated obstacle height to that shown in Figure 7.8 was observed.

7.4 Discussion

The low ART values suggest that for the lead limb, voluntary responses cannot be the first line of defense: reflexes are necessary to recover from a trip. The range of ART for the lead limb (50 to 140 ms) suggests that in most cases a polysynaptic response for recovery from a trip could be adequate. While previous experimental results have suggested that the CNS uses polysynaptic reflexes to recover from an unexpected perturbation, no published work has commented on the possibility of voluntary reactive response to a trip.

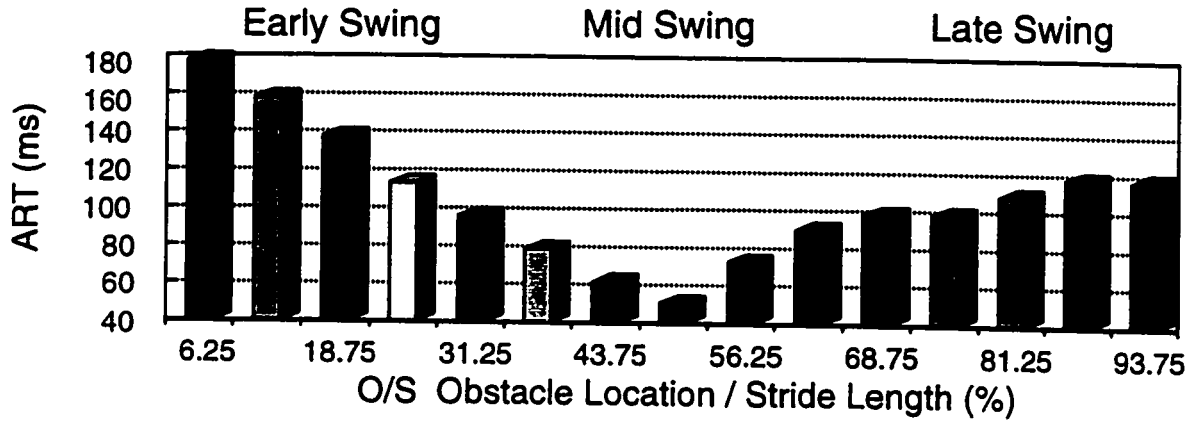

Figure 7.7: **Dependence of ART to O/S ratio. Anticipated obstacle height was 10 cm.**

The available response time for recovery from a trip during early swing is much greater than mid and late swing. This suggests that we can afford to be lax with the trailing limb as the threat of tripping is less severe. Note that in experimental studies accidental trips usually occur with the trailing limb and not the leading limb.

ART provides some insights on the O/S ratio used by humans when stepping over various size obstacles. Young adults step over small and medium obstacles with an O/S ratio of 60%. They increase this ratio to 70% when stepping over very large obstacles ($38cm$). This causes the subjects to encounter the obstacle later in the swing phase. By this time, the velocities of the hip and toe have not only reduced [83], but also the lead toe has traveled more anterior to the center of mass of the body. ART seems to increase (see Figure 7.7) when the threat of obstacle height to the control of balance increases.

ART also gives some insights to the adjustments of the CNS to the O/S ratio, due to aging and vision deficits. Patla et al. [33] observed that in healthy elderly populations the O/S ratio increased to 70% compared to 60% observed in young population. However, this ratio was maintained around 70% for cataract patients after the first and second surgery, and did not change significantly (Figure 7.10). The results of the simulation (Figure 7.7) show that by increasing the O/S ratio from

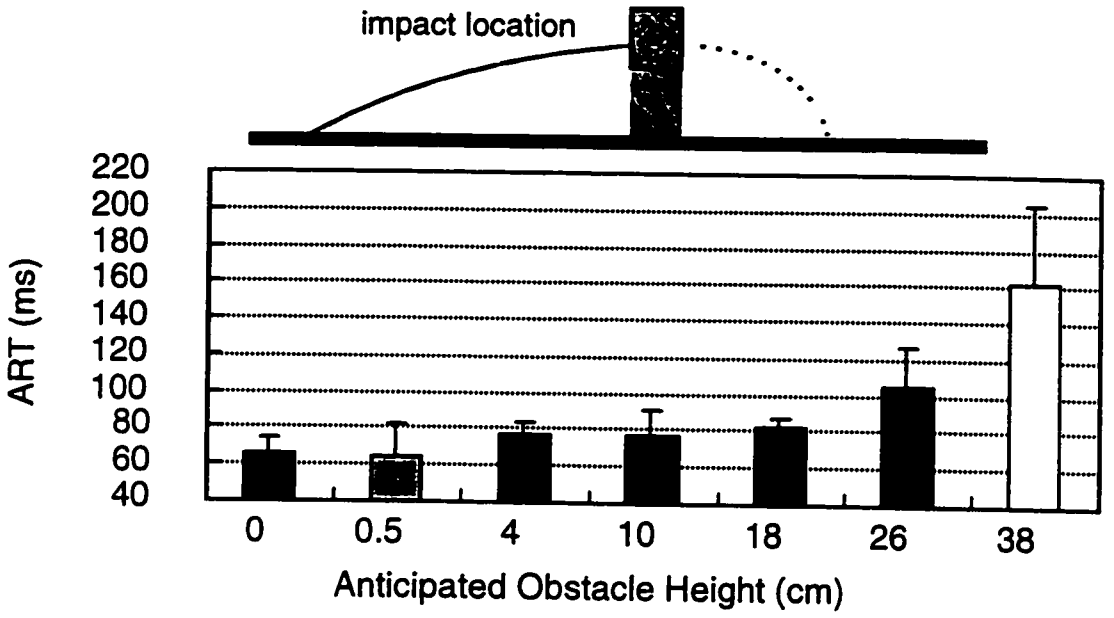

Figure 7.8: **Dependence of ART to the anticipated obstacle heights.**

60% to 70%, some safety margin will be added due to the increase in ART; however, not much will be gained with further increase in the O/S ratio. Therefore, even the elderly (who step more conservatively over obstacles) and people with vision deficits do not tend to increasae their O/S ratio to more than 70%.

The values of ART also suggest that it is more important to control the velocity of the center of mass and foot, than positioning the center of mass back further (i.e., increasing the distance between the lead toe and the center of mass). This conclusion can be arrived at by comparing Figures 7.8 and 7.9. The increase in ART with anticipation of larger size obstacles is both due to the relative location of the center of mass with respect to the leading toe, and the velocity of the center of mass and the leading toe. ART is also affected by the impact force on the foot and the active muscle forces (Figure 7.5). However these effects are minimized in Figure 7.8, because the same obstacle characteristics were used for all the simulations shown. By performing the simulation with the impact location at mid swing for various obstacle sizes, the effect of the O/S ratio to the ART was also removed. In Figure 7.9, the only remaining parameter for the regulation of ART was the effect of the center of

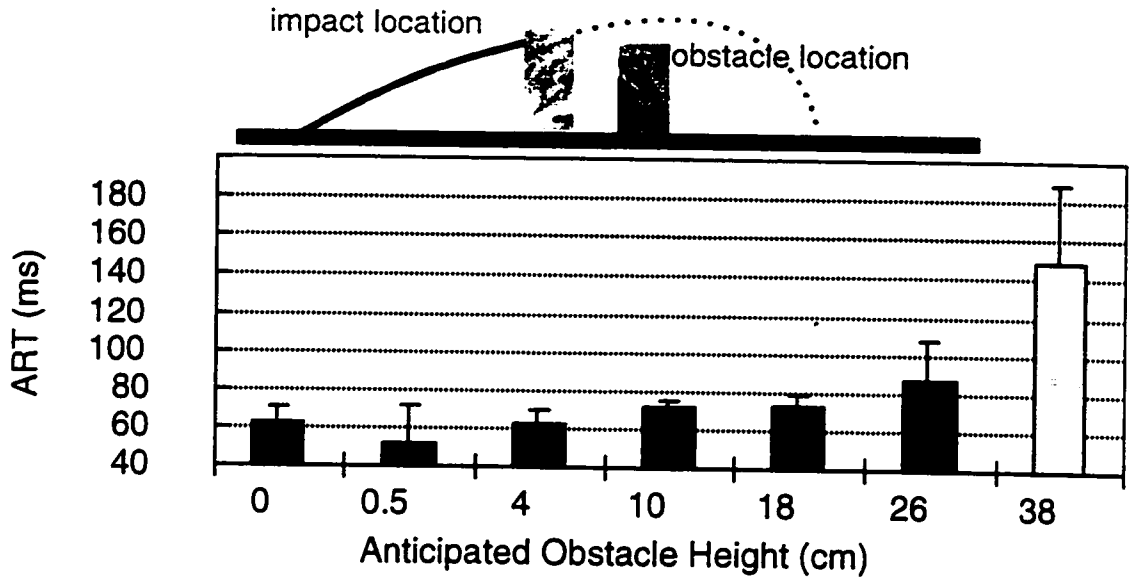

Figure 7.9: **Change of ART when impact location is at 50% of stride length.**

mass velocity. The similar trends in Figures 7.9 and 7.8 demonstrate that the center of mass velocity has the most dominant effect on the observed increase of ART with anticipated obstacle height. This is consistent with the results of Chen et al. [14] who concluded that the reduction of the horizontal velocities of the toe and of the center of mass when stepping over obstacles are important.

The values obtained for ART are usually overestimated. This is because of the assumption that the trunk stays perpendicular to the pelvis. In real life, however, while stepping over obstacles, the trunk is behind the pelvis and travels slower than it. This causes an overestimation of ART which is an additional reason why a voluntary response to recovery from a trip is not possible.

The final point worthy to note is that ART, as defined, is not the ultimate indicator of the recovery from a trip. The body momentum at the time of impact, and whether or not the muscle forces trap this momentum, are the major indicators of the possibility of recovering from the trip. However, such definition would largely rely on the state of the muscles at the time of impact. Our choice of ART will put these results on the conservative side: before the center of mass passes the leading

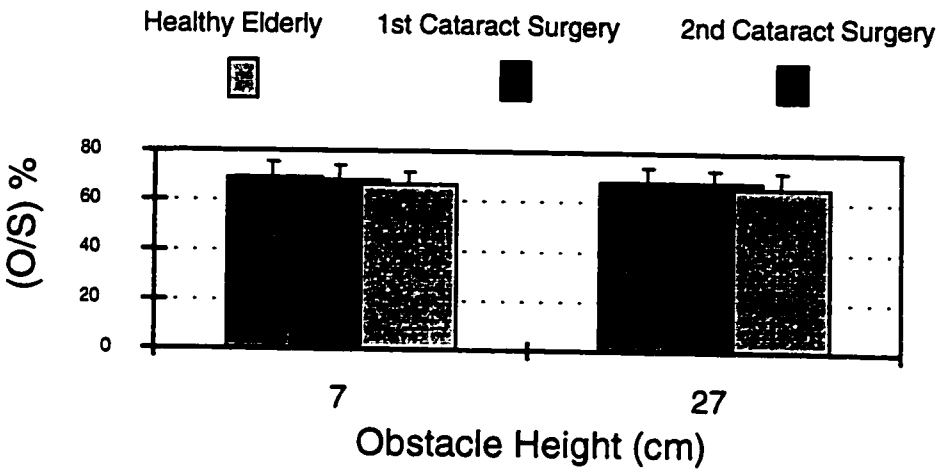

Figure 7.10: O/S **Ratio in Healthy Elderly and Patients with First and Second Cataract Surgery.**

toe, the recovery from the trip may or may not be possible. After that, the chances of recovery from the trip would be very slim, since both feet would be behind the obstacle. A more detailed definition of the ART cannot offer much improvement to the results. This is because the accuracy of the model prediction is limited by many approximations (six degree of freedom model, rigid links, and one or two degree of freedom joints).

7.5 Conclusions

The available response time provides some insight to the possibility of voluntary and/or type of reflexive response to the tripping over obstacles. The available response time after a trip increases with obstacle compliance, size, and its location with respect to the stride length. It also depends on the velocity of the swing foot and the location of the center of mass at the time of impact. The simulation suggests that at normal speeds and smaller obstacles, polysynaptic responses to tripping are the only possible option for the human locomotor. Only if the obstacle is hit in early swing is a voluntary response to the trip possible.

Chapter 8

Conclusion

The contributions of this work and recommendations for future directions in continuing this research are now presented on a chapter by chapter basis:

8.1 Summary of Conclusions

In Chapter 2 we proposed that a biomechanical model of the swing phase of locomotion would be useful to understand the role of active torques and forces and intersegmental dynamics during the swing phase of locomotion over both level ground and obstacles. Simulations based on this model have shown that mechanical interactions between segments provide energy efficiency for walking on level ground and over obstacles. It is clear that the control system exploits these features of the effector system to regulate locomotor patterns over different terrains.

A summary of the most important results obtained are as follows:

- During level ground walking, there are no initial conditions at toe-off that can produce a swing that provides adequate ground clearance and stable landing. However, minimal active control exerted at the ankle joint is sufficient to achieve a normal swing phase.

- Obstacle avoidance strategies used by subjects to elevate the limb are economical in terms of energy cost while ensuring stable landing. Specifically, translational energy applied at the hip joint provides a given toe elevation for minimal energy cost but severely compromises subsequent landing. This strategy is most effective when it is initiated during the double support phase.

- The contribution of intersegmental dynamics is greater when active (flexor) control is implemented at the knee joint compared to the hip joint.

The experimental results [61] and the planar model of Chapter 2 demonstrated the dominant contribution of translational hip energy to swing toe elevation when stepping over obstacles. In Chapter 3 the model was expanded to 3-D in order to investigate the potential strategies for elevating the hip. The results are as follows:

- Gravity, via intersegmental dynamics, helps elevate the limb during the swing phase.

- The above strategy, together with increasing hip vertical translational energy at toe-off, are the most effective strategies for obtaining maximum toe elevation when stepping over obstacles.

- Lead limb ankle push-off during the double support phase appears to be the most effective strategy for increasing the hip translational energy at toe-off.

In Chapter 4 we showed how force plate data (forces of constraint) can be used effectively in the Lagrangian formulation of the equations of motion. This will help to simplify the solution to the equations of motion of the link-segment model.

We also looked at reactive control strategies (Chapter 7). The concept of the available response time (ART) provides some insight to the possibility of voluntary and/or reflexive response needed to recover from a trip:

- The available response time following a trip increases with obstacle compliance, size, and its location with respect to the stride length. It also depends on the

velocity of the swinging foot and the location of the center of mass at the time of impact.

- The simulations show that at normal speeds and smaller obstacles, polysynaptic reflexes are the only possible recovery option available. Only if the obstacle is hit in early swing might a voluntary response to the trip be possible.

The possible objectives that the central nervous system may consider in planning a strategy for stepping over an obstacle was investigated in Chapter 5. A direct optimization approach with multi-objective criteria was performed to satisfy postulated objectives of landing stability, obstacle clearance, and efficiency of the movement. The results showed that:

- Use of bi-articular muscles is sufficient to clear a range of obstacles with the trailing limb. Stride length or landing stability objectives need not be specified suggesting a simpler control of limb trajectory by the CNS.
- While the use of bi-articular muscles can be sufficient to clear the obstacle with the leading limb, a stable landing and smooth toe and knee trajectories are compromised without suitable initial conditions at toe-off.

The optimization results were expanded in Chapter 6 by using a neuro-fuzzy-genetic algorithm. This model of the central system was also used to study adaptation of human locomotion in performing obstacle avoidance strategies. The results showed that:

- The final population of solutions is less sensitive to the swing ankle velocity at toe-off.
- For the leading limb stepping over an obstacle, less active control during the swing phase and more planning during the double support phase is required.

- With no active control, the hip elevation velocity at toe-off controls the toe clearance and the location of maximum toe elevation. The knee flexor velocity at toe-off mostly affects the stable landing.

- The model suggests that the reason that individuals use approximately 60% obstacle location to stride length ratio, could be explained by the minimal requirement of active control when the obstacle is encountered in mid swing.

- For the trailing limb, modifying the initial velocities at toe-off are not sufficient to achieve obstacle clearance and landing stability: addition of muscles are required to produce a satisfactory trajectory.

- Finally, the model was able to achieve an adaptive behavior. It demonstrated a satisfactory performance over a range of obstacles without re-learning the neural weights and activation functions.

In this work, the large search space, the non-linear interaction of the free parameters, and existence of local minima in the search space made the neuro-fuzzy-genetic optimization a more attractive approach than gradient descent techniques.

8.2 Future Directions

Although the proposed dynamic models provide some insight on the control of the limb trajectory when stepping over obstacles, many questions remain unanswered. A natural follow up to this work is to identify empirically the contribution of various sources to the observed hip elevation. It is also important to examine experimentally the contribution of ankle push-off during the double support phase to the observed hip elevation.

Stepping over obstacles involves shifting the center of mass in sagittal and frontal planes. A model considering the shift of the center of mass in the frontal plane would be a natural extension to the 3-D models introduced in this work.

In order to compare the subject specific experimental data with the model predictions, extended optimization models must address the contribution of single joint muscles. By inclusion of the line of pull and the variable moment arm length for each muscle, subject specific information could be gained from the optimization approach. The optimization model must also be extended to address the contribution of the single articular muscles to limb elevation. In addition, as discussed in Chapter 5, a fuzzy logic approach (instead of manual guidance) will be useful in directing the optimization to the field of attraction of the global minimum.

A natural follow up to the study of reactive control (Chapter 7) is to determine the strategies used to recover from a trip, and this can be done using optimization methods. The inclusion of the trunk movements and the calculation of velocities of the center of mass and toe during contact can provide more insights. In addition, the model can be extended to include the case in which the obstacle topples over when hit by the foot of the subject.

Finally, modelling the other blocks of the Figure 6.1 and integrating their functions would be a natural progression of the study of adaptive locomotion. In addition, the neuro-fuzzy-genetic network can be improved to include individuals with variable string size in the genetic pool. As well, other operators as discussed in appendix F can improve the performance of this network.

Appendix A

Equations of Motion for a 4 DOF Link Segment Model

The equations of motion for the planar model are derived using Lagrange equations. The equation and it's terms are defined as follows:

$$D(\theta)\,\ddot{\theta} + C(\theta,\dot{\theta}) + \Phi(\theta) = \tau - M(\theta,\dot{\theta}) \tag{A.1}$$

The inertia matrix:

$$D(\theta) = \begin{bmatrix} K_1 & C_2cos(\theta_1-\theta_2) & C_3cos(\theta_1-\theta_3) & C_4cos(\theta_1-\theta_4) \\ C_2cos(\theta_1-\theta_2) & K_2 & C_1cos(\theta_2-\theta_3) & C_5cos(\theta_2-\theta_4) \\ C_3cos(\theta_1-\theta_3) & C_1cos(\theta_2-\theta_4) & K_3 & C_6cos(\theta_3-\theta_4) \\ C_4cos(\theta_1-\theta_4) & C_5cos(\theta_2-\theta_4) & C_6cos(\theta_3-\theta_4) & K_4 \end{bmatrix} \tag{A.2}$$

The velocity dependent terms:

$$C(\theta,\dot{\theta}) = \left\{ \begin{array}{l} C_2\dot{\theta_2}^2 sin(\theta_1-\theta_2) + C_3\dot{\theta_3}^2 sin(\theta_1-\theta_3) + C_4\dot{\theta_4}^2 sin(\theta_1-\theta_4) \\ -C_2\dot{\theta_1}^2 sin(\theta_1-\theta_2) + C_1\dot{\theta_3}^2 sin(\theta_2-\theta_3) + C_5\dot{\theta_4}^2 sin(\theta_2-\theta_4) \\ -C_3\dot{\theta_1}^2 sin(\theta_1-\theta_3) - C_1\dot{\theta_2}^2 sin(\theta_2-\theta_3) + C_6\dot{\theta_4}^2 sin(\theta_3-\theta_4) \\ -C_4\dot{\theta_1}^2 sin(\theta_1-\theta_4) - C_5\dot{\theta_2}^2 sin(\theta_2-\theta_4) - C_6\dot{\theta_3}^2 sin(\theta_3-\theta_4) \end{array} \right\} \quad (A.3)$$

The potential terms:

$$\phi(\theta) = \left\{ \begin{array}{l} W_1 cos(\theta_1) \\ W_2 cos(\theta_2) \\ W_3 cos(\theta_3) \\ W_4 cos(\theta_4) \end{array} \right\} \quad (A.4)$$

The right hand side of the equation of motion (A.1) includes external torques and damping forces:

$$\tau(t) - M(\theta,\dot{\theta}) = \left\{ \begin{array}{c} -\tau_s \\ \tau_h - \tau_k - M_k \\ \tau_k - \tau_a + M_k - M_p - M_d \\ \tau_a + M_p + M_d \end{array} \right\} \quad (A.5)$$

where: M_k, M_p, and M_d are the non-linear damping forces opposing knee hyper-extension, ankle plantar-flexion, and ankle dorsi-flexion respectively.

τ_s, τ_h, τ_k, and τ_a are the external torques applied to stance limb, hip, knee, and ankle. The equation constants are defined in Appendix B.

When hip elevation is applied as constrained trajectory, the following terms are added to the left hand side of the equation A.1:

$$H = \left\{ \begin{array}{l} A_1 \ddot{h} cos(\theta_1) \\ \frac{W_2}{g} \ddot{h} cos(\theta_2) \\ \frac{W_3}{g} \ddot{h} cos(\theta_3) \\ \frac{W_4}{g} \ddot{h} cos(\theta_4) \end{array} \right\} \quad (A.6)$$

When it was desired to constrain the ankle movement (rigid ankle) the differential form of constraint ($\ddot{\theta}_4 - \ddot{\theta}_3 = 0$) along with the equations of motion was formulated by using augmented method [23]:

$$\begin{bmatrix} D & B^T \\ B & 0 \end{bmatrix} \begin{Bmatrix} \ddot{\theta} \\ \lambda \end{Bmatrix} = \begin{Bmatrix} C + \phi \\ G \end{Bmatrix} + \begin{Bmatrix} \tau - M \\ \dot{g} \end{Bmatrix} \quad . \tag{A.7}$$

where $[B]$ is the Jacobian constraint, $\{G\} = -[\dot{B}]\{\dot{\theta}\}$, $\{g\} = [B]\{\dot{\theta}\}$, and the rest of the terms are as defined above. The Jacobian constraint in the case of a rigid ankle will be: $\{B\} = \{0\ 0\ -1\ 1\ 0\}$, and $\{G\} = \{\dot{g}\} = 0$.

Appendix B

Constants of the Equations of Motion for the Planar Link Segment Model

The followings are the constants used in the equations of motion in the previous appendix:

g	Gravitational acceleration
I_S	Moment of inertia of the stance limb around the ankle
I_1, I_2, I_3	Moments of inertia at the C.M. of the thigh, shank, and foot
m_H	Concentrated mass of hip, arm, and trunk
m_l, m_1, m_2, m_3	Masses of stance limb, swing thigh, shank, and foot
l_1, l_2, l_3	Lengths of thigh, shank, and foot respectively
z	Distance from the proximal joint to the centre of mass of the stance limb
z_1, z_2, z_3	Distances from the proximal joint to the centre of mass of swing thigh, shank, and foot respectively
T_h, T_k, T_a	External joint torques applied at hip, knee, and ankle
h	Hip elevation vertical distance

$$l = l_1 + l_2 + l_3$$

$$W_1 = (2m_l + m_H)gl - m_l gz$$

$$W_2 = (m_1 z_1 + m_2 l_1 + m_3 l_1)g$$

$$W_3 = (m_2 z_2 + m_3 l_2)g$$

$$W_4 = m_3 z_3 g$$

$$K1 = I_S + (2m_H + m_1 + m_2 + m_3)l^2$$

$$K2 = I_1 g + m_1 {z_1}^2 + (m_2 + m_3){l_1}^2$$

$$K_3 = I_2 + m_2 {z_2}^2 + m_3 {l_2}^2$$

$$K_4 = I_3 + m_3 {z_3}^2$$

$$C_1 = m_2 l_1 z_2 + m_3 l_1 l_2$$

$$C_2 = m_1 l z_1 + m_2 l l_1 + m_3 l l_1$$

$$C_3 = m_2 l z_2 + m_3 l l_2$$

$$C4 = m_3 l z_3$$

$$C_5 = m_3 l_1 z_3$$

$$C_6 = m_3 l_2 z_3$$

Appendix C

Understanding the Control of Locomotion

The objective of this section is to draw a general picture of the neural aspects of the control of human locomotion. The materials presented in this section for most follows that of references [43, 33].

C.1 Human Movement

The human motor system produces three overlapping classes of movements: reflex responses, voluntary movements, and rhythmic movements. Voluntary movements are the purposeful, goal directed movements, which are largely learned and improved by practice. As the skills of any movement improve, the conscious participation for performing those movements reduces. Reflex responses (such as knee jerk) are rapid, stereotyped movements with minimal conscious participation. Rhythmic movements (such as walking and running) require conscious participation for the start and the end of the movement but may continue automatically without any need for external stimuli. During locomotion animals utilize all three classes of movement.

All three classes of movements rely on sensory information, and are performed by translating the neural information to mechanical energy produced by muscles. For

the motor system to perform any movement, it is necessary to get information from the surroundings, the relative position of the body parts, the equilibrium state of the body, and the motor plant (that is, the knowledge of the human musculo-skeletal system and the effect of intersegmental dynamics).

The classes of movement rely on a hierarchy of the control system that utilizes the necessary sensory information. The control strategies used can be classed under feedback (reactive) and feed-forward (proactive) control. The reactive control detects an unexpected (sensed) movement and is followed by a stabilizing response. This type of response in biological systems is usually slow and is mostly used for regulating posture and slow movements. To perform fast movements, such as catching a ball thrown to us, it takes several hundred milliseconds for a visual cue to be responded to. Note that the response to a quick movement may take only 150 to 200 milliseconds. Therefore, proactive (feed-forward) control is a necessary part of the movement.

The proactive response may be due to visual identification of the upcoming event for which the motor system estimates the required modifications in locomotor movements to avoid the potential threat to body stability. For example, by detecting an obstacle in the path of movement, the locomotor may increase limb elevation, change direction, or stop.

Other type of proactive response may be evoked by prediction of an expected perturbation caused by a concurrent voluntary movement. For example, if the arms are decided to be thrown forward (an action that pushes the centre of mass of the body forward), prior to this event, the humans back and thigh muscles (erector spinae and hamstrings) become active to push the centre of mass of the body backward to counteract the upcoming event.

These two strategies utilize three types of sensory information which flow through three organizational neural control levels. Prior to describing each of the neural control levels, we briefly discuss the type of sensory information used in locomotion.

C.2 Sensory Systems Used During Locomotion

The role of the sensory system is to provide the body with the perception of the surroundings, as well as movement and orientation of the musculo-skeletal system. Three types of sensory systems are used in the hierarchy of control of locomotion: kinaesthetic, vestibular, and visual systems.

The kinaesthetic system is mainly responsible for sensing relative position and movement of the limbs, orientation of the body relative to the supporting surface, and muscle tension. Muscle spindles, Golgi tendon organs, joint receptors, and cutaneous receptors are the major players in this system. A brief outline of the type of information each modality conveys follows:

Muscle spindles are sensitive to muscle stretch. They convey information about relative orientation, and changes in the velocities of the limbs. Golgi Tendon Organs convey information about the muscle tension. Cutaneous receptors provide information about support surface and joint position. Joint receptors convey information about joint position, and are more sensitive to the joint limits.

During locomotion, the visual system is mostly used for proactive control. It provides information on orientation and movement of body parts relative to each other and to the external environment. The visual sampling of movement is intermittent. It can be appreciated that such a feature enables our visual system to remain reserved for other important activities during locomotion.

The vestibular system, located in the inner ear, is the organ of sensing balance. It senses the angular and linear acceleration of the head with reference to gravity.

The existence of several sensing organs for detecting one feature of a movement may introduce a sensory conflict, an important factor in the hierarchy of the human control system. Note that in most cases, sensory information are not utilized in a parallel manner, as such, loss of information from one can affect the task to be performed. However, the loss of that information may not result in a complete failure in performing a task. The hierarchy of the control system has to consider such conflicts

and set priorities in utilizing the type of sensory information available.

C.3 Control of Locomotion in Human

There are three levels to the motor control system for human movement: the spinal cord, brain stem, and the cortical motor areas (Figure C.1). These three levels are organized both hierarchically and in parallel. The levels have some common organizational features: all receive sensory information; all contain somato-topic maps (spatial relations are preserved so neurons influencing adjacent body parts are adjacent to each other); and higher levels can suppress the sensory information that they receive. Two additional subcortical systems, the cerebellum and basal ganglia, play major roles in motor regulation. All of the levels of control are under the influence of these subcortical systems. A brief description of each level follows:

The spinal cord is the lowest level in the hierarchy of the motor control. It contains neural circuits that mediate a variety of automatic and stereotyped reflexes. These reflexes are part of the general mechanism used for locomotion. The gain of these reflexes can be modulated by higher levels of control. As well, these reflexes form a closed loop feedback mechanism that can operate even when the cord is disconnected from the rest of the brain. The spinal circuitry is the final common pathway for mediating the voluntary movements.

Spinal reflexes are modulated during locomotion. These modulations are under the influence of both spinal and supra spinal mechanisms. Another important aspect of the spinal circuitry of neurons and interneurones is that they form part of the pathway for the pattern generators. The spinal pattern generators are responsible for developing rhythmic patterns for locomotion.

The second level of the motor control system is the brain stem. The brain stem receives inputs from the cerebellum, basal ganglia, cerebellar cortex, and sensory information from vestibular, visual, and kinaesthetic systems. The information is mediated to the spinal level through its five major tracts: vestibula-spinal tract,

rubro-spinal tract, reticula-spinal tract, tecta-spinal tract, and cortico-spinal tract. These tracts play an important role in modulation of the locomotor patterns during various phases of locomotion. As well, via dorsal and ventral tegumental fields, the brain stem is responsible for setting the posture and initiating the locomotion.

The cerebellum is responsible for accuracy and timing of movement. Most importantly, it acts as a comparator between the ongoing motor commands and the resulting responses. As expected, the cerebellum receives information from all sensory modalities, the efferent copy of the motor act (the actual neural firings that resulted in performing a movement), and the planning centers of the cerebellar cortex. It is also known that it has a role in motor learning.

The basal ganglia is the other subcortical component. It does not receive direct sensory information, however, it receives processed sensory information from the somato sensory cortex. The anatomical and lesion studies on Parkinson patients suggests that the basal ganglia's role is more related to planning and initiation of movement. The activity of the basal ganglia is usually related to directionally selective passive and active movements of single joints [43].

The highest level of control includes the three areas of the primary motor cortex, premotor area , and supplementary motor area. The supplementary and premotor areas are more responsible for planning and complicated sequential movements. They also receive information from the primary motor cortex (responsible for voluntary motor acts), the parietal cortex and hippocampus (responsible for cognitive mapping and memory storage). The primary motor cortex has both direct pathways to the spinal level and indirect pathways through the brain stem.

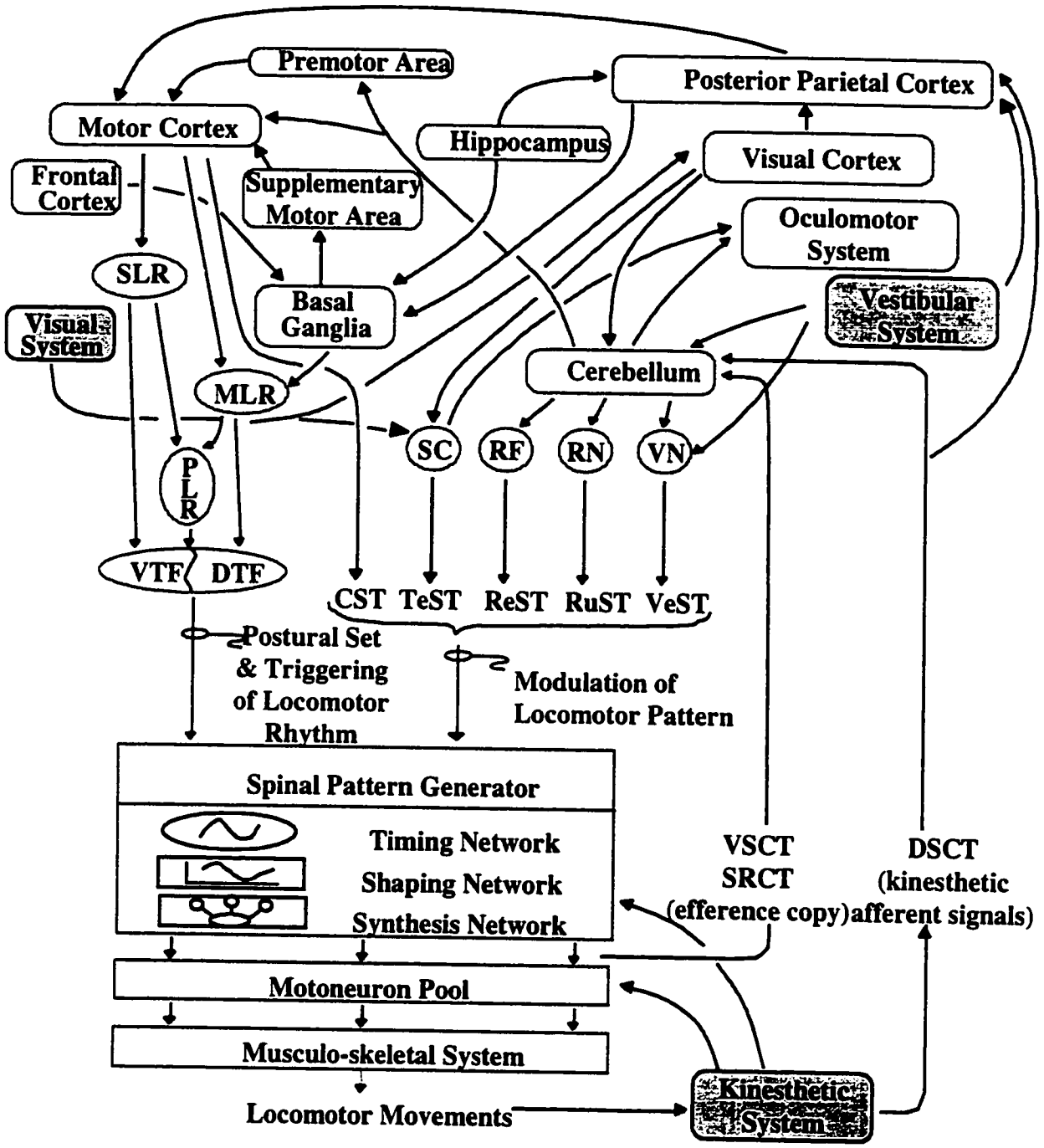

Figure C.1: A simplified diagram showing various efferent and afferent connections in the locomotor control system. Legends: SLR, subthalamic locomotor region; MLR, mesensephalic locomotor region; PLR, pontine locomotor region; VTF, ventral part of the cadual tagmental field; CST, cortico-spinal tract; REST, reticulo-spinal tract; RUST, rubro-spinal tract; SRCT, spino-reticulo-cerebellar tract; DSCT, dorsal spino-cerebellar tract; RF, reticular formation; RN, red nucleus; VN, vestibular nuclei [33].

Appendix D

Fuzzy Logic

The fuzzy reasoning approach can model the qualitative aspects of human knowledge and reasoning processes without employing precise quantitative analysis. This approach provides an efficient way to cope with imperfect information and imprecise knowledge. It offers some kind of flexibility in decision making processes and is especially useful when a process can be controlled by a skilled human without knowledge of its underlying dynamics.

Since Zadeh's [89] introduction of the linguistic approach and system analysis based on fuzzy set theory, fuzzy logic controllers have been widely used for various practical applications. The research of Mamdani and colleagues [45, 49] on the development of the fuzzy controller for a steam engine was widely followed by other researchers for various applications. Examples of some of these works are water quality control [78], automatic train operation system [88], nuclear reactor control [9], hardware system [86], and memory devices [77].

D.1 Fuzzy Sets and Ordinary Sets

A key characteristic in the fuzzy set theory is the gradual loss of information. Let the universe U be a collection of objects denoted generically by u. U is called the universe of discourse while u is a generic element of U. For an ordinary set O in U

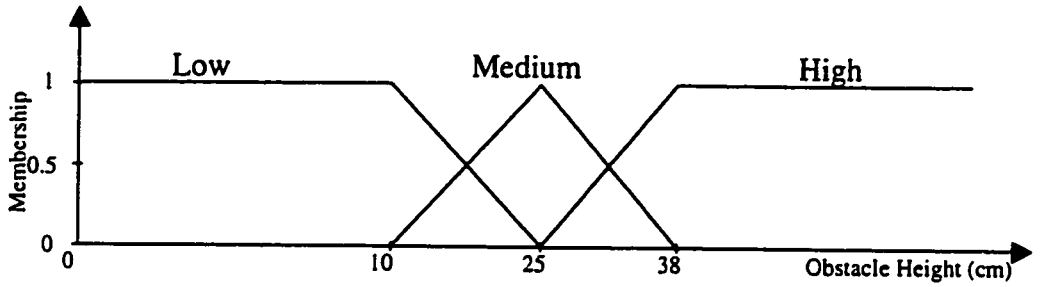

Figure D.1: **Triangular membership functions.**

the elements of U are either inside O or outside O. We could assign binary value 1 to all the elements which are members of this set and 0 to the non-members of this set. Fuzzy sets, however, allow degrees of membership. For example, assume a universe consisting of different size obstacles. An ordinary set defined as "high obstacles", may include all the obstacles higher than 30cm. A 32cm obstacle and a 42cm obstacle are members of "high obstacle" set equally while a 29cm obstacle is not considered "high obstacle". For the fuzzy sets this sharp definitions would be modified to a new interpretation (Figure D.1). A 32cm obstacle has a membership in the range of {0,1} in the fuzzy set of "high obstacles". This obstacle size might as well have a membership in the fuzzy set of "medium obstacles". The triangles in Figure D.1, which are one possible function for defining the membership of each set, are called *membership functions*. The domain of each triangle defines the fuzzy set. Most common membership functions often used in fuzzy logic control have triangular, bell curved, trapezoidal, or a sigmoid function shape. As a formal definition a fuzzy set F in U may be represented as a set of ordered pairs of a generic element u and its grade of membership function: $F = \{(u, \mu_f(u)) \mid u \in U\}$.

We can employ fuzzy sets to represent some linguistic variables. In the example of Figure D.1, obstacle height is a linguistic variable, and the universe of discourse is divided into the term sets (or linguistic values) {low, medium, high }.

The approximate reasoning of fuzzy systems is achieved by a fuzzy rule base. The fuzzy rule base combines the linguistic variables in the following format:

If *antecedent* Then *consequent*

The antecedent and consequent are usually a combination of linguistic variables and their values. As an example:

If obstacle is low AND its location is far THEN apply a small hamstring force

In this example obstacle height, obstacle location, and hamstring force are three linguistic variables. Low, far, and small are their linguistic sets respectively. Examples of other variations of fuzzy rule base are given in [76, 88].

One method of storing fuzzy rules is using a fuzzy associative memory (FAM) matrix. The example of Figure D.2 demonstrates a FAM matrix for two inputs X and Y and one output Z. The universe of discourse for the two inputs is divided into three linguistic sets of Negative (N), Zero (ZE) and Positive (P), while the output Z consists of five linguistic sets of Negative small (NS), Negative Large (NL), Zero (ZE), Positive Small (PS) and Positive Large (PL). The elements of the FAM matrix produce the fuzzy subsets. The number of antecedents (premises) of the fuzzy rules determine the dimensionality of the FAM matrix. Three inputs produce a FAM matrix that looks like a three-dimensional cube. Higher number of inputs produce hypercube matrices.

Most commonly, more than one rule applies to a condition. Therefore, an inference mechanism is required to determine the proper action to be taken by the process output.

D.2 Fuzzy Inference Mechanism

The structure of a fuzzy inference system (Figure D.3) includes the following blocks (It is interesting to compare this with Figure 6.3; if the cerebellum is removed, the blocks are identical).

- A knowledge base includes:

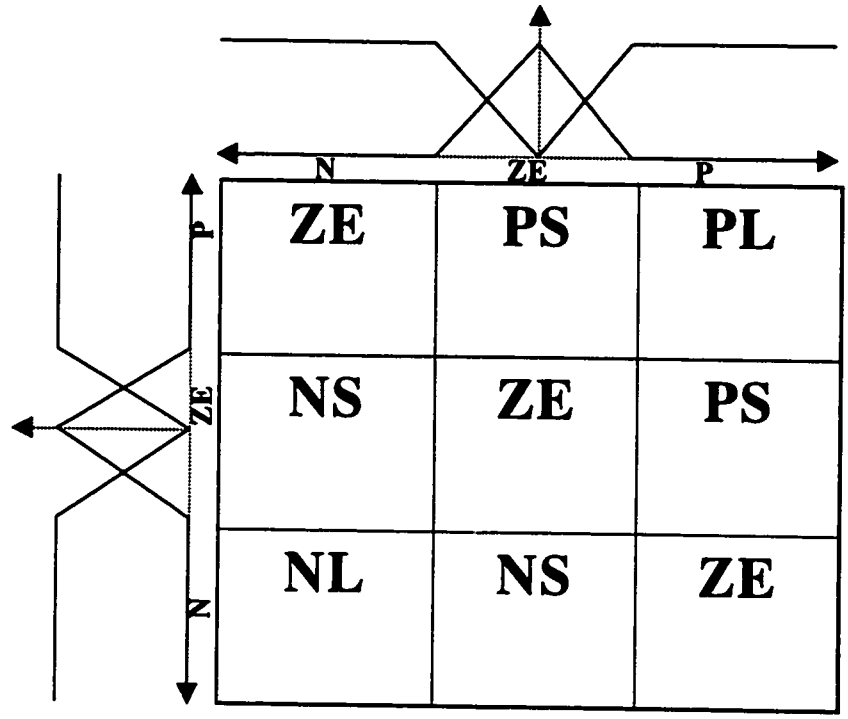

Figure D.2: **Fuzzy associative memory.**

1. A *database* that defines the membership functions of the fuzzy sets (Figure D.1)
2. A *rule base* that consists of a number of conditional statements as described (FAM matrix)

- A fuzzification interface that transforms the crisp values to the linguistic values
- A decision making logic that performs inference operation on rules
- A defuzzification interface that transforms the inference operation results to crisp values.

The fuzzification interface measures the values of input variables, performs scale mapping that transfers the ranges of values of the input variables into the corresponding universe of discourse, and finally performs the function of fuzzification that converts input data to a suitable linguistic values (memberships of the linguistic sets).

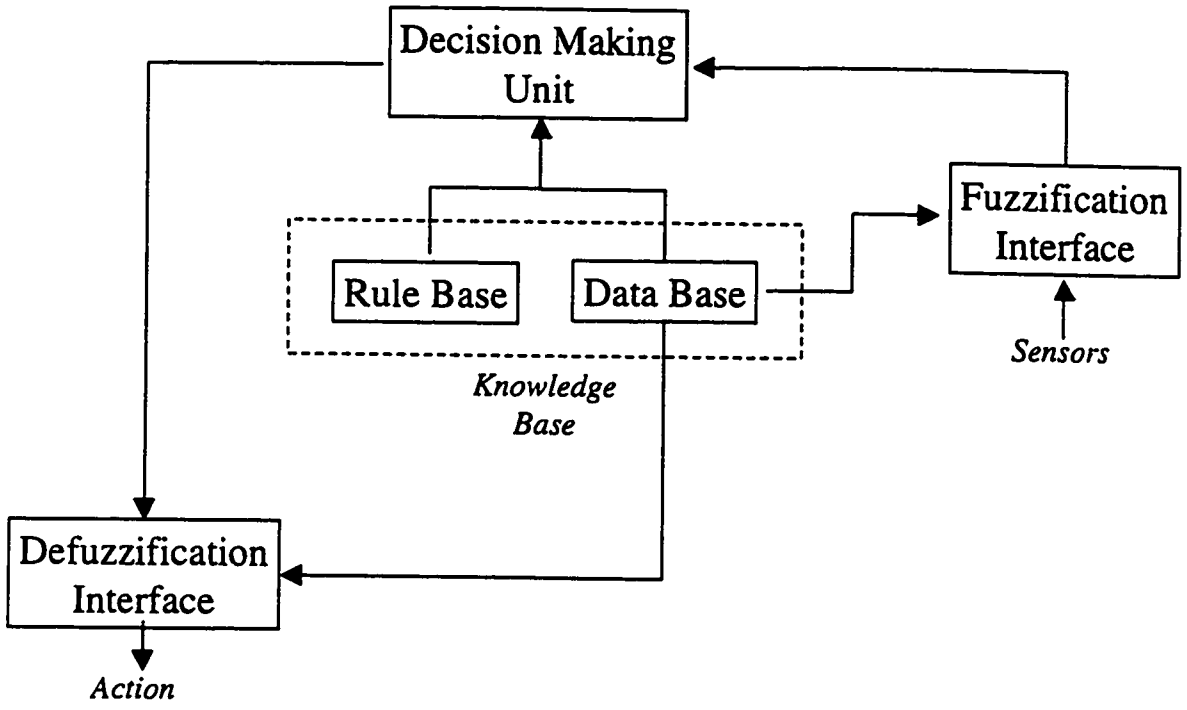

Figure D.3: **Fuzzy inference system.**

As indicated, for example, a 10cm high obstacle has a membership in both linguistic sets of "small" and "medium" obstacles. Therefore a minimum of two rules applies to this obstacle:

IF obstacle is small AND ... THEN ...

IF obstacle is medium AND ... THEN ...

Performing these rules requires some fuzzy operators (e.g. AND). Several operators are defined for fuzzy sets. The most common of these include:

1. The union of two sets, $P \cup N$, corresponds to the OR function and is defined by

$$\mu_{P \cup N} = max(\mu_P(x), \mu_N(x)) \tag{D.1}$$

2. The intersection of two sets, $P \cap N$, corresponds to the AND function and is defined by

$$\mu_{P \cap N} = min(\mu_P(x), \mu_N(x)) \tag{D.2}$$

3. The complement of a set P corresponds to the NOT function and is defined by

$$\mu_{\bar{N}} = 1 - \mu_N(x) \tag{D.3}$$

The decision making unit may derive an overall fuzzy output from the premises of the if-then rules in various ways. One of the more common ways in fuzzy logic control, also used in this work, is the application of the min-max operation to the qualified outputs. Figure D.4 illustrates an example of the decision making operations. The universe of discourse for the two references of obstacle height and obstacle location is defined such that the obstacle heights of [0,1] meters are mapped to the universe of [0,4], As well, the location of the obstacles [-.5, .5] is mapped to the universe of [-2,2]. It is assumed that obstacle size of x has membership in two linguistic sets, as is the obstacle location y. The minimum operation results in the mapping of the smaller membership of each of the two rules(membership of 0.1 corresponding to x in rule 1 and membership of 0.6 corresponding to membership of y in rule 2) from the premises of these rules to their consequent. Finally the max operation (OR operation) is performed on the areas of the two consequent rules to find the overall fuzzy output.

The output of the inference process is an overall fuzzy set specifying a possibility of distribution of the output (control action). The defuzzification interface produces a crisp value (a non-fuzzy control action) that best represents the possibility distribution of the overall fuzzy output. Again there is no standard method and several methods have been proposed. Some of the more common methods are (see [46]): the maximum criterion method, the mean-of-maximum method, and the center-of-area method. Among these we have chosen to use the center-of-area method which is most often used and has been shown to lead to superior results [11]). This method generates the center of gravity of the possibility distribution of the overall fuzzy output. For the triangular linguistic sets of the same slope, the center-of-area method will lead to :

$$I = \sum(\mu_n \times U_n) / \sum \mu_n \tag{D.4}$$

where n is the number of conditional statements applied.

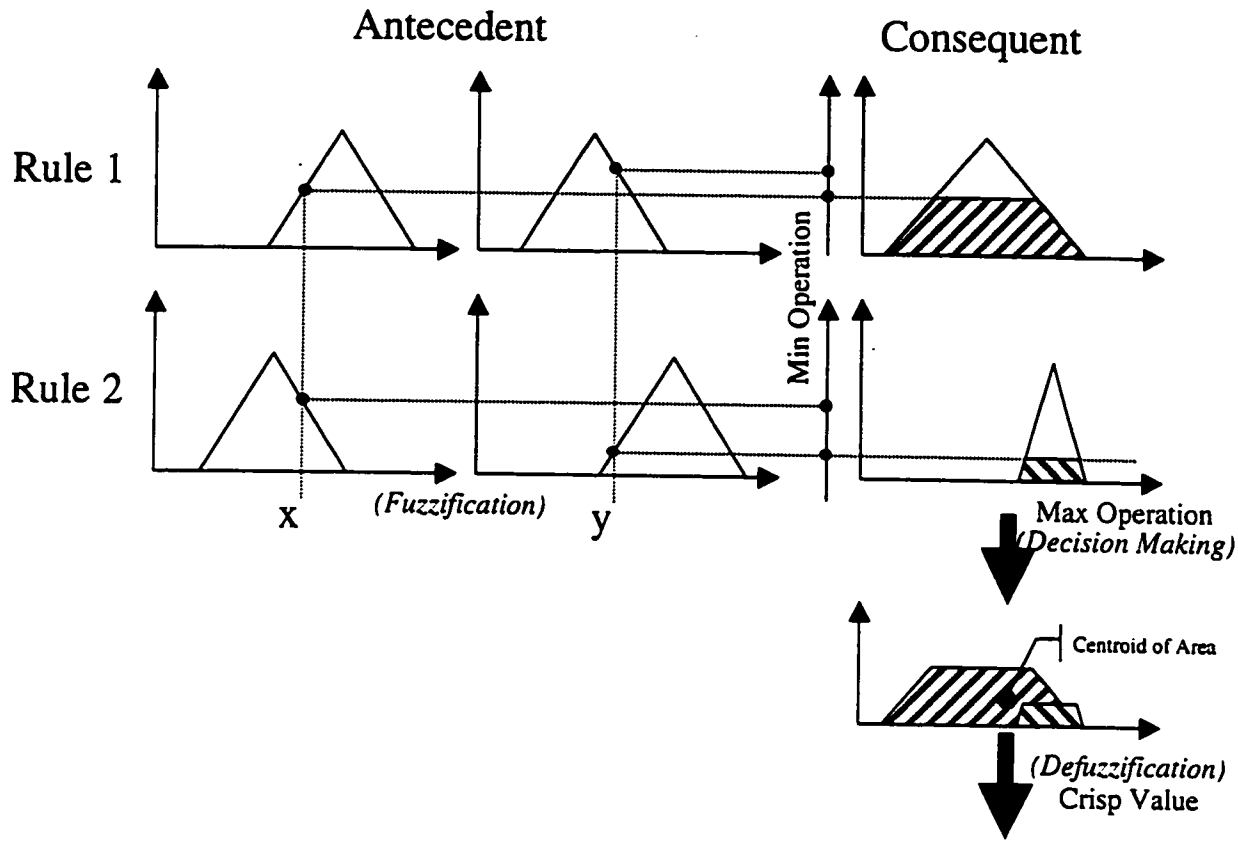

Figure D.4: **Fuzzy decision making system for two inputs (x and y).**

In this work we have used 3 to 5 linguistic sets of triangular shape for each references(obstacle size and location). For each of the control inputs (muscle pulses and the initial conditions at the toe-off) five linguistic sets are usually used (see Figure 5.2 for the definitions of the muscle pulse parameters).

Appendix E

Neural Networks

The power of the human brain in problem solving, thinking and remembering has stimulated researchers to create models that imitate the accepted structure of the brain. Artificial Intelligence emerged from the belief that intelligent human behavior can be formalized and mechanized, and problem solving is according to rules. Connectionist models, however, carried the idea that intelligent behavior, or the problem solving according to rules, is just an emergent property of the underlying mechanisms. These models, with the goal of developing the microstructure of cognition, focused on physiologically plausible models that were inspired by biological neurons. This has resulted in the development of Artificial Neural Networks; a structure that processes information using simple computational elements called neurons. Neurons operate in parallel and pass signals to each other via interconnections. The strength of the connections (the weights) determine the behavior of the system. Figure E.1 illustrates the topology of a standard multi-layer Network.

The important features of a Neural Network, which make it different from other computing methods, are as follows:

- The network generates its own computing rules for given input/output relationships. This is done by using a learning algorithm, which determines the appropriate weights.

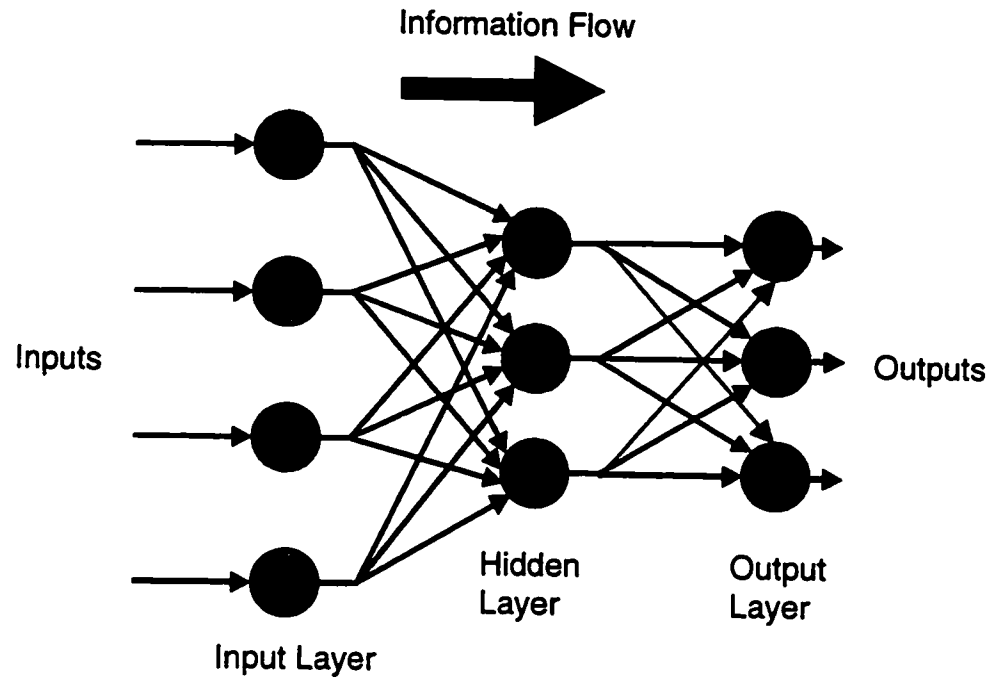

Figure E.1: **The Topology of Neural Networks.**

- Neural networks store information in distributed memory units (weights). This characteristic enables the network to estimate a response when an incomplete or noisy input is presented.
- They are fault tolerant. This means that if a computing element is damaged or destroyed, the behavior of the network does not change dramatically.
- The network can perform non-linear mapping between input/output pairs.
- Neural networks can handle high computational rates. This feature makes them suitable for pattern recognition applications.
- They are capable of synthesizing complex continuous functions.

The above features make neural networks suitable for a variety of applications including pattern recognition, signal processing, system modelling, functional synthesis and control of complex mechanical systems and processes.

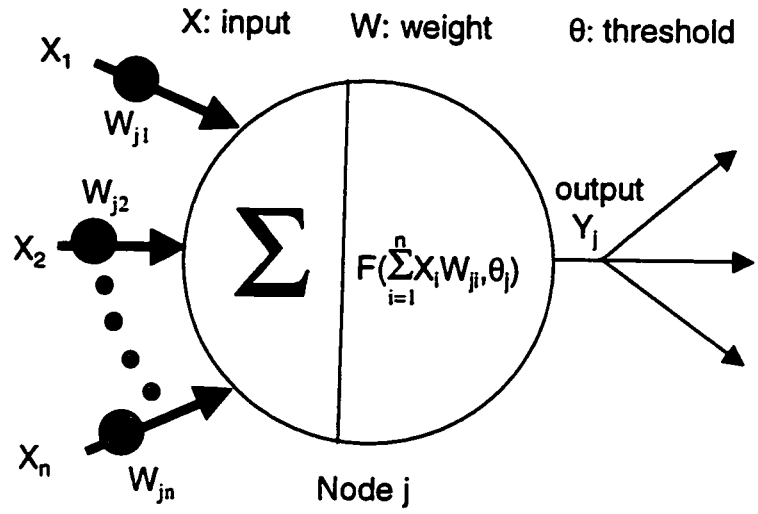

Figure E.2: **The Structure of a Single Node.**

E.1 Terminology

The basic element of an ANN is called a Neuron, Node or Unit. The basic function of a node is shown in Figure E.2. Each node receives input signals from other nodes. These signals may be excitatory or inhibitory. When the signal is excitatory, the output value increases with an increase of the input value, and the node is more likely to "fire". The output of a node receiving an inhibitory input, decreases with increasing value and is less likely to fire. In order to determine whether the output fires or not, the sum of the inputs is compared with a threshold value. When the input value exceeds the threshold, the node sends its output signal to other nodes through weighted connections. The weights of the connections determine the degree of effect of each input on the overall behavior of the node and of the network in general. To control the performance of the Network, the weights are usually modified by using various learning algorithms.

As shown in Figure E.2, the output from a node is related to the sum of the inputs to the node via an activation function, $f(\sum (x_i\ W_{ji}))$. Four common activation functions are:

- Linear Activation Function: this function has the form $f(x) = \alpha.x$ in which α magnifies the node input x.

- Non-linear Ramp Function: this is a linear function in the range $[-\delta, \delta]$.

- Step Threshold function: this is a binary function which usually gets the values 0 and 1.

- Sigmoid Function: this is a bounded and monotonic (output uniformly increases or decreases with input) function. It is usually in the form of a logistic or hyperbolic function and provides a graded nonlinear response.

In the ANN, nodes are arranged in layers or groups. The nodes in each layer are generally activated simultaneously. Figure E.2 illustrates the two types of layer commonly used, namely output and hidden. The output layer emits to the environment the processed signals received from a hidden layer (or sometimes the inputs). The hidden layers consist of intermediate nodes between the network inputs and the output layer nodes. They emit the signals received from the inputs or the previous hidden layer, to the next hidden layer or the output layer.

The type of connections used between the nodes depends on the usage of the network. Figure E.3 shows three types of the common node connections. The standard feed-forward network [68] has only connections between the nodes in the consecutive layers. The inter-layer connections are mostly used for pattern classification applications [48]. Recurrent connections [68], which loop back to the same node, are suitable for representing the dynamic behavior of a system.

Learning is the most important feature of the ANN. When a data vector is applied to the input nodes, a 'learning rule' is used to adapt the weights between the layers so that the desired output results. If the desired network response is not provided, the learning is called unsupervised. In this type of learning structure, only the input vector is shown to the network. The network then internally organizes itself to form a cluster of similar sets in the input space [48].

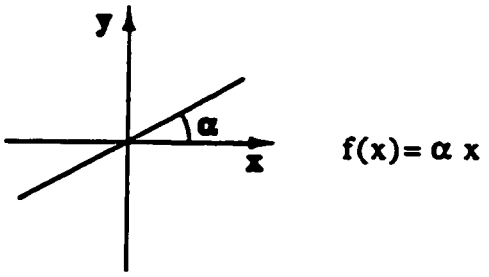

(a) linear function

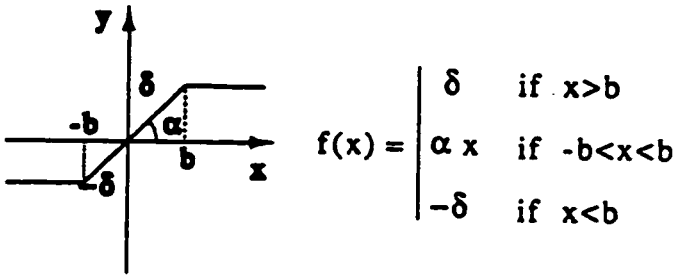

(b) non-linear ramp function

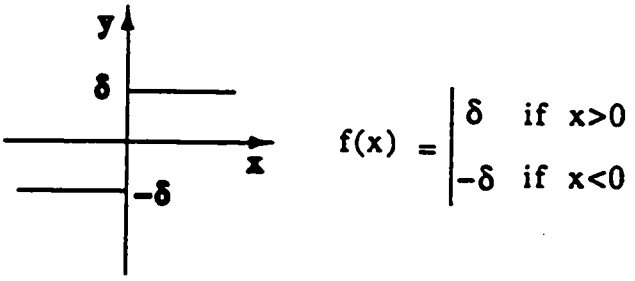

(c) step threshhold function

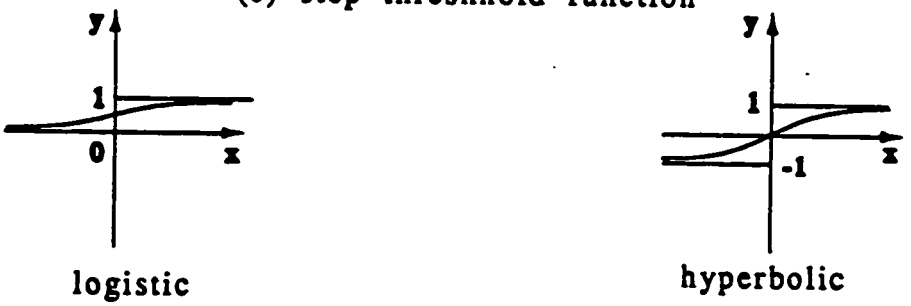

(d) sigmoid function

Figure E.3: Types of Connections in the Neural Networks.

If the desired network response is provided, the learning is referred to as supervised learning. In supervised learning, for each input vector a desired output vector is presented, and the network is gradually trained to achieve approximately the desired input/output mapping. When the desired output vector is the same as the input vector, the Network is called auto-associative. This type of network is useful for pattern recognition applications, where a degraded or incomplete input pattern is presented, and the Network recalls the complete pattern. If the desired output vector is not the same as input vector, the network is called hetero-associative [48].

E.2 Multi-layer Networks

A multi-layer network is essentially a feed-forward network with one or more hidden layers between the input vector and output layer. The main advantage of a multi-layer network over a perceptron (network without hidden layer) is its ability to perform non-linear mapping. This can be best understood by comparing the decision regions that these two networks produce [48]. However, the convergence of the multi-layer net to a correct input/output mapping is not guaranteed. This is the problem of being trapped in a local minimum, which is discussed in the following section.

E.3 Error Propagation

The application of multi-layer nets was limited before 1986 when Rumelhart et al. [68] presented a back propagation technique for adapting the weights. Since then, multi-layer nets have been used in variety of applications.

Back-propagation uses a gradient search technique to minimize a cost function equal to the square difference between the desired and the actual plant outputs. An input vector is presented to a feed-forward multi-layer net. The resultant output vector is compared to a target output vector. If there is a difference between actual and target outputs, all the connections may be responsible. The error is propagated

backward to the previous layer modifying the weights. This process repeats until the input layer is reached.

The rule for changing the weight for a perceptron with a linear activation function is:

$$\Delta_p W_{jk} = \eta(t_{pj} - o_{pj}) i_{pk} = \eta \delta_{pj} i_{pk} \tag{E.1}$$

where: η is the learning rate (between 0 and 1)

$\Delta_p W_{jk}$ is the change of the weight from input k to output j

t_{pj} is the j^{th} component of the target output

o_{pj} is the j^{th} component of the actual output

i_{pk} is the k^{th} element of input due to pattern p

δ_{pj} is the error signal for j^{th} component of the output due to pattern p.

A single step linear system can do all the computations possible with a multiple step linear system [68]. Therefore, multi-layer networks with a linear activation function provide no advantage over single-layer networks. The rule of changing the weight for a network with a non-linear activation function is:

$$\Delta_p W_{kj} = \eta \delta_{pj} o_{pk} \tag{E.2}$$

where o_{pk} is the output of node k as defined in Figure E.2. This is the generalized delta rule used for weight adaptation. In order to feed-back the error, the error signal should reflect the effect of the change of the error to the change of the node output. For a monotonic semi-linear activation function, the error signal for any output node j would be:

$$\delta_{pj} = (t_{pj} - o_{pj}) f'_j \left(\sum W_{jk}\, o_{pk}\right) \tag{E.3}$$

where W_{jk} is the weight between the nodes k and j and f'_j is the first derivative of the activation function of the node j.

If node j is in a hidden layer, the error signal would be:

$$\delta_{pj} = f'_j(\sum W_{jk}\ o_{pk})\ \sum \delta_{pk} W_{kj} \tag{E.4}$$

A common example for a good activation function is the logistic function. This function is continuous, nonlinear and monotonic. It has been found to be a useful activation for variety of applications of multi-layer networks. It has the form:

$$o_{pj} = \frac{1}{1 + exp(-(\sum W_{jk}\ o_{pk} + \theta_j))} \tag{E.5}$$

where θ_j is the threshold, and its value is learned similar to the other weights. It is assumed as a node which is always on.

When the generalized delta rule is used for a network without hidden units, the error surface, in the weight space, gets the shape of a bowl with only one minimum. In this case, the net convergence to the desired respond is guaranteed. With a multi-layer network, the error surface may have several local minima and there is a possibility of getting trapped in these. In the next appendix we introduce Genetic Algorithms as a global search technique which tries to overcome the problem of trapping in local minima.

E.4 Reinforcement Learning

Learning of behavior based on trial and error without an explicit teacher is referred to as reinforcement learning. Like supervised learning, these models get some feed-back from the environment. However, the signal is in the form of reward (reinforcement signal), which is evaluative and not instructive. This means that the signal does not indicate the correct behavior. It is a single scalar and the goal is to maximize the cumulative reward received over time. Reinforcement learning is also called learning with a critic, as opposed to learning with a teacher [36].

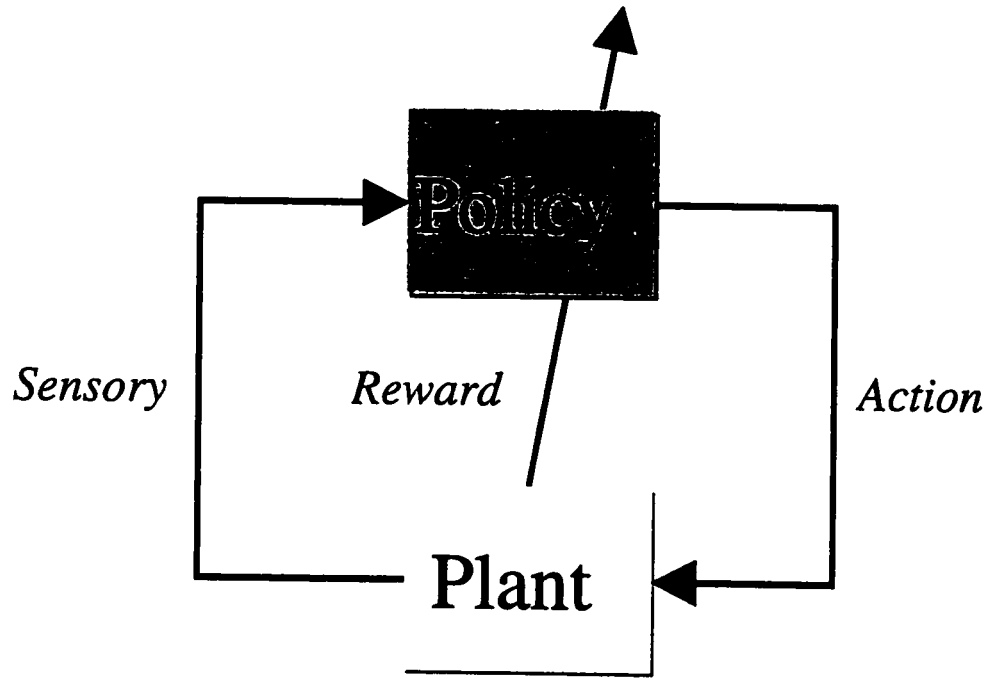

Figure E.4: **A Simple Reinforcement Learning Network.**

Reinforcement learning involves the learning of the mapping that indicates what action is taken in a certain state. The mapping is called policy [75] and can be a neural network or a heuristic system. The reward is taken from the environment and used to change the weights of the neural network, if the policy is a neural network (Figure E.4).

The reinforcement learning architectures have improved considerably to include more sophisticated problems. For instance one problem with the architecture shown in the Figure E.4 is that a low reward for a certain state (action-sensory mapping), may be the highest attainable for another state. To resolve this problem, reinforcement-comparison algorithm were proposed [6]. These algorithms include a model predictor network whose output is the reward signal (Figure E.5). After the model prediction gets close enough to the reward signal from the environment, it would be directly used to train the policy network. These architectures are effective for immediate reward. Actions, however, not only affect the next reward but also the next states. Adaptive

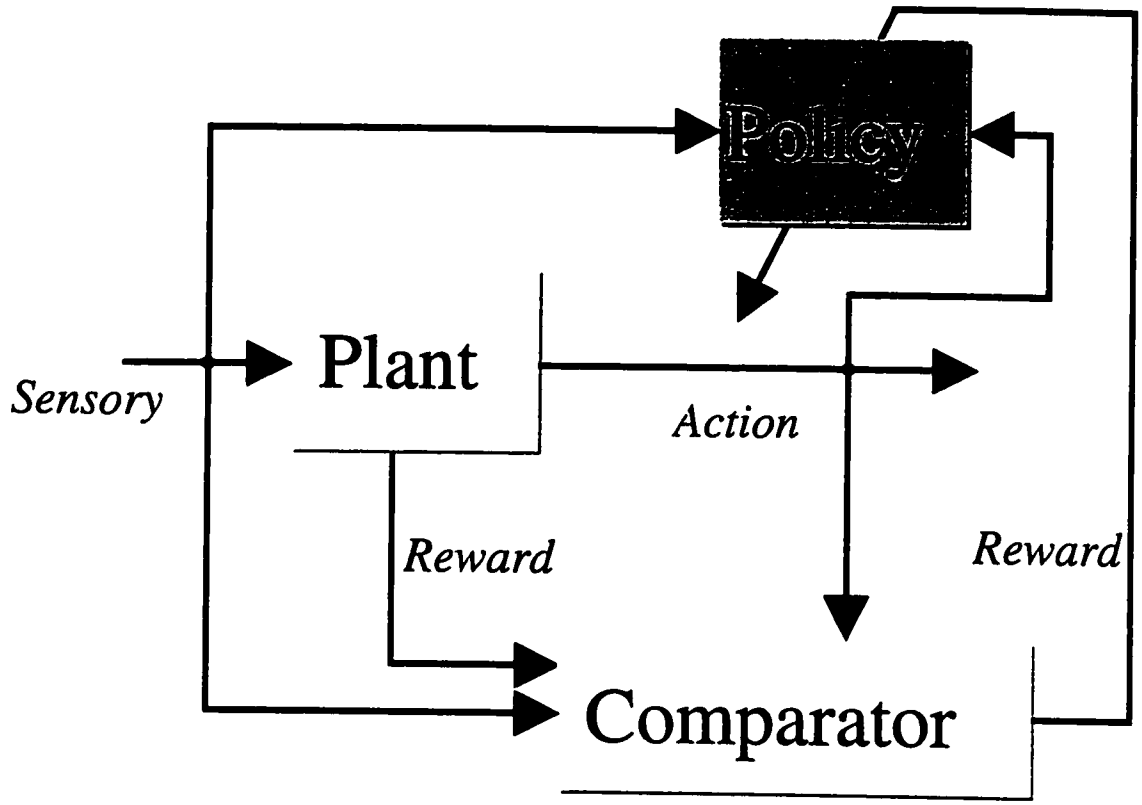

Figure E.5: **learning with Reinforcement and Comparison.**

heuristic networks with critics was designed to take such delayed effects into account [74]. Descriptions of the evolution of the types of reinforcement learning, are nicely described by Sutton [75].

E.5 Adaptive Neural Networks

Another notation used in Chapter six is the adaptive neural network. An adaptive neural network is a superset of all kinds of feed-forward networks. In these networks the links and the node thresholds are modified by learning algorithms. Moreover, the activation functions of all or some of the neurons in adaptive networks include parameters that are modified with the learning algorithm (Figure 6.2). Adaptive nodes are shown by a square instead of a circle. In adaptive neural networks, the

type of activation functions can also be different. In the neuro-fuzzy network used in this work the form of parameters and activation functions for the nodes of each layer is specific to that layer. This has to be taken into account when using back-propagation learning.

Appendix F

Genetic Algorithms

Genetic algorithms (GA) are highly parallel mathematical algorithms that solve problems in the same way that living organisms solve the problem of adapting to the harsh realities of life in a hostile world: evolution. Because of their parallel organization, genetic algorithms are capable of performing optimization on nonlinear multimodal (many local maxima and minima) functions. Although their convergence to a global maximum or minimum is not guaranteed, GAs have been experimentally realized as a robust optimization tool in many problems. The use of GAs as a global search routine for training neural networks instead of gradient search algorithms (such as back propagation) has also been examined successfully [81, 55].

GAs were first introduced by Holland [38], as a form of search technique modeled on Darwinian evolution. Good introductions to GAs are by Goldberg [29], Grefensette [31] and Schaffer [70].

For a multi-dimensional search problem with several possible solutions, a genetic code representation is chosen such that each point in the search space is represented by a string of binary characters called a genotype (Figure F.1). Each string represents a behavioral architecture in an organism, or a network structure in a connectionist model (phenotypes). A number of initial random genotypes (called individuals) is produced that form the initial population. Each of the genotypes are evaluated with an appropriate evaluation function and are given a fitness value. The next generation

of individuals is generated from the present population by selection and reproduction. The selection process is based on the fitness of the present population such that the individuals with more than average fitness contribute more to the new population (survival of the fittest). This is done probabilistically. Genetic operators, such as mutation and crossover (will be discussed in more detail), operate on the new reproductive pool of genotypes. With these operations, the original genotypes (parents) are transformed to new off-spring (children) (Figure F.2). In this way, a new generation of the genotypes is created. This generation inherits some useful information from the older generation. This is mainly because of two reasons: a) the selection process has favored the reproduction of the individuals with a higher than average fitness value, b) the crossover operators favor performing operations on individuals with higher fitness. The process of selection and reproduction followed by other genetic operations (crossover and mutation) are then performed on the new pool and the process will repeat until the solution is reached (other criteria for termination of the search algorithm may be considered as well).

The main theorem that demonstrates the fitness improvement of the genetic pools through generations is Holland's [38] schema theorem. His theorem proves that schemata (the building blocks in his genetic representation) of above average fitness will receive exponentially increasing numbers of trials and errors in successive generations. Hence, improvement will result. He also showed that in a population of size n, the number of schemata being processed is on the order of n^3 for the binary strings. In other words, the algorithm is efficient. This is referred to as implicit parallelism in GAs. These results are the only underlying theoretical foundations for GAs, at present.

In the design of GAs, several decisions have to be made. Some of these include: size of the population, use of the fixed or variable size genotype, type of genetic operators, the termination criteria, and the choice of selection technique. Some of these issues will be discussed in more detail:

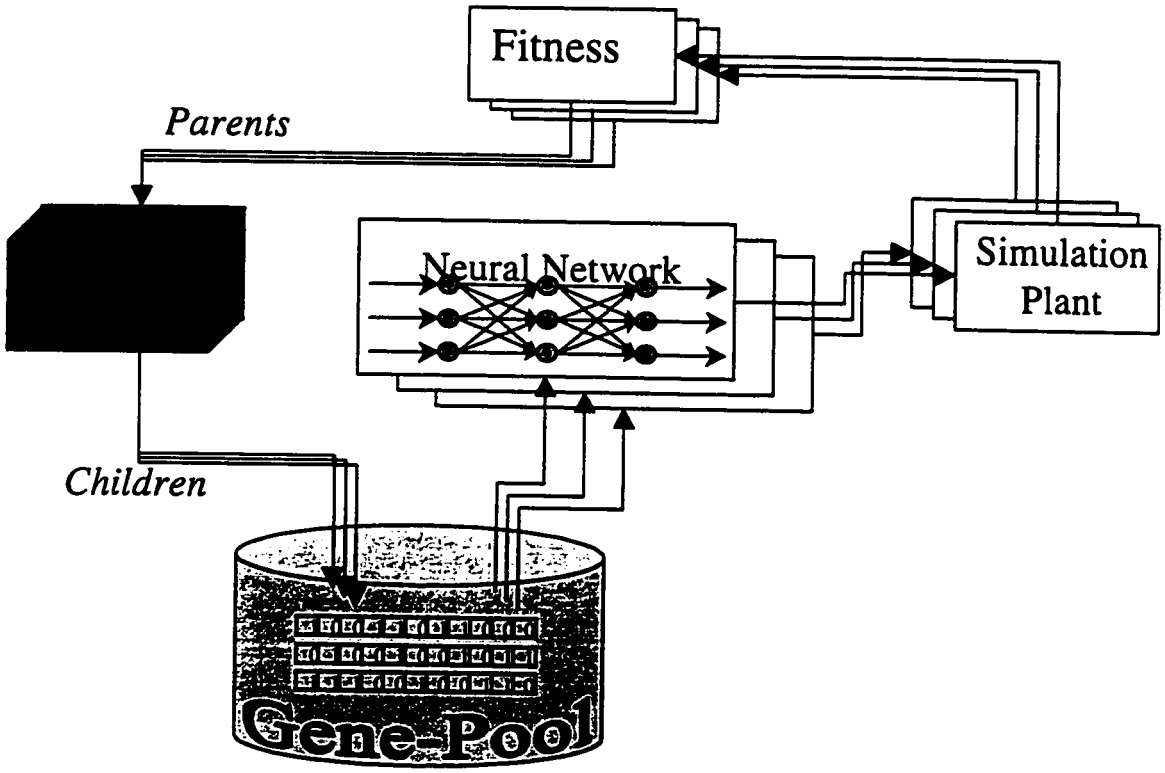

Figure F.1: **A GA Architecture.**

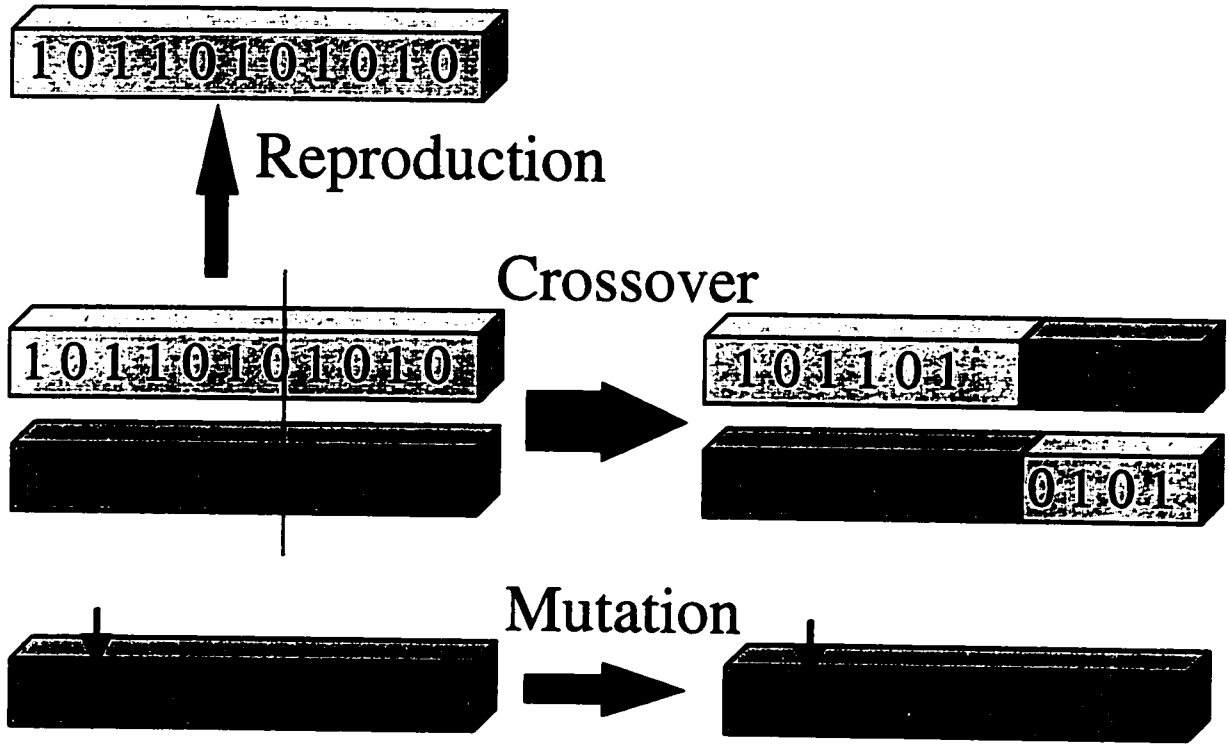

Figure F.2: **Crossover and Mutation Operators.**

F.1 Genotype Representation

Representation is a key issue in GAs as the algorithms directly manipulate the coded representation of the problem. A fixed representation scheme (such as fixed length genotypes) limits the window by which the system observes its world (see [41]). For example a binary length of 8 bits divides the sensory input information range into 2^8 discrete levels. This is a limitation for problems where the size and shape of the solution and the possible range of inputs are unknown in advance. However, the schemata theorem is proven and valid for fixed length (as apposed to variable length) genotypes. In this work, we have chosen to use a representation of binary strings of 8 to 16 bits per variable.

F.2 Selection Techniques

A recurring problem in the choice of selection technique is to keep a balance in selective pressure. Too little selective pressure results in small fitness improvement per generation. Too much selective pressure, on the other hand, leads to premature convergence and the lack of diversity needed to escape from local minima.

In this work we use standard Baker's SUS algorithm for the selection technique. In the SUS algorithm the fitness of the genotypes in the pool are rearranged such that:

$$f'_n = f'_{n-1} + \frac{f_n}{\bar{f}} \tag{F.1}$$

where:

f'_n : the new fitness of the n^{th} genotype,

f_n : the original fitness of the n^{th} genotype,

$\bar{f}$: the average fitness of the pool

In this pool the fitness of each individual is the partial sum of the previous fitness divided by the average fitness of the pool. Therefore, the fitness of the last individual in the pool will become equal to the size of the pool.

In the SUS algorithm, the partial sum of each individual is compared with an incrementing random number. The result is that the genotypes with higher than average fitness will be favored for reproduction.

We have also included an aging factor in the SUS algorithm. Only the individuals that are older than the average age of the pool (number of generations) are qualified for reproduction. In this way we ensure that the individuals which are selected for reproduction, have already survived through several trials. This characteristic is especially important for simulations where the reference sensory input for each trial is selected randomly. Thus a specific individual may exhibit a high fitness to one set of sensory inputs, while its fitness might reduce significantly when exposed to another set of sensory inputs.

F.3 Genetic Operators

Several genetic operators have been proposed and used for GAs. The two original biologically inspired operators, crossover and mutation (Figure F.2), are common in all GA applications. Other genetic operators, such as addition and deletion operators, are introduced in other works (e.g., [18]). In this work we only use crossover and mutation operators.

Mutation operators randomly change the value of a single bit of some individuals in the pool. They preserve the diversity of the pool, by protesting against the focusing effect of recombination(crossover) operators. Thus, they prevent premature convergence to a local solution. By increasing the effect of mutation, the genetic search will become more similar to the random search. Mutation operators are mostly required for smaller size pools, where the probability of immature convergence increases. For a pool size of 100-500 individuals, we found the mutation rate of 0.1% to be most

effective.

Crossover or recombination operators transform two parents strings of genotypes into new off-spring (Figure F.2). This is done by exchanging a portion of the strings between two parents. The string lengths (at least in our model) in the off-spring will remain the same as their parents. This mating may result in transformation of schemata carried by each parent to the child, hence creating the possibility for the child to be more fit than the parents. The crossover may occur on several points (n-point crossover). As well, other forms of recombination within a gene are also used in the literature (Segregation crossover). For this work we have chosen to use only two sites of crossover at a time (Figure F.2). As well, a crossover rate of 60% is maintained throughout the simulations. The values of the crossover rate and the mutation rate used were also recommended by Davidor [18].

F.4 Scaling

As the GA progresses, the average fitness of the population improves. As there is an upper bound for the maximum fitness, the difference between the minimum and the maximum fitness continuously reduces. After several generations, fitness values get very close. Therefore, the fitter strings will not have that much of an advantage when the time for crossover reaches.

Scaling is a remedy to this situation. Scaling magnifies the distance between the upper and lower fitness value. In this way, the individuals at higher bounds of the fitness values will be more prone to crossover. However, scaling has two dangers. First, it changes the topology of the surface that the GA is climbing on. This change may produce a misleading bias against the original peaks. Second, scaling increases the probability of premature convergence.

Because of the above two dangers and the fact that in most of our trials a small percentage of the individuals with considerable low fitness were present, we chose to not apply scaling to the fitness function. Moreover, the goal of this work was to find a

pool of individuals with higher fitness (and not necessarily the best fitness). The high fitness would indicate that the locomotor has cleared the obstacle efficiently and has landed safely. We were willing to compromise maximum safety and efficiency for a pool of individuals including more than one solution to the problem. In other words, various hills with acceptable heights were more desirable than just one maximum peak.

In summary, the use of the GA is advocated when at least one of the following conditions exist:

- the search space is so large that other approaches are computationally infeasible,
- reliance on global information and robustness is crucial,
- certain degree of nonlinearity exists in the problem,
- the storage capacity and processing power are not critical,
- real-time response is not necessary.

Appendix G

D-H Convention and Pareto Optimality

The Denavit-Hartenberg or D-H convention is a method for the systematic placement of frames of reference and is commonly used in robotics applications. With this convention, the relation between two consecutive frames of reference can be established by two rotations and two translations. Thus, the three Euler angles and the three translation components relating two consecutive frames can be expressed by only four parameters. To satisfy D-H convention the two consecutive frames $x_0y_0z_0$ and $x_1y_1z_1$ are assigned such that

1. The axis x_1 must be perpendicular to the axis z_0
2. The axis x_1 must intersect with the axis z_0

For more detailed descriptions consult reference [72].

Definition of local Pareto optimal solution taken from reference [69]: $x^* \in X$ is said to be a local Pareto optimal solution to the multi-objective non-linear programming problem if and only if there exists a real number δ such that x^* is Pareto optimal in $X \cap N(x^*, \delta)$ i.e. there does not exist another $x \in X \cap N(x^*, \delta)$ such that $f_i(x) \leq f_i(x^*)$ for all i and $f_j(x) \neq f_j(x^*)$ for at least one j, where $N(x^*, \delta)$ denotes the δ neighborhood of x^* defined by $\{x \in R^n | \; || \; x - x^* \; || < \delta\}$.

Bibliography

[1] F. M. L. Amirouche. *Computational Methods in Multibody Dynamics.* Prentice Hall, 1992.

[2] F. M. L. Amirouche, S. K. Ider, and J. Trimble. Analytical method for the analysis and simulation of human locomotion. *Journal of Biomechanical Engineering*, 112:379–386, 1990.

[3] F. M. L. Amirouche and J. Tongyi. Pseudo uptriangular decomposition method for constrained multibody system's using kane's equations. *Journal of Guidance Control and Dynamics AIAA*, 11(1):39–46, 1988.

[4] C. M. Angle and R. A. Brooks. Small planetary rovers. *IEEE/RSJ International Workshop on Intelligent Robots and Systems IROS, Ikabara, Japan*, pages 383–388, 1990.

[5] M. Armand, A. E. Patla, and J. P. Huissoon. Modelling of human leg motion during locomotion. *Proceedings of the 8th Biennial Conference, Canadian Society for Biomechanics, Calgary*, pages 94–95, 1994.

[6] A. G. Barto and R. S. Sutton. Landmark learning: An illustration of associative search. *Biological Cybernetics*, 42:1–8, 1981.

[7] R. D. Beer. *Intelligence as Adaptive Behavior.* Academic Press Inc., 1990.

[8] M. Belanger and A. E. Patla. Corrective responses to perturbations applied during walking in humans. *Neuroscience Letters*, 49:291–295, 1984.

[9] J. A. Bernard. Use of rule-based system for process control. *IEEE Control Systems Magazine*, 8(5):3–13, 1988.

[10] N. Bernstein. *The Coordination and Regulation of Movements.* Pergamon Press, Oxford, UK, 1967.

[11] M. Braae and D. A. Rutherford. Fuzzy relations in a control setting. *Kybernetes*, 7(3):185–188, 1978.

[12] R. A. Brooks. A robust layered control system for a mobile robot. *IEEE Journal of Robotics and Automation*, RA-2(1):14–23, 1986.

[13] T. S. Buchanan and D. A. Shreeve. An evaluation of optimization techniques for the prediction of muscle activation patterns during isometric tasks. *Journal of Biomechanical Engineering*, 118:565–574, 1996.

[14] H. C. Chen, J. A. Ashton-Miller, N. B. Alexander, and A. B. Schultz. Stepping over obstacles: Gait patterns of healthy young and old adults. *Journal of Gerontology: Medical Sciences*, 46(6):196–203, 1991.

[15] L. Chou and L. F. Draganich. Stepping over an obstacle increases the motions and moments of the joints of the trailing limb in young adults. *Journal of Biomechanics*, 30(4):331–337, 1997.

[16] J. J. Collins. Redundant nature of locomotor optimization laws. *Journal of Biomechanics*, 28(3):251–267, 1995.

[17] R. D. Crownshield and A. B. Brand. A physiologically based criterion of muscle force prediction in locomotion. *Journal of Biomechanics*, 14(11):793–801, 1981.

[18] Y. Davidor. *Genetic Algorithms and Robotics - A Heuristic Strategy for Optimization.* World Scientific Publishing, 1991.

[19] V. Dietz. Human neuronal control of automatic functional movements: Interaction between central programs and afferent input. *Physiological Reviews*, 72:33–69, 1992.

[20] V. Dietz, J. Quintern, and W. Berger. Obstruction of the swing phase during the gait: Phase-dependent bilateral leg muscle coordination. *Brain Research*, 384:166–169, 1986.

[21] T. Drew and S. Rossignol. A kinematic and electromyographic study of cutaneous reflexes evoked from the forelimb of unrestrained walking cats. *Journal of Neurophysiology*, 57:1160–1184, 1987.

[22] J. Duysens and G. E. Loeb. Modulation of ipsi and contralateral reflex responses in unrestrained walking cats. *Journal of Neurophysiology*, 44:1024–1037, 1980.

[23] J. Duysens, M. Trippel, G. A. Hortsmann, and V. Dietz. Gating and reversal of reflexes in ankle muscle during human walking. *Experimental Brain Research*, 82:351–358, 1990.

[24] G. M. Edelman. *Neural Darwinism.* Basic Books, New York, 1987.

[25] J. J. Eng, D. A. Winter, and A. E. Patla. Strategies for recovery from a trip in early and late swing during human walking. *Experimental Brain Research*, 102:339–349, 1994.

[26] R. Fletcher. *Practical Methods of Optimization.* Wiley, New York, 1988.

[27] H. Forssberg, S. Grillner, and S. Rossignol. Phasic gain control of reflexes from the dorsum of the paw during spinal locomotion. *Brain Research*, 132:121–139, 1977.

[28] L. Gauthier and S. Rossignol. Contralateral hindlimb responses to cutaneous stimulation during locomotion in high decerebrate cats. *Brain Research*, 207:303–320, 1981.

[29] D. E. Goldberg. *Genetic Algorithms in Search, Optimization and Machine Learning.* Addison-Wesley, Massachusetts, 1989.

[30] H. Goldstein. *Classical Mechanics.* Addison-Waseley, 1980.

[31] Editor J. J. Grefenstette. *Proceedings of International Conference on Genetic Algorithms.* Lawrence Erlbaum Associates, Hillsdale, N.J., 1985.

[32] S. W. Groesberg. *Advanced Mechanics.* John Wiley & Sons, 1968.

[33] A. E. Patla. Neuro-bio-mechanical Bases for the Control of Human Locomotion. In A. Bronstein et al., editor, *Clinical Aspects of Balance and Gait Disorders.* Edward Arnold, U.K., 1994.

[34] D. E. Hardt. Determining muscle forces in leg during normal human walking-an application and evaluation of optimization methods. *Journal of Biomechanical Engineering*, 100:27–78, 1978.

[35] H. Hemami and F. C. Weimer. Modeling of nonholonomic dynamic systems with applications. *Journal of Applied Mechanics*, 48:177–182, 1981.

[36] J. Hertz, A. Krogh, and R. G. Palmer. *Introduction to the Theory of Neural Computation.* Addison-Wesley publishing, Redwood, California, 1991.

[37] W. Herzog and T.R. Leonard. Validation of optimization models that estimate the forces exerted by synergistic muscles. *Journal of Biomechanics*, 24:31–39, 1991.

[38] J. Holland. *Adaptation in Natural and Artificial Systems.* University of Michigan Press, Ann Arbor, USA, 1975.

[39] M. Ishac and D. A. Winter. *KINGAIT Software.* Waterloo, Canada, 1994.

[40] J. R. Jang. Anfis: Adaptive-network-based fuzzy inference system. *IEEE Transactions on Systems, Man, and Cybernatics*, 23(3):665–684, 1993.

[41] K. De Jong. On using genetic algorithms to search program spaces. In J. J. Grefenstette, editor, *Proceedings of Second International Conference on Genetic Algorithms.* Lawrence Erlbaum Associates, 1987.

[42] J. W. Kamman and R. L. Huston. Dynamics of constrained multibody systems. *Journal of Applied Mechanics*, 51:899–903, 1984.

[43] E. R. Kandel, J. H. Schwartz, and T. M. Jessell. *Principles of Neural Science.* Appleton & Lange, Norwalk, Connecticut, 1992.

[44] J. Kim, Y. Moon, and B . P. Zeigler. Designing fuzzy net controllers using genetic algorithms. *IEEE Control Systems Magazine*, pages 66–72, 1995.

[45] P. J. King and E. H. Mamdani. The application of fuzzy control systems to industrial processes. *Automation*, 13(3):235–242, 1977.

[46] C. C. Lee. Fuzzy logic in control systems: Fuzzy logic controller. *IEEE Transactions on Systems, Man, Cybernetics*, 20(2):404–434, April 1990.

[47] M. A. Lewis, A. H. Fagg, and G. A. Bekey. Genetic algorithms for gait synthesis in a hexapod robot. In Y. F. Zheng, editor, *Recent Trends in Mobile Robots.* World Scientific Publishing Co., 1993.

[48] R. P. Lippmann. An introduction to computing with neural nets. *IEEE ASSP Magazine*, pages 4–22, 1987.

[49] E. H. Mamdani and S. Assilian. An experiment with linguistic synthesis with a fuzzy logic controller. *International Journal of Man Machine Studies*, 7(1):1–13, 1976.

[50] B. J. McFadyen and D. A. Winter. Anticipatory locomotor adjustments during obstructed human walking. *Neuroscience Research Communications*, 9(1):37–44, 1991.

[51] T. McGeer. Passive dynamic walking. *International Journal of Robotics Research*, pages 62–82, 1990.

[52] D. Mena, J. M. Mansour, and S. R. Simon. Analysis and synthesis of human swing leg motion during gait and its clinical applications. *Journal of Biomechanics*, 14:823–832, 1981.

[53] S. Mochon and T. A. McMahon. Ballistic walking. *Journal of Biomechanics*, 13:49–57, 1980.

[54] S. Mochon and T. A. McMahon. Ballistic walking: An improved model. *Journal of Mathematical Biosciences*, 52:241–260, 1981.

[55] D. J. Montana and L. Davis. Training feed forward neural networks using genetic algorithms. *Proceedings of the 11th International Joint Conference on Artificial Intelligence*, pages 762–767, 1989.

[56] J. A. Nelder and R. Mead. A simplex method of function minimization. *Comput. Journal*, 7:308–313, 1965.

[57] S. Onyshko and D. A. Winter. Synthesis of human walking: A planar model for single support. *Journal of Biomechanics*, 13:361–368, 1980.

[58] M. G. Pandy and N. Berme. A mathematical model for the dynamics of human locomotion. *Journal of Biomechanics*, 21(12):1053–1060, 1988.

[59] M. G. Pandy, F. E. Zajac, E. Sim, and W. S. Levine. Optimal control model for maximum-height human jumping. *Journal of Biomechanics*, 23(12):1185–1198, 1990.

[60] A. E. Patla, S. Prentice, C. Robinson, and J. Neufeld. Visual control of locomotion: Strategies of changing directions and going over obstacles. *Journal of Experimental Psychology [Human Perception]*, 17(3):603–634, 1991.

[61] A. E. Patla and S. D. Prentice. The role of active forces and intersegmental dynamics in the control of limb trajectory over obstacles during locomotion in humans. *Experimental Brain Research*, 106:499–504, 1995.

[62] A. E. Patla, S. D. Prentice, M. Armand, and J. P. Huissoon. The role of effector system dynamics on the control of limb trajectory over obstacles during locomotion: Empirical and modelling approaches. In T. Taguchi, editor, *Vestibular and Neural Front*, pages 333–336. Elsevier Science Publishers B.V.: North-Holland, 1994.

[63] A. E. Patla and S. Rietdyk. Visual control of limb trajectory over obstacles during locomotion: Effect of obstacle height and width. *Gait & Posture*, 1:45–60, 1993.

[64] A. Pedotti, V.V. Krishman, and L. Stark. Optimization of muscle force sequencing in human locomotion. *Mathematical Biosciences*, 38:57–76, 1978.

[65] C. A. Pratt, J. A. Buford, and J. L. Smith. Adaptive control for backward quadrupedal walking v. mutable activation of bifunctional thigh muscles. *Journal of Neurophysiology*, 75(2):832–842, 1996.

[66] J. N. Reeke and G. M. Edelman. Real brains and artificial intelligence. *Daedalus*, 117(1):143–173, 1988.

[67] S. Rietdyk and A. E. Patla. Context dependent reflex control: Some insights into the role of balance. *Experimental Brain Research*, 1997.

[68] D. E. Rumelhart, G. E. Hinton, and R. J. Williams. *In Parallel Distributed Processing, Volume 1.* MIT Press, Cambridge, Massachusetts, 1986.

[69] M. Sakawa. *Fuzzy Sets and Interactive Multi-objective Optimization.* Plenum Press, NewYork and London, 1993.

[70] Editor J. D. Schaffer. *Proceedings of Third International Conference on Genetic Algorithms.* Morgan Kaufmann, San Mateo, California, 1989.

[71] R. P. Singh and P. W. Likins. Singular value decomposition for constrained dynamical systems. *Journal of Applied Mechanics*, 52:943–948, 1985.

[72] M. W. Spong and M. Vidyasagar. *Robot Dynamics and Control.* John Wiley and Sons, 1989.

[73] R. E. Stein. Reflex modulation during locomotion: Functional significance. In A. E. Patla, editor, *Adaptability of human Gait*, pages 21–36. Elsevier Science Publishers B.V.: North-Holland, 1991.

[74] R. S. Sutton. Learning to predict by the methods of temporal differences. *Machine Learning*, 3:9–44, 1988.

[75] R. S. Sutton. Reinforcement learning architectures for animats. In J. A. Meyer and S. W. Wilson, editors, *Proceedings of the First International Conference on Simulation of Adaptive Behavior*, pages 288–296. The MIT Press, Cambridge, 1991.

[76] T. Takagi and M. Sugeno. Derivation of fuzzy control rules for human operator's action. *Proceedings of the IFAC Symposuim on Fuzzy Information, Knowledge Representation and Decision Analysis*, pages 55–60, July 1983.

[77] M. Togai and H. Watanabeh. Expert system on a cheap: An engine for approximate real time reasoning. *IEEE Expert Systems Magazine*, 1:55–62, 1986.

[78] R. M. Tong, M. B. Beck, and A. Latten. Fuzzy control of the activated sludge wastewater treatment process. *Automation*, 171:669–690, 1980.

[79] V. Torczon. On the convergence of the multidirectional search algorithm. *SIAM Journal of Optimization*, 1(1):123–145, 1991.

[80] C. Wernicke. The symptom-complex of aphasia. In A. Church, editor, *Diseases of Nervous System.* Appleton, New York, 1908.

[81] D. Whitley. Applying genetic algorithms to neural network learning. In *Proceedings of the Seventh Conference for the Study of Artificial Intelligence and Simulated Behavior, Sussex, England.* Pitman Publishing, 1989.

[82] D. A. Winter. *The Biomechanics and Motor Control of Human Gait: Normal, Elderly, and Pathological.* 2nd edition, 1991.

[83] D. A. Winter. *Biomechanics and Motor Control of Human Movement.* John Wiley and Sons Inc., 1992.

[84] D. A. Winter. Foot trajectory in human gait, a precise and multifunctional motor control task. *Physical Therapy*, 72:45–56, 1995.

[85] G. T. Yamaguchi and F. E. Zajac. Restoring unassisted natural gait to paraplegics with functional neuromuscular stimulation: A computer simulation study. *IEEE Transactions on Biomedical Engineering*, 37(9):886–902, 1991.

[86] T. Yamakawa and K. Miki. The current mode fuzzy logic integrated circuits fabricated by standard cmos process. *IEEE Transactions on Computer*, C-35(2):161–167, 1986.

[87] J. F. Yang and R. B. Stein. Phase-dependent reflex reversal in human leg muscles during walking. *Journal of Neurophysiology*, 63:1109–1117, 1990.

[88] S. Yasunobu and S. Miyamoto. Automatic train operation by predictive fuzzy control. In M. Sugeno, editor, *Industrial Application of Fuzzy Control*, pages 1–18. Amesterdam, North-Holland, 1985.

[89] L. A. Zadeh. The concept of linguistic variable and its application to approximate reasoning. *Information Science*, 8:199–249, 1975.

[90] R. Zernicke, K. Schneider, and J. A. Buford. Intersegmental dynamics during gait: Implications for control. In A. E. Patla, editor, *Adaptability of human Gait.* Elsevier Science Publishers B.V., North-Holland, 1991.

IMAGE EVALUATION
TEST TARGET (QA-3)

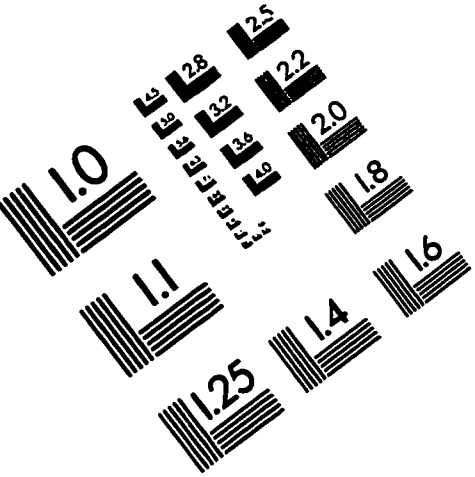

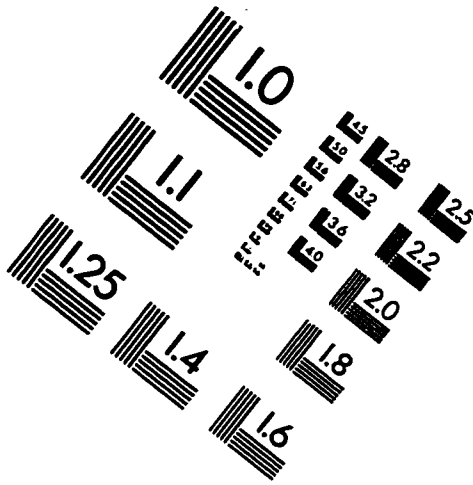

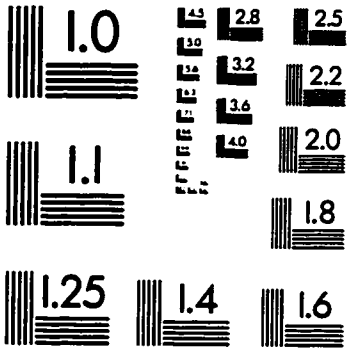

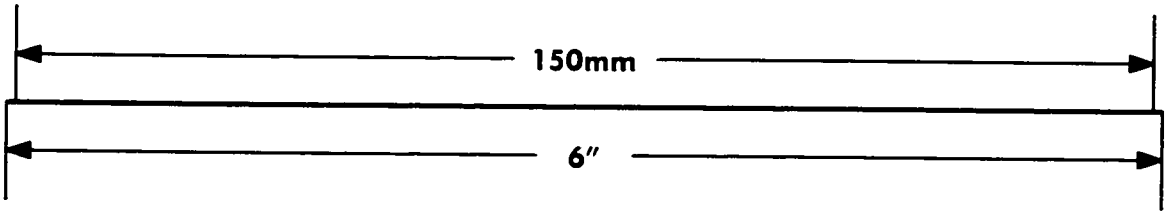

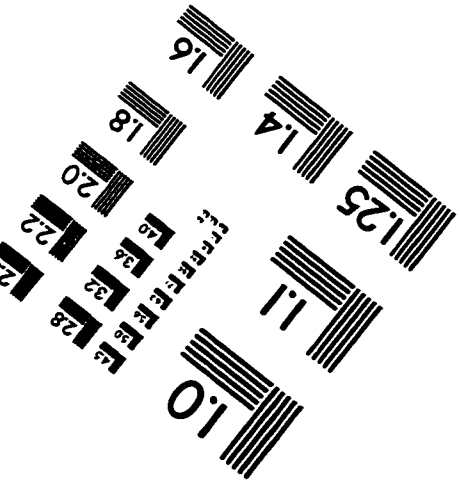

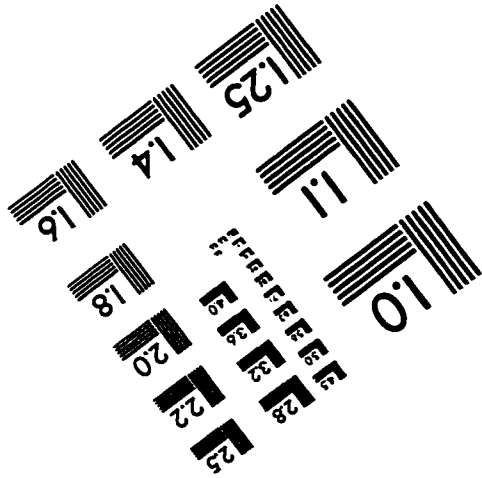

APPLIED IMAGE, Inc
1653 East Main Street
Rochester, NY 14609 USA
Phone: 716/482-0300
Fax: 716/288-5989

© 1993, Applied Image, Inc., All Rights Reserved